BSc thesis in Mathematics and Physics

Effects of orbital resonance on the giants in the early Solar System

Joran Haasnoot

August 2024

- Instructors: dr. P.M.Visser & prof.dr. S.Stallinga
- Faculty: Faculty of Electrical Engineering, Mathematics and Computer Science, Delft

Abstract

One of the most popular descriptions of the evolution of our Solar System is known as the Nice model which places the giants Jupiter, Saturn, Uranus and Neptune in proximate orbits which influence each other greatly due to a phenomenon known as ”orbital resonance”. To attain this the planets were placed into near co-planar orbits with small eccentricities and inclinations, with semi-major values of $5.45\text{AU}, 8.65\text{AU}, 11 - 13\text{AU}$ and $13.5 - 17\text{AU}$. Furthermore, a disk of planetoids outside of the outer planet's radius was placed to emulate to effect of planetoids on this evolution. Furthermore, the model often includes a disk of planetoids beyond the outer planet's radius to simulate their influence on planetary evolution. However, in this research, the effects of orbital resonance were investigated by running numerical simulations without the presence of these planetoids, using the Leapfrog method as the numerical integrator. First, we considered the 1:1 resonance of test-particles in the Lagrange point L_4. After this the 2:1 resonance was investigated by placing a test-particle in resonance with a planet and afterwards replacing the test particle with another planet. From this it could be found that resonance has significant effects on planets, most importantly causing their semi-major axis and eccentricity to oscillate. With this knowledge the Nice model was researched (with Uranus and Neptune swapped to their current order) without this disk of planetoids in order to investigate the effects of resonance on the early Solar System. From this, qualitative effects were found such as the oscillation of eccentricities due to orbital resonance and the effect of ”locking”, which is the effect that once two orbits cross each other it's difficult for them to separate. During this locking there were a number of opportunities in which for the crossing orbits to close-encounter and to send each other into eccentric orbits, or to eject a planet from the Solar System entirely. Finally, to investigate the certainty of the results more accurate simulations were executed with the use of adaptive time-steps, from these simulations the same features could be seen with the total energy deviating a few percents.

Contents

1 Introduction **1**

2 Gravity model **5**
2.1 The N-body problem . . . 5
2.2 Ellipse . . . 5
2.3 The one-body problem . . . 7
2.4 Three-body problem . . . 8
2.4.1 The movement of the two bodies . . . 8
2.4.2 The mechanics of a rotating frame. . . . 9
2.4.3 Jacobi integral . . . 11
2.4.4 Lagrange points . . . 12
2.4.5 Stability of Lagrange points . . . 13
2.4.6 Different orbits . . . 15
2.5 Orbital elements . . . 16
2.5.1 Definition of orbital elements . . . 16
2.5.2 Calculating orbital elements from Cartesian coordinates . . . 19
2.6 Perturbations of the planets' motion . . . 22
2.7 Orbital resonance . . . 23
2.8 Nice model . . . 26

3 Numerical method **29**
3.1 Mechanics . . . 29
3.2 Initialisation . . . 30
3.3 Adaptive time-steps . . . 31

4 Results **33**
4.1 The 1:1 resonance, L_4 . . . 33
4.2 2:1 Resonance with test-particle . . . 37
4.3 2:1 resonance tests of planets . . . 45
4.4 Four planets in resonance chain . . . 51
4.4.1 Resonance chain with adaptive time-steps . . . 59

5 Conclusion **61**

6 Further Research **63**

List of Figures

1.1 Two clocks in 2:1 resonance. As the upper clock makes two full rotations, the lower clock makes one full rotation. It can be observed that the clocks are in the same position when both arrows point up. . . . 2
1.2 A figure showing 3 snapshots of the evolution of the Nice model. The first snapshot shows the initial conditions. . . . 2

2.1 Representation of an ellipse highlighting three key distances: the semi-major axis a, the semi-minor axis b, and the distance from the center to the foci c. These characteristic distances define the shape and geometry of the ellipse. . . . 6
2.2 An example of a planetary orbit around the Sun. . . . 8
2.3 Illustration of the circular motion of two bodies. The distances are proportional to the mass of the other body to balance the center of mass. . . . 10
2.4 All the Lagrange points and contour lines of the potential U for $\mu_2 = 0.2$ in the ξ, η-plane. . . . 13
2.5 A so-called "horseshoe" orbit which was obtained by initialising a system of $\mu_2 = 0.000953875$ at $\xi = -1.02745, \eta = \dot{\xi} = 0, \dot{\eta} = 0.04032$. . . . 16
2.6 A so-called "tadpole" orbit which was obtained by initialising a system of $\mu_2 = 0.000953875$ at $\xi = -0.097668, \eta = \dot{\xi} = 0, \dot{\eta} = -0.06118$. . . . 17
2.7 A procedure illustrating the transition between the blue orientation and the pink orientation by Euler angles. First rotating about Ω around the z-axis to be able to rotate the plane by an angle of I correctly. Finally, rotating ω around the z-axis to obtain the correct orientation within the plane. . . . 18
2.8 A figure showing a few notable quantities within the plane of an orbit. The reference direction refers to the direction through which the plane has been rotated. The perihelion and the Aphehlion are the closest and farthest point away from the Sun respectively and have values of $(1-e)a$ and $(1+e)a$. ω is the angle from the reference direction to the perihelion and ν is the angle from the perihelion to the body. 19
2.9 A figure showing the initial conditions of a small inner body in a Kepler orbit and a large outer body in a circular orbit. . . . 24
2.10 The disturbing potential $\mathcal{R}$. Notice that there's some base-level shown by the grey dotted line and peaks. . . . 25
2.11 The oscillation function for $e = 0.3$. This function describes the distance divided by the semi-major axis from the focal point closest to the periapsis to a point that makes a pseudo-angle ϕ relative to the periapsis. . . . 26
2.12 Evolution of the Solar System as depicted in the Nice model [Tsiganis et al., 2005]. This $a/q/Q$ plot displays the semi-major axis a (where $q = a(1-e)$), the perihelion distance q, and the Aphelion distance Q (where $Q = a(1+e)$). The plot illustrates how the semi-major axis and eccentricity of the planets evolve over time, providing insights into the dynamic changes and resonant interactions within the Solar System. 28

4.1 A plot of the relative distance from L_4, that is, the distance divided by the distance between the two large masses d. This simulation was ran with time-steps of 10^4 seconds. . . . 34
4.2 A similar plot to that of 4.1 but with time-steps of 10^5 seconds. . . . 34
4.3 The path of an object starting close to L_4. It can be seen that it oscillates about this point. Additionally, this shape seems similar to that of a cycloid. . . . 35
4.4 The x and y values divided by the separation between the Sun and the planet. . . . 35
4.5 The maximum relative deviation against the time-steps of the simulation. A linear relation can be observed between $\log \mathrm{dt} = \log \frac{\Delta x}{d}$. It follows from the slope of 2 decades per decade that the error is quadratic in dt. . . . 36

4.6 The numerical solution and the analytical solution near L_4 with starting conditions $x - x_0/d = y - y_0/d = 10^-5$ after 900yr. After this time the numerical solutions seems to lag behind the analytical solution with about 9.419yr 36

4.7 Similar test to 4.6 where the numerical and analytical solution of motion near L_4 with starting conditions $x - x_0/d = y - y_0/d = 10^{-5}$ are compared after 900yr. . . . 37

4.8 These figures show the variance of orbital elements of different 2:1 resonances over a time-scale of 100 circulations of an outer body with $\mu_2 = 0.001$. In each plot a is the semi-major axis (on a scale from 3AU to 3.25AU), e represents the eccentricity (on a scale from 0 to 0.2), ϖ longitude of periapsis (on a scale from $-\pi$ to π rad) and φ a quantity defined by $2\nu_2 - \nu_1 - 2\varpi$ (on a scale from $-\pi$ to π rad). The initial values are given in table 4.1. All of these figures were created with time-steps of 10^5s. 41

4.9 Plots of different orbital elements for different types of 2:1 resonances, described more precisely in figure 4.8, which is identical to these plots except that time-steps of 10^5s were used to create the plots instead of 10^6s, which were used for these plots. 44

4.10 Orbital elements of two planets starting over a time-scale of 1000 circulations of the outer body. The inner and outer body were given the masses of Jupiter and Saturn respectively. In each plot a is the semi-major axis (on a scale from on a scale from 5.2 to 5.6AU for the inner body and 8.25 to 8.9AU for the outer), e represents the eccentricity (on a scale from 0 to 0.2 for both), ϖ longitude of periapsis (on a scale from $-\pi$ to π rad) and φ a quantity defined by $2\nu_2 - \nu_1 - 2\varpi$ (on a scale from $-\pi$ to π rad). The initial values are given in table (4.1). 48

4.11 The orbital elements of initial conditions (b) and (f) respectively for 1000 outer periods. The specifics of these initial conditions are also given in the titles of the respective plots. These plots were shown for 100 outer periods in 4.3 and were both plotted because the eccentricity e did not appear periodic in these plots. It is in this figure that that this is indeed the case. 49

4.12 Orbital elements of Jupiter and Saturn initialised as in the Nice model. a is the semi-major axis (on a scale from on a scale from 5.2 to 5.6AU for the inner body and 8.25 to 8.9AU for the outer), e represents the eccentricity (on a scale from 0 to 0.2 for both), ϖ longitude of periapsis (on a scale from $-\pi$ to π rad) and φ a quantity defined by $2\nu_2 - \nu_1 - 2\varpi$ (on a scale from $-\pi$ to π rad). 50

4.13 Run of our Nice model depicting oscilations due to resonance. 51

4.14 Run of our Nice model depicting Uranus and Neptune closing in on each other, after which at around $t \approx 0.3 \times 10^6$yr they have a close encounter and Neptune is ejected into an eccentric orbit. 52

4.15 Run of our Nice model depicting an ejection of Uranus at around $t \approx 0.1 \times 10^6$yr, after which Neptune is knocked into a more eccentric orbit with higher semi-major axis. 52

4.16 Run of our Nice model depicting Uranus influencing Saturn's and Neptune's orbit strongly due to the distance between the orbits from around $t = 0.5 \times 10^6$yr. After chaotic changes, Uranus is ejected from the Solar System at around 0.7×10^6yr, after which Saturn and Neptune keep changing each other's orbit. 53

4.17 Relative deviation of total energy, linear momentum and angular momentum of figure 4.13. It can be observed that all the conserved quantities have a noise-like error which is on the scale of 10^{-3} for the energy and the angular momentum, while it is on the scale of 10^{-1} for the momentum. 54

4.18 Relative deviation of total energy, linear momentum and angular momentum of figure 4.14. A discontinuity can be observed in the energy and angular momentum plot around $t = 0.3 \times 10^6$yr. Additionally, the angular momentum and the linear momentum increase their noise-like error after this event. 55

4.19 Relative deviation of total energy, linear momentum and angular momentum of figure 4.15. A discontinuity can be observed in the energy and linear momentum plot around $t = 0.1 \times 10^6$yr. Additionally, the noise of the linear momentum increases after this point. Because of the moving center of mass (the average of p is not constant) the angular momentum's error increases linear from $t = 0.1 \times 10^6$yr. 57

4.20 Relative deviation of total energy, linear momentum and angular momentum of figure 4.16. Significant results can be found around $t = 0.5 \times 10^6$yr, during which all the conserved quantities change and an event around 0.7×10^6yr after which the angular momentum linearly increases, suggesting an ejection, as can be verified from figure 4.16. 58
4.21 Run of our Nice model with adaptive time-steps. Most notable is the ejection of Uranus at approximately $t = 0.8 \times 10^6$yr 59
4.22 Relative deviation of total energy and momentum of figure 4.21. From the angular momentum plot it can be seen that there are 2 significant events at around 0.45×10^6yr and 0.8×10^6yr. By comparing the timescale with that of figure 4.21 it can be seen that the first event is when Uranus starts having close encounters with Saturn and Neptune, changing its semi-major axis significantly and the last event is the ejection of Uranus. 60

1 Introduction

The current leading theory for the extinction of the dinosaurs is that a large meteor impacted the Earth, ejecting a thick layer of dust into the atmosphere, which in turn globally suppressed photosynthesis, resulting in extinction events. This theory was first proposed in [Alvarez et al., 1980], referred to as the "Alvarez hypothesis" in the literature.

Meteors also cause damage on smaller scales. On February 15, 2013, a meteor impacted close to Chelyabinsk, Russia. The pressure from the impact destroyed the village's windows, which caused most of the damage to the 1,500 people affected; fortunately, there were no casualties.

If one wishes to take preventative actions, it is of utmost importance to detect planetoids before they become meteors, i.e., before they cross their orbits with that of the Earth. Planetoids only dimly reflect light from other objects, which means that they are difficult to detect. Thus, it is helpful to predict where cluster of asteroids may reside and estimate their size in order to place observational satellites near these clusters. Predicting this depends heavily on understanding the history and evolution of planetoids and their interactions within the Solar System..

In 2005 a series of papers [Gomes et al., 2005], [Morbidelli et al., 2005], [Tsiganis et al., 2005] were published conjecturing initial conditions for the distribution of planetoids in the early Solar system: four giant planets (being Jupiter, Saturn, Uranus and Neptune) were placed very close together compared to their positions now, with a disk of small planetoids residing outside of the outer planet's orbit. Additionally, the planets were placed in such a way that they would have close-encounters near the same point in their orbit, a phenomenon known as orbital resonance.

To describe what orbital resonance is, we can draw an analogy to a clock. The minute and hour hand of a clock are said to be in a so-called "12:1 resonance", because the minute hand makes 12 full rotations in 12 hours whereas the hour hand only 1. In this case, the hands do not meet at the same point, which can be verified by considering the approximate locations at times like 2:10 and 3:15. The hands only meet at the same point when the resonance is of the form $n : n - 1$, such as 2:1. Imagine a hand which counts every minute and one which counts every two minutes, as shown in figure (1.1). As can be seen in the figure, the clocks meet again at the same position.

The initial conditions and evolution of the original Nice papers are shown in figure 1.2. The results of these initial conditions showed significant correspondence with current observed properties of the Solar system [Tsiganis et al., 2005]. This model is called the "Nice model" (named after the city Nice in France) in the literature and is one of the most successful models of the evolution of the Solar system.

Recent research has expanded on the Nice model, exploring the "jumping Jupiter" scenario, where Jupiter experiences a rapid shift in the orbit's semi-major axis. This could be explained by placing an additional fifth giant in the original Nice model, which is later on ejected. This planet causes Jupiter to move quickly when it's close to this fifth giant before its ejection [Li et al., 2023].

The relevance of the history of the Solar system in taking preventative actions against planetoids crossing the orbit of Earth and the recent utilisation of the Nice model in the literature motivates us to investigate the Nice model. In this thesis the Nice model is researched by neglecting the effects of planetoids to the orbits of the planets. In other words, this research investigates the effects of orbital resonance on the planets of our Solar System in close proximity.

The structure of this thesis is as follows. First, the basic mechanics of gravity are reviewed, focusing on Newtonian gravity and the derivation of planetary orbits as approximate ellipses around the Sun. The three-body problem is then introduced to explain the gravitational interactions between the Sun, Jupiter, and smaller bodies, which lead to the formation of asteroid clusters in resonant orbits.

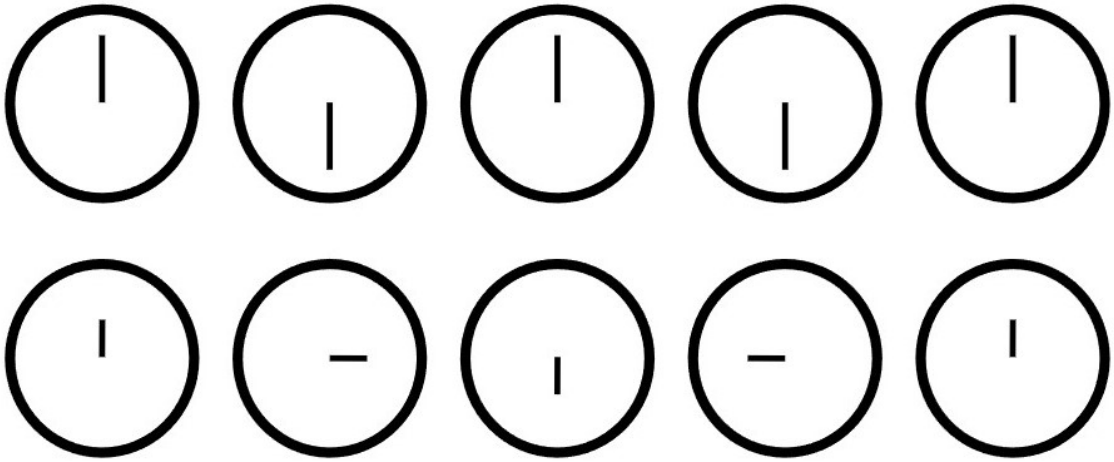

Figure 1.1: Two clocks in 2:1 resonance. As the upper clock makes two full rotations, the lower clock makes one full rotation. It can be observed that the clocks are in the same position when both arrows point up.

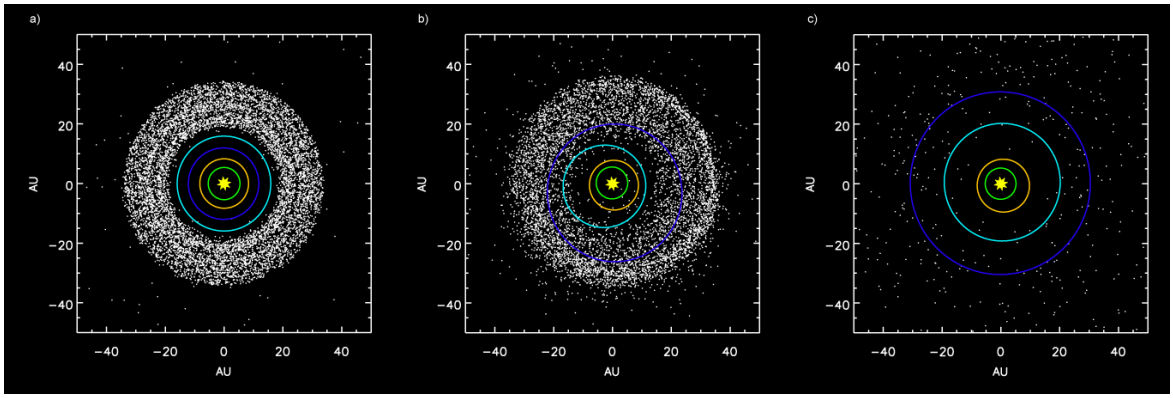

Figure 1.2: A figure showing 3 snapshots of the evolution of the Nice model. The first snapshot shows the initial conditions.

Following this, the slow changes in these elliptical orbits are described using parameters known as ”orbital elements.” This framework is then used to demonstrate the effects of orbital resonance. After establishing this theoretical foundation, the Nice model is introduced, outlining its initial conditions and relevance.

The methodology is then detailed, describing the approach taken in the research. Next, the results are presented. These include simulations of the 1:1 resonance at Lagrange point L_4, the 2:1 resonance both with and without test particles, and a simulation of the Nice model without a disk of planetoids. The thesis concludes with an analysis of these results and their implications.

2 Gravity model

This thesis aims to investigate how the positions of gas giants, along with the Sun, influence each other under specific initial conditions. To achieve this, it is crucial to select an appropiate model that describes the changes in the positions of the planets: the equations of motion. In this research, these equations will be modeled purely by gravity. This chapter aims to describe the model of gravity and its properties to allow for a sufficient understanding of the evolution of the Solar system.

2.1 The N-body problem

In this research, the Solar system will be considered within the framework of Newtonian mechanics. Newtonian mechanics has been chosen over general relativity since general relativity is more complex but not significantly more accurate in this context. A number of bodies are idealised as point-masses, and the gravitational forces them are considered. This is known as "the N-body problem".

In Newtonian mechanics any mass m_i experiences a gravitational force from a mass m_j with a value given by:

$$\vec{F}_{j\to i} = -\frac{\mathcal{G}m_i m_j}{\left\|\vec{r}_i - \vec{r}_j\right\|^3}(\vec{r}_i - \vec{r}_j), \tag{2.1}$$

where $\mathcal{G}$ refers to the gravitational constant which has a value of $6.67430 \pm 0.00015 \times 10^{-11}\mathrm{Nm}^2/\mathrm{kg}^2$ [NIST, 2022]. Additionally, $\vec{r}_i$ and $\vec{r}_j$ refer to the positions of body i and body j, respectively. In Newtonian mechanics, the force is related to the motion of a particle by $\vec{F} = m\vec{a}$, where $\vec{a}$ is the acceleration, or the second order derivative of position. This means that the acceleration of a mass m_i due to a mass m_j is

$$\vec{a}_{j\to i} = -\frac{\mathcal{G}m_j}{\left\|\vec{r}_i - \vec{r}_j\right\|^3}(\vec{r}_i - \vec{r}_j). \tag{2.2}$$

If the contributions of all masses other than that of body i are summed, the acceleration of body i can be found as

$$\vec{a}_i = -\sum_{j\neq i} \frac{\mathcal{G}m_j}{||\vec{r}_i - \vec{r}_j||^3}(\vec{r}_i - \vec{r}_j). \tag{2.3}$$

This results in a non-linear system of differential equations which in general is hard to solve. An analytical solution to this problem is known [Wang, 1991], but it is an infinite series expression with very slow convergence, and therefore not practically useful. Because of this limitation, simplifications to the N-body problem shall be made in theoretical discussions, and numerical solutions shall be utilised for the experiments.

2.2 Ellipse

This section's purpose is to inform the reader about the properties of the ellipse, as this shape will be recurrent in the following chapters. If the reader is familiar with the properties of the ellipse, understanding this thesis should not be compromised by skipping this section.

An ellipse can be defined in the following way:

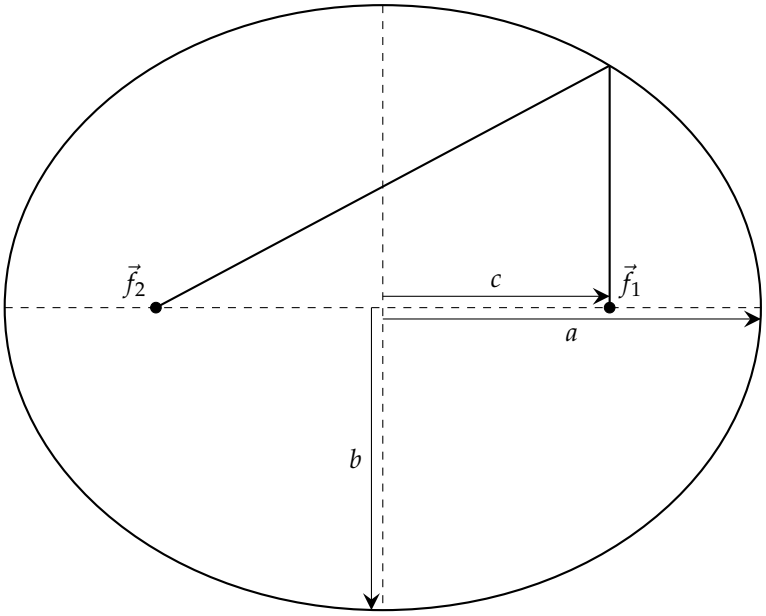

Figure 2.1: Representation of an ellipse highlighting three key distances: the semi-major axis a, the semi-minor axis b, and the distance from the center to the foci c. These characteristic distances define the shape and geometry of the ellipse.

Definition 2.2.1 (Ellipse)**.** An ellipse is a set of points $\{\vec{r} \in \mathbb{R}^2 : ||\vec{r} - \vec{f}_1|| + ||\vec{r} - \vec{f}_2|| = 2a\}$.

In words, this means that an ellipse is created by picking two points $\vec{f}_1$ and $\vec{f}_2$ and a distance $2a$. Then, the ellipse is found by finding all the points such that going from $\vec{f}_1$ to such a point and then going to $\vec{f}_2$ covers a distance exactly equal to $2a$. An example of an ellipse has been provided in figure 2.1. There are three important variables describing the different characteristic distances of the ellipse illustrated in the figure: a, b and c. a describes the distance from the center to the rightmost point, also known as the "semi-major axis", b is the distance between the center and the top, known by "semi-minor axis", and c describes the distance from the center to one of the points chosen in the definition, such a point is known as a "focus", and c is given the name "linear eccentricity".

Notice that in figure 2.1 a is mentioned as the length from the center to the right-most point. This is consistent with definition (2.2.1). Consider the right-most point, then the two distances would be $a - c$ and $a + c$, adding up to $2a$, proving consistency. The uppermost point can also be considered in a similar way to find a relation between a, b and c, the two distances are equal and equate to $\sqrt{b^2 + c^2}$, meaning that $2\sqrt{b^2 + c^2} = 2a \implies b^2 + c^2 = a^2$. Since there is an equation relating the three variables, two parameters are needed to describe the shape of an ellipse since the three variables got reduced to two. Since a is seen in the definition it is natural to take a as one of these parameters, describing the size of the ellipse. For the second parameter a quantity which describes the shape of the ellipse is chosen: the eccentricity, defined by $e = \frac{c}{a}$ which takes values from 0 to 1. For $e = 0$, the focuses coincide and one obtains a circle.

Since algebraic computations of the ellipse will be necessary in the following sections, the algebraic shape of an ellipse oriented like the one in the example is given as: [Wikipedia, 2024a]

$$\left(\frac{x}{a}\right)^2 + \left(\frac{y}{b}\right)^2 = 1. \tag{2.4}$$

However, for the purposes of this paper, the Sun, which is one of the focuses, is most naturally placed at the origin. For this reason, the ellipse is shifted to the left resulting in the expression

$$\left(\frac{x+c}{a}\right)^2 + \left(\frac{y}{b}\right)^2 = 1. \tag{2.5}$$

When this equations is written completely in terms of the ellipse parameters, this would give

$$\left(\frac{x+ae}{a}\right)^2+\left(\frac{y}{\sqrt{1-e^2}a}\right)^2=1. \tag{2.6}$$

In conclusion, the ellipse is a shape defined by the combined distance of two focuses. The ellipse is determined by two parameters a and e, known as the semi-major axis and the eccentricity. This shape is described by equation (2.6) algebraically when the Sun is placed at the origin and the perihelion at the positive x-axis (which shall be the convention in this paper).

2.3 The one-body problem

The N-body problem has been described but there's a significant difference in tools necessary to describe a dust cloud of gravitational particles and that of describing the Solar system; the Solar system has bodies orbiting in ellipses around the Sun while a dust cloud does not. The Solar System therefore requires a simpler analysis of the N-body problem because of this structure, the goal of this section is to illustrate why this structure emerges.

The reason why the planets orbit around the Sun instead of around each other as well is the fact that it's the heaviest object in the Solar system, approximately 1,000 times heavier than Jupiter, the heaviest planet. More specifically, the equations of motions of a body can be well approximated by neglecting the other planets. Additionally, because the Sun is vastly more heavy than the other objects it can also be considered as the center of mass (which in reality is just outside of the Sun's surface). Neglecting all other masses and pinning the Sun at the origin modifies equation (2.3) into

$$\ddot{\vec{r}}=-\frac{\mathcal{G}M_\odot}{r^3}\vec{r}, \tag{2.7}$$

which is also referred to as "the one-body problem". In this equation r is the distance from the Sun, or center of mass, and $M_\odot$ is the Solar mass which has a value of 2.0×10^{30}kg [Murray and Dermott, 2000, p. 22]. This differential equation is not trivial to solve but solutions can be found by applying the first two Kepler laws: [Murray and Dermott, 2000, p. 3]

1. The planets move in ellipses with the Sun at one focus.
2. A radius vector from the Sun to a planet sweeps out equal areas in equal times.

These laws describe the evolution of the body because the path is known by the first law and the speed at which the path is traversed by the second law. The initial conditions then give the specifics: which ellipse and at what rate is area traversed. This means that the orbits of the planets are all ellipses which slowly change over time because of perturbations from other planets. An example of an orbit has been provided in figure 2.2. Two labels have been given to the outermost points: the perihelion and the aphelion. The perihelion will be mentioned a number of times throughout the paper as it gives a reference direction for the ellipse and because the mechanics are relatively simple at that point because of the symmetry, allowing for the calculation of conserved quantities.

The "third Kepler law"

$$n^2a^3=GM_\odot, \tag{2.8}$$

where n is the angular velocity, is a direct consequence from the first two Kepler laws (2.3). In section 2.5.2, it is demonstrated that at the periapsis, the position and velocity vector are given by

$$\vec{r}=\begin{pmatrix}a(1-e)\\0\\0\end{pmatrix}\qquad\text{and}\qquad\vec{v}=\begin{pmatrix}0\\\sqrt{\frac{GM_\odot}{a}\frac{1+e}{1-e}}\end{pmatrix}.$$

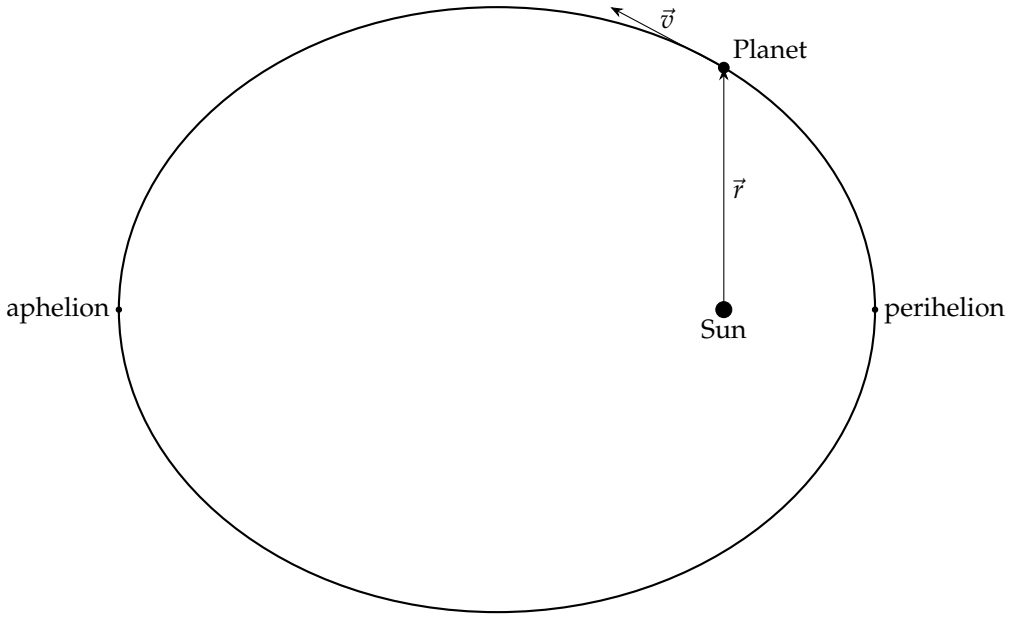

Figure 2.2: An example of a planetary orbit around the Sun.

From these, the rate of area being swept out can be derived as $\frac{1}{2}\|\vec{r}\times\vec{v}\| = \frac{1}{2}\sqrt{GM_{\odot}a(1-e^2)}$. By considering that the area of an ellipse is $\pi ab = \pi a^2\sqrt{1-e^2}$, the period can be derived as

$$T = \frac{\pi ab}{\frac{1}{2}\sqrt{GM_{\odot}a(1-e^2)}} = \frac{2\pi a^{3/2}}{\sqrt{GM_{\odot}}}. \tag{2.9}$$

Using the relationship that the frequency $n = \frac{2\pi}{T}$, the third Kepler law, equation (2.8), is then derived.

2.4 Three-body problem

The three-body problem involves analyzing the mutual gravitational interactions between three bodies. This problem is crucial for testing numerical methods and understanding 1:1 "orbital resonance," which will be further discussed in section 2.7. In its most general form, the three-body problem is notoriously difficult to solve, with known solutions being slowly-converging infinite series [Sundman, 1913], from which the general solution of the N-body problem [Wang, 1991] was inspired. For simplicity, we impose the following restrictions: firstly, the third mass is negligible and does not affect the orbits of the first two bodies; secondly, the orbits of the first two bodies are perfect circles around their common center of mass (CM), simplifying the equations of motions. This section explores the motion of the third, negligible mass.

2.4.1 The movement of the two bodies

To understand the motion of the third body, we first need to precisely determine the motion of the two primary bodies, which can be analyzed by solving the two-body problem. Instead of deriving a solution from scratch, we will present a known solution and verify that it satisfies the equations governing the two-body problem.

The proposed solutions of both bodies are:

$$\vec{r}_1 = \begin{pmatrix} x_1 \\ y_1 \\ z_1 \end{pmatrix} = \begin{pmatrix} -\cos(nt)\mu_2 d \\ -\sin(nt)\mu_2 d \\ 0 \end{pmatrix} \tag{2.10}$$

and

$$\vec{r}_2 = \begin{pmatrix} x_2 \\ y_2 \\ z_2 \end{pmatrix} = \begin{pmatrix} \cos(nt)\mu_1 d \\ \sin(nt)\mu_1 d \\ 0 \end{pmatrix}, \tag{2.11}$$

where d is the distance between the two points and μ_1 and μ_2 are relative weights with values of $m_1/(m_1+m_2)$ and $m_2/(m_1+m_2)$ respectively. Key observations from this solution include:

1. The bodies are in circular motion with both bodies having the same angular frequency. A rotation by

$$\hat{R} = \begin{pmatrix} \cos(nt) & \sin(nt) & 0 \\ -\sin(nt) & \cos(nt) & 0 \\ 0 & 0 & 1 \end{pmatrix}, \tag{2.12}$$

   or nt radians in the negative direction, keeps $\vec{r}_1$ and $\vec{r}_2$ stationary.

2. The distance between the two bodies remains constant, $\vec{r}_1 - \vec{r}_2 = \frac{m_1+m_2}{m_2}\vec{r}_1 = d\hat{r}_1$. This is a direct implication from the previous observation.

3. The center of mass remains stationary at the origin: $m_1\vec{r}_1 + m_2\vec{r}_2 = \vec{0}$.

To verify the solution, the expressions are substituted into the equations of motion:

$$\ddot{\vec{r}}_1 = -\frac{\mathcal{G}m_2}{r_{12}^3}(\vec{r}_1 - \vec{r}_2) \qquad \text{and} \qquad \ddot{\vec{r}}_2 = -\frac{\mathcal{G}m_1}{r_{12}^3}(\vec{r}_2 - \vec{r}_1), \tag{2.13}$$

which then turns into

$$-n^2\vec{r}_1 = -\frac{\mathcal{G}(m_1+m_2)}{d^3}\vec{r}_1 \qquad \text{and} \qquad -n^2\vec{r}_2 = -\frac{\mathcal{G}(m_1+m_2)}{d^3}\vec{r}_2. \tag{2.14}$$

This confirms that the proposed solution satisfies the equations, provided that

$$n^2 = \frac{\mathcal{G}(m_1+m_2)}{d^3}. \tag{2.15}$$

An example of such a motion has been displayed in figure 2.3

2.4.2 The mechanics of a rotating frame.

The three-body problem is complex due to the time-dependent interactions between moving bodies. To simplify the analysis, particularly for the restricted three-body problem, we use a rotating frame of reference where the two primary bodies are stationary. This section details how Newtonian mechanics transform in this rotating frame.

Consider the linear transformation $\hat{R} : \vec{r} = (x, y, z) \to \vec{r'} = (\xi, \eta, \zeta)$ represented by the matrix $\hat{R}$ as in equation 2.12, which rotates the system by nt radians into the negative direction. In this new (ξ, η, ζ) frame the two massive masses are stationary. $\frac{d^2}{dt^2}\vec{r} = \vec{a}$ needs to be determined to understand how the mechanics change.

Starting from the expression $\vec{r} = R^{-1}\vec{r'}$, this expression is differentiated twice to obtain:

$$\vec{a} = \frac{d^2\hat{R}^{-1}}{dt^2}\vec{r'} + 2\frac{d\hat{R}^{-1}}{dt}\vec{v'} + \hat{R}^{-1}\vec{a'}. \tag{2.16}$$

The $\hat{R}^{-1}$ has to be evaluated further to get a more direct expression. First note that

$$\hat{R}^{-1} = \begin{pmatrix} \cos(nt) & -\sin(nt) & 0 \\ \sin(nt) & \cos(nt) & 0 \\ 0 & 0 & 1 \end{pmatrix}. \tag{2.17}$$

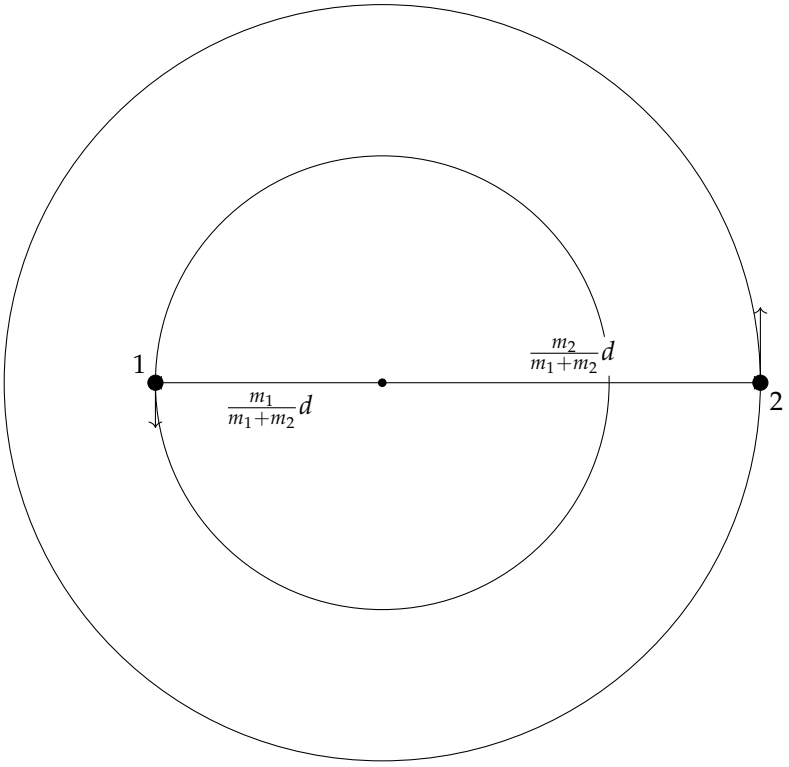

Figure 2.3: Illustration of the circular motion of two bodies. The distances are proportional to the mass of the other body to balance the center of mass.

To get the derivative, simple term by term geometric differentiation gives that

$$\frac{d}{dt}\hat{R}^{-1}\vec{b'} = \begin{pmatrix} -n\sin(nt) & -n\cos(nt) & 0 \\ n\cos(nt) & -n\sin(nt) & 0 \\ 0 & 0 & 0 \end{pmatrix} \begin{pmatrix} b_\xi \\ b_\eta \\ b_\zeta \end{pmatrix}, \tag{2.18}$$

but this can also be rewritten as

$$\hat{R}^{-1}\vec{b'} = n \begin{pmatrix} \cos(nt) & -\sin(nt) & 0 \\ \sin(nt) & \cos(nt) & 0 \\ 0 & 0 & 1 \end{pmatrix} \begin{pmatrix} -b_\xi \\ b_\eta \\ 0 \end{pmatrix}, \tag{2.19}$$

which can be represented symbolically by $n\hat{R}^{-1}\vec{b}_{p,L}$. So

$$\frac{d\hat{R}^{-1}}{\mathrm{dt}}\vec{b} = n\hat{R}^{-1}\vec{b}_{p,L}, \tag{2.20}$$

where p stands for projected (onto the ξ, η-plane) and L for rotated to the left. This means that equation (2.16) can be rewritten as

$$\vec{a} = -n^2\hat{R}^{-1}\vec{x'}_p + 2n\hat{R}^{-1}\vec{v'}_{p,L} + \hat{R}^{-1}\vec{a'} \tag{2.21a}$$

$$-n^2\vec{x'}_p + 2n\vec{v'}_{p,L} + \vec{a'} = \hat{R}\vec{x}. \tag{2.21b}$$

This means that

$$\ddot{\xi} - 2n\dot{\eta} = n^2\xi - \frac{\mu_1}{r_{13}^3}(\xi - \frac{m_2}{m_1+m_2}d) - \frac{\mu_2}{r_{23}^3}(\xi - \frac{m_1}{m_1+m_2}d) \tag{2.22a}$$

$$\ddot{\eta} + 2n\dot{\xi} = n^2\eta - \frac{\mu_1}{r_{13}^3}\eta - \frac{\mu_2}{r_{23}^3}\eta \tag{2.22b}$$

$$\ddot{\zeta} = -\frac{\mu_1}{r_{13}^3}\zeta - \frac{\mu_2}{r_{23}^3}\zeta. \tag{2.22c}$$

Note that this equation can also be written as

$$\ddot{\xi} - 2n\dot{\eta} = -U_{\xi} \tag{2.23a}$$
$$\ddot{\eta} + 2n\dot{\eta} = -U_{\eta} \tag{2.23b}$$
$$\ddot{\zeta} = -U_{\zeta}, \tag{2.23c}$$

where

$$U = -\frac{1}{2}n^2(\xi^2 + \eta^2) - \frac{\mu_1}{r_{13}} + \frac{\mu_2}{r_{23}}. \tag{2.24}$$

2.4.3 Jacobi integral

In the three-body problem, the test particle has a conserved quantity known as the Jacobi integral. This subsection will derive the Jacobi integral and demonstrate how it can be calculated. This can be used to validate numerical tests, by testing whether this quantity is indeed conserved.

Starting from the dot-product of equation (2.23) and the velocity gives

$$\vec{v'} \cdot \vec{a'} = -\vec{v'} \cdot \vec{\nabla} U, \tag{2.25}$$

which represents the derivative of

$$\frac{1}{2}v'^2 = -U - \frac{1}{2}C_J \tag{2.26a}$$
$$\implies C_J = -2U - v'^2 \tag{2.26b}$$
$$= n^2(\xi^2 + \eta^2) + 2(\frac{\mu_1}{r_{13}} + \frac{\mu_2}{r_{23}}) - (\dot{\xi}^2 + \dot{\eta}^2 + \dot{\zeta}^2). \tag{2.26c}$$

This C_J is the integration constant and is a conserved quantity for a particle in the restricted three-body problem. It can be thought of as the "energy" of this frame which is being rotated. The $n^2(\xi^2 + \eta^2) + 2(\frac{\mu_1}{r_{13}} + \frac{\mu_2}{r_{23}})$ can be thought of as the "potential term" and $-(\dot{\xi}^2 + \dot{\eta}^2 + \dot{\zeta}^2)$ the "kinetic term".

Since later on simulations are ran in the inertial reference frame it is useful to also be able to calculate the Jacobi integral in this frame. Most of the conversion is trivial: $\xi^2 + \eta^2, \mu_1/r_{13}$ and μ_2/r_{23} are all functions of the distance and can thus immediately be expressed in their x, y, z-equivalent. The kinetic-energy term $\dot{\xi}^2 + \dot{\eta}^2 + \dot{\zeta}^2$ is non-trivial, however. To find this quantity, consider that $\vec{v}' = \frac{d}{dt}\vec{r}' = \frac{d}{dt}\hat{R}\vec{r}$. By the product-rule and considering the symmetry to equation (2.20) this simplifies to

$$\vec{v}' = n\hat{R}\vec{r}_{p,R} + \hat{R}\vec{v}. \tag{2.27}$$

Taking the dot-product of $\vec{v}'$ with itself simplifies the formula to

$$\dot{\xi}^2 + \dot{\eta}^2 + \dot{\zeta}^2 = \vec{v} \cdot \vec{v} + 2n\vec{v} \cdot \vec{r}_{p,R} + n^2\vec{r}_{p,R} \cdot \vec{r}_{p,R} \quad = (\dot{x}^2 + \dot{y}^2 + \dot{z}^2) - 2n(x\dot{y} - y\dot{x}) + n^2(\xi^2 + \eta^2). \tag{2.28a}$$

This helps in the transformation of the Jacobi integral in inertial coordinates:

$$C_J = 2\left(\frac{\mu_1}{r_{13}} + \frac{\mu_2}{r_{23}}\right) + 2n\left(x\dot{y} - y\dot{x}\right) - \left(\dot{x}^2 + \dot{y}^2 + \dot{z}^2\right). \tag{2.29}$$

Thus there is a quantity known as the Jacobi integral which arises as an integration constant. This constant has a simple form in both the rotated and the inertial frame and can therefore be of great utility in analysing the 3-body problem.

2.4.4 Lagrange points

In the 3-body problem there are particular stables points. These can, for example, be observed in space by particular clumps of asteroids. This subsection identifies stationary points–where the forces cancel out–indicating potential positions where a particle remains stationary if it starts there. These points, known as "Lagrange points," are candidates for stable points.

Remark. In the following subsections a lot of algebraic manipulations will be performed. For simplification, a different system of units is used: the distance unit is chosen such that $d = 1$, and the unit of time is chosen such that $\mathcal{G}(m_1 + m_2) = 1$. Consequently, $n^2 = \frac{\mathcal{G}(m_1+m_2)}{d^3} = 1$, leading to $n = 1$.

With these new units the accelerations obtained by dividing force by mass are given by:

$$a_{g1} = -\frac{\mu_1}{r_{13}^3}\vec{r_{13}}, \tag{2.30a}$$

$$a_{g2} = -\frac{\mu_2}{r_{23}^3}\vec{r_{23}}, \tag{2.30b}$$

$$a_c = \vec{r_p}, \tag{2.30c}$$

which can be deduced by differentiating each term in the potential (2.24).

When the forces cancel out, the total gravitational accelerations equal the negative of the centrifugal acceleration, implying that these accelerations are parallel. This has two key implications. First, since $a_c \propto \vec{r_p}$, the centrifugal acceleration can not balance the ζ-axis, meaning all forces and vectors lie in the (ξ, η)-plane. Consequently, $\vec{r_p} = \vec{r}$, simplifying the equations. Additionally, because $\vec{r}$ is parallel to the centrifugal acceleration and this acceleration is parallel to the sum of the gravitational accelerations, it means that $(\vec{a_{g1}} + \vec{a_{g2}}) \times \vec{r} = 0$. Solving this, gives that $\frac{m_1}{r_{13}^3}\vec{r_1} + \frac{m_2}{r_{23}^3}\vec{r_2} = 0$, which means that two terms of $a_{g1} + a_{g2}$ together cancel to 0, leaving the last two terms to be $-(\frac{\mu_1}{r_{13}^3} + \frac{\mu_2}{r_{23}^3})\vec{r}$. Comparing the amplitudes between $a_{g1} + a_{g2}$ and a_c gives that

$$\frac{\mu_1}{r_{13}^3} + \frac{\mu_2}{r_{23}^3} = 1. \tag{2.31}$$

The solutions to this equation are then the stationary points. However, these equations are difficult to solve. To simplify these equations an additional quantity is derived: remember that $m_1\vec{r_1} = -m_2\vec{r_2}$. Multiplying this equation by $\vec{a_1} + \vec{a_2}$ gives that $m_1\vec{a_2} \times \vec{r_{13}} = -m_2\vec{a_1} \times \vec{r_{23}}$, (write $\vec{r_1} = \vec{r_{13}} + \vec{r}$ and note that $a_1 \propto \vec{r_{13}}$ and that $a_1 + a_2 \propto \vec{r}$). Since these vectors have the same directions, this means that $m_1 a_2 r_{13} = m_2 a_1 r_{23}$. This in turn means that $r_{13} = r_{23} = d$ by utilising equation (2.31). This gives two stationary points which lie on an equilateral triangle together with the other objects, these points are known as L_4 and L_5.

This approach assumes that not all points lie on the same line. Indeed, the norm of the cross product was compared but this norm is zero in the 1-dimensional case. If they do lie on the same line, all of the coordinates can be represented by ξ-coordinates which means that equation (2.31) becomes $\frac{m_1}{(\xi+\mu_2)} + \frac{m_2}{\mu_1-\xi} = m_1 + m_2$, which can be translated into the polynomial

$$(\mu_1 - \xi)^3(\mu_2 + \xi)^3 = \mu_1(\mu_1 - \xi)^3 + \mu_2(\mu_2 + \xi)^3. \tag{2.32}$$

This polynomial can be solved numerically or approximations can be made to find 3 other stationary points [Murray and Dermott, 2000, p. 77], these stationary points are known as L_1, L_2 and L_3.

To illustrate the stationary points, or Lagrange points, a plot has been made of the potential $U = \frac{1}{2}(\xi^2 + \eta^2) + \frac{\mu_1}{r_{13}} + \frac{\mu_2}{r_{23}}$ shown in figure 2.4, where the stationary points reside on the critical points of the multi-dimensional function.

The stationary points have been found by manipulating the equations relating the forces on the test particle. However, as mentioned this does not show that the particle does not stay close as it could accelerate away after a small deviation. Instead, stability has to be shown.

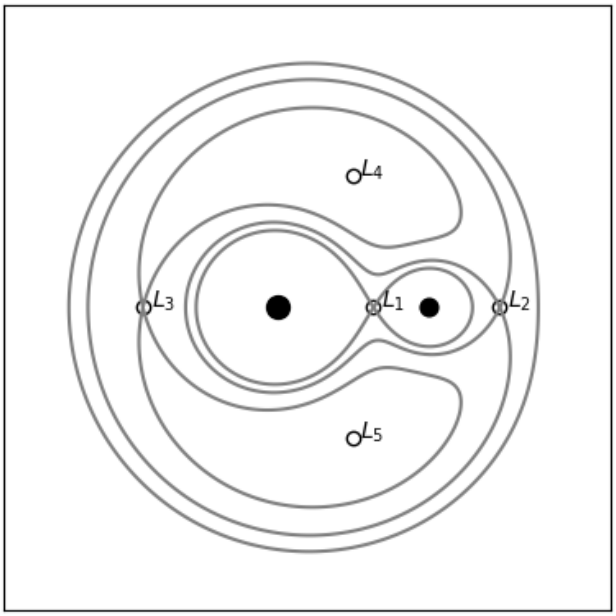

Figure 2.4: All the Lagrange points and contour lines of the potential U for $\mu_2 = 0.2$ in the ξ, η-plane.

2.4.5 Stability of Lagrange points

This subsection aims to show that particular Lagrange points are stable. To show this a general procedure is outlined and is executed for the points L_4 and L_5. From these equations of motion it can be shown that L_4 and L_5, the points corresponding to the equilateral triangle, are in fact stable.

In equation (2.23) the equation on the right-side could be written as $-\nabla U$, this equation is approximated by a second-order Taylor expansion.

$$\ddot{\xi} - 2\dot{\eta} = U_{\xi\xi}\xi + U_{\xi\eta}\eta \tag{2.33a}$$

$$\ddot{\eta} + \dot{\xi} = U_{\eta\eta}\eta + U_{\eta\xi}\xi \tag{2.33b}$$

$$\ddot{\zeta} = U_{\zeta\zeta}\zeta \tag{2.33c}$$

are then the equations describing movement close to the stationary points, where it has been used that $U_\xi = U_\eta = U_\zeta = 0$ due to the fact only stationary points are considered and $U_{\xi\zeta} = U_{\eta\zeta} = 0$ due to the symmetry in the ζ-axis at those points. It can be observed that the equations of ξ and η influence each other, while ζ evolves independently. So an analysis has can be made of ξ and η, and ζ independently.

The ζ-motion is analysed first due to it being simpler. To find the motion of ζ $U_{\zeta\zeta}$ has to be found, which is equal to $-\frac{\mu_1}{r_{13}^2} - \frac{\mu_2}{r_{23}^2}$. This quantity is always negative so the equation of motion can be rewritten as

$$\ddot{\zeta} = -k\zeta, \tag{2.34}$$

where k is some positive number. The solutions of this differential equation are well known and is in general a sum of a sine and cosine, hence the solution is stable. So it only has to be shown that the motion of ξ and η coupled together is stable as well.

To analyse the motion of ξ and η, the equations of motion shall be rewritten in the form of the linear equation

$$\frac{d}{\mathrm{d}t}\begin{pmatrix}\xi\\ \eta\\ \dot{\xi}\\ \dot{\eta}\end{pmatrix} = \begin{pmatrix}0 & 0 & 1 & 0\\ 0 & 0 & 0 & 1\\ U_{\xi\xi} & U_{\xi\eta} & 0 & -2\\ U_{\eta\xi} & U_{\eta\eta} & 2 & 0\end{pmatrix}\begin{pmatrix}\xi\\ \eta\\ \dot{\xi}\\ \dot{\eta}\end{pmatrix}. \tag{2.35}$$

The matrix helps with the analysis because stability occurs if the eigenvalues of this matrix all have non-positive real parts. So it's essential to be able to find these eigenvalues. These eigenvalues can be found by equating $\det \hat{A} - \lambda \hat{I}$ to zero, which results in

$$\lambda^4 + \lambda^2\left(4 - U_{\xi\xi} - U_{\eta\eta}\right) + U_{\xi\xi}U_{\eta\eta} - U_{\xi\eta}^2 = 0. \tag{2.36}$$

To find the solution to this equation the values of $U_{\xi\xi}, U_{\eta\eta}$ and $U\xi\eta$ have to be found explicitly. These values are

$$U_{\xi\xi} = 1 - A + B \tag{2.37a}$$
$$U_{\eta\eta} = 1 - A + C \tag{2.37b}$$
$$U_{\xi\eta} = D, \tag{2.37c}$$

where

$$A = \frac{\mu_1}{(r_{13}^3)_0} + \frac{\mu_2}{(r_{23}^3)_0} \tag{2.38a}$$
$$B = 3\left[\frac{\mu_1}{(r_{13}^5)_0}(x_0+\mu_2)^2 + \frac{\mu_2}{(r_{23}^5)_0}(x_0-\mu_1)^2\right] \tag{2.38b}$$
$$C = 3y_0^2\left[\frac{\mu_1}{(r_{13}^5)_0} + \frac{\mu_2}{(r_{23}^5)_0}\right] \tag{2.38c}$$
$$D = 3y_0\left[\frac{\mu_1}{(r_{13}^5)_0}(x_0+\mu_2) + \frac{\mu_2}{(r_{23}^5)_0}(x_0-\mu_1)\right]. \tag{2.38d}$$

This then turns equation (2.36) into

$$\lambda^4 + \lambda^2(2 + 2A - B - C) + (1 - A + B)(1 - A + C) - D^2 = 0. \tag{2.39}$$

The solutions to this equation are found by considering the fact it's a second order polynomial in λ^2 which means that the quadratic equation gives the solutions

$$\lambda_{1,2} = \pm\left[\frac{1}{2}(B + C - 2A - 2) - \frac{1}{2}\left[(B + C - 2A - 2)^2 - 4((1 - A + B)(1 - A + C) - D^2)\right]^{1/2}\right]^{1/2} \tag{2.40a}$$

$$\lambda_{3,4} = \pm\left[\frac{1}{2}(B + C - 2A - 2) + \frac{1}{2}\left[(B + C - 2A - 2)^2 - 4((1 - A + B)(1 - A + C) - D^2)\right]^{1/2}\right]^{1/2}. \tag{2.40b}$$

So if these quantities all have a non-positive real part, the system can be said to be stable. Note however that $\lambda_1 = -\lambda_2$ and $\lambda_3 = -\lambda_4$, so each negative real part is coupled by a positive real part, this means that the equations must be purely imaginary in that case.

Since L_1, L_2 and L_3's location are not known exactly the analysis is difficult, too difficult for the scope of this subsection, and shall therefore be skipped. Instead only L_4 and L_5 shall be considered.

For L_4, L_5 the position are known from the fact that $r_{13} = r_{23} = d \equiv 1$, which means that $x_0 = (\frac{1}{2} - \mu_1)$ and $y_0 = \pm\frac{1}{2}\sqrt{3}$. This means that A, B, C, D take on the values

$$A = \mu_1 + \mu_2 = 1 \tag{2.41a}$$
$$B = 3\left[\frac{1}{4}\mu_1 + \frac{1}{4}\mu_2\right] = \frac{3}{4} \tag{2.41b}$$
$$C = 3\left[\frac{3}{4}\mu_1 + \frac{3}{4}\mu_2\right] = \frac{9}{4} \tag{2.41c}$$
$$D = \pm 3\frac{\sqrt{3}}{2}\left[\frac{1}{2}\mu_1 - \frac{1}{2}\mu_2\right] = \pm\frac{3\sqrt{3}}{2}. \tag{2.41d}$$

Which then means that the solutions given by equation (2.40) are

$$\lambda_{1,2} = \pm\left[-\frac{1}{2} - \frac{1}{2}\left[27\mu_2^2 - 27\mu_2 + 1\right]^{1/2}\right]^{1/2} \tag{2.42a}$$

$$\lambda_{3,4} = \pm\left[-\frac{1}{2} + \frac{1}{2}\left[27\mu_2^2 - 27\mu_2 + 1\right]^{1/2}\right]^{1/2}, \tag{2.42b}$$

which have to be purely imaginary. For this the following two cases are considered:

1. $27\mu_2^2 - 27\mu_2 + 1 < 0$, in which case an imaginary number is added to the $-\frac{1}{2}$ term in equations (2.42). This means that the term in brackets is mixed real and imaginary, which always has a non-zero real part after taking the square root which means that either λ_1 or λ_2 has a positive real part. Therefore this case results in instable equilibrium point.
2. $27\mu_2^2 - 27\mu_2 + 1 \geq 0$, in which case a real number is added to the $-\frac{1}{2}$ term in equations (2.42), which if it is $\leq \frac{1}{2}$ will result in a term ≤ 0, and therefore purely imaginary, meaning that the point is stable. If $27\mu_2^2 - 27\mu_2 + 1 > 1$ $\left[-\frac{1}{2} + \frac{1}{2}\left[27\mu_2^2 - 27\mu_2 + 1\right]^{1/2}\right]^{1/2}$ will be positive real and the point is therefore unstable.

The function $27\mu_2^2 - 27\mu_2 + 1$ shall therefore be considered. It has the same roots as $\mu_2^2 - \mu_2 + \frac{1}{27}$, which has roots $\frac{1}{2} \pm \sqrt{\frac{1}{4} - \frac{1}{27}}$. These roots have the approximate values of 0.0385 and 0.9615. At $\mu_2 = 0$ and $\mu_2 = 1$ the function has value 1. This means that if $0 \leq \mu_2 \leq \frac{1}{2} - \sqrt{(\frac{1}{2})^2 - \frac{1}{27}} \approx 0.0385$ and the parallel case $1 \geq \mu_2 \geq \frac{1}{2} + \sqrt{(\frac{1}{2})^2 - \frac{1}{27}} \approx 0.9615$ the point will be stable.

From considering the second-order Taylor approximation for the potential it has been found that L_4 and L_5 have non-positive eigenvalues for the cases $0 \leq \mu_2 \leq \frac{1}{2} - \sqrt{(\frac{1}{2})^2 - \frac{1}{27}} \approx 0.0385$ and $1 \geq \mu_2 \geq \frac{1}{2} + \sqrt{(\frac{1}{2})^2 - \frac{1}{27}} \approx 0.9615$. This means that it can be concluded that L_4 and L_5 are stable points.

2.4.6 Different orbits

Since the eigenvalues are all imaginary for $L4$ and L_5 and come in pairs of positive and negative the general solution has the form

$$\xi = A_1\cos(\lambda_1 t) + B_2\sin(\lambda_1 t) + C_1\cos(\lambda_2 t) + D_1\sin(\lambda_2 t) \tag{2.43a}$$
$$\eta = A_2\cos(\lambda_1 t) + B_2\sin(\lambda_1 t) + C_2\cos(\lambda_2 t) + D_2\sin(\lambda_2 t). \tag{2.43b}$$

The solutions were then found for $\mu_2 = 0.01$ with eigenvalues with value of $\lambda_1 \approx 0.963$ and $\lambda_2 \approx 0.268$, with an initial deviation of 10^{-5} from $x_0 = (1 - \mu_2)$ and 10^{-5} from $y_0 = \frac{1}{2}\sqrt{3}$ and an angular velocity of $n \equiv 1$. The values were first calculated with $e^{\hat{A}t}\vec{s}$, where $\hat{A}$ is the matrix in

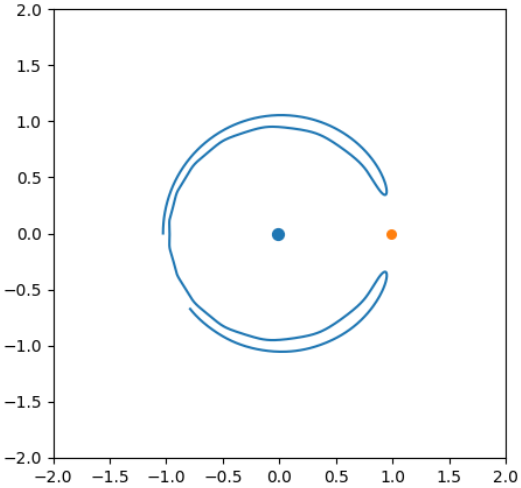

Figure 2.5: A so-called "horseshoe" orbit which was obtained by initialising a system of $\mu_2 = 0.000953875$ at $\xi = -1.02745, \eta = \dot{\xi} = 0, \dot{\eta} = 0.04032$.

equation (2.35) and $\vec{s}$ the state corresponding to the initial conditions outlined. These values were then fitted to the solutions described in equation (2.43). From this the values

$$A_1 = -2.45 \times 10^{-5}, B_1 = -8,55 \times 10^{-5}, C_1 = 3.45 \times 10^{-5}, D_1 = 3.07 \times 10^{-4} \tag{2.44a}$$

$$A_2 = -4.20 \times 10^{-5}, B_2 = 4.91 \times 10^{-5}, C_2 = 5.20 \times 10^{-5}, D_2 = -1.76 \times 10^{-4} \tag{2.44b}$$

were obtained.

Aside from the close points to L_4 it is also possible for asteroids to orbit around both $L_4, L5$ and L_1 by getting caught in orbits close to contour lines outlined in figure 2.4. These result in so-called "horseshoe" orbits (2.5) and "tadpole" (2.6) orbits.

2.5 Orbital elements

In section 2.3, the idea was introduced that planetary orbits are ellipses. Beyond the variables a and e discussed in section 2.2, which describe the shape of the ellipse, three additional variables Ω, ω and I are used to define the orientation of the orbit. Moreover, there's a final variable, ν or M_0, which specifies the position of the body in the orbit. These six variables, collectively known as "orbital elements," are particularly useful for analyzing the dynamics of the Solar System, due to their geometric nature. However, these elements are not perfectly constant, as they change over time due to the gravitational influence of other planets. This gradual evolution of orbits, driven by perturbations, will be discussed further in section 2.6, showing the importance of orbital elements in understanding both the current state and the long-term evolution of planetary orbits.

2.5.1 Definition of orbital elements

Orbital elements consist of six variables, of which a and e have already been talked about in sufficient detail and shall therefore be listed immediately:

a : The semi-major axis of the orbit.

e : The eccentricity of the orbit.

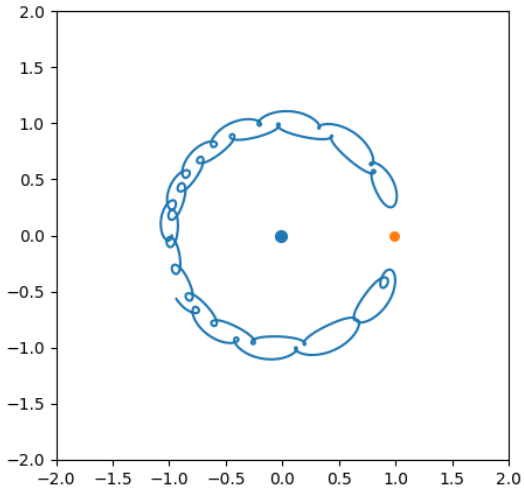

Figure 2.6: A so-called "tadpole" orbit which was obtained by initialising a system of $\mu_2 = 0.000953875$ at $\xi = -0.097668, \eta = \dot{\xi} = 0, \dot{\eta} = -0.06118$.

This ellipse is embedded in 3-dimensional space, the next three variables aim to describe this position. In figure 2.2 it can be seen that the Sun, which is one of the focuses, is always located at the origin according to the Kepler laws (2.3). So the only degree of freedom stems from the orientation (as opposed to displacement as well). To describe this orientation a procedure is described which will result in three quantities Ω, ω and I, which are three additional orbital elements. The description is similar to that of Euler angles:

- Start with an ellipse oriented along the positive x-axis, with the periapsis in this direction and the angular velocity pointing along the positive z-axis. The goal is to rotate this initial configuration into the desired orientation.
- Identify the point where the ellipse crosses the (x, y)-plane, where the orbiting body moves from a negative to a positive z-coordinate. This point is called the "ascending node."
- Rotate the ellipse until the periapsis aligns with the ascending node. The angle of this rotation, measured around the z-axis, is called the longitude of the ascending node, Ω.
- Next, rotate the ellipse around the periapsis to adjust the tilt of the orbit. The angle of this tilt, relative to the reference plane, is the inclination, I.
- Finally, rotate the ellipse within the orbital plane to align the periapsis with the desired end position. The angle of this rotation, within the plane, is the argument of periapsis, ω.

In figure 2.7 the procedure is outlined visually. This procedure is also described by executing the transformations

$$\begin{pmatrix} \cos\Omega & -\sin\Omega & 0 \\ \sin\Omega & \cos\Omega & 0 \\ 0 & 0 & 1 \end{pmatrix} \begin{pmatrix} 1 & 0 & 0 \\ 0 & \cos I & -\sin I \\ 0 & \sin I & \cos I \end{pmatrix} \begin{pmatrix} \cos\omega & -\sin\omega & 0 \\ \sin\omega & \cos\omega & 0 \\ 0 & 0 & 1 \end{pmatrix} = \hat{R}_y(\Omega)\hat{R}_x(I)\hat{R}_z(\omega) \quad (2.45)$$

on the ellipse which can be parameterised by

$$\begin{pmatrix} -ae + a\cos E \\ a\sqrt{1-e^2}\sin E \\ 0 \end{pmatrix}. \quad (2.46)$$

Note that these procedures are in reverse order (rotation by ω is first) because the axes do not move together with the ellipse, so all rotations have to applied in the "rest system". These procedures

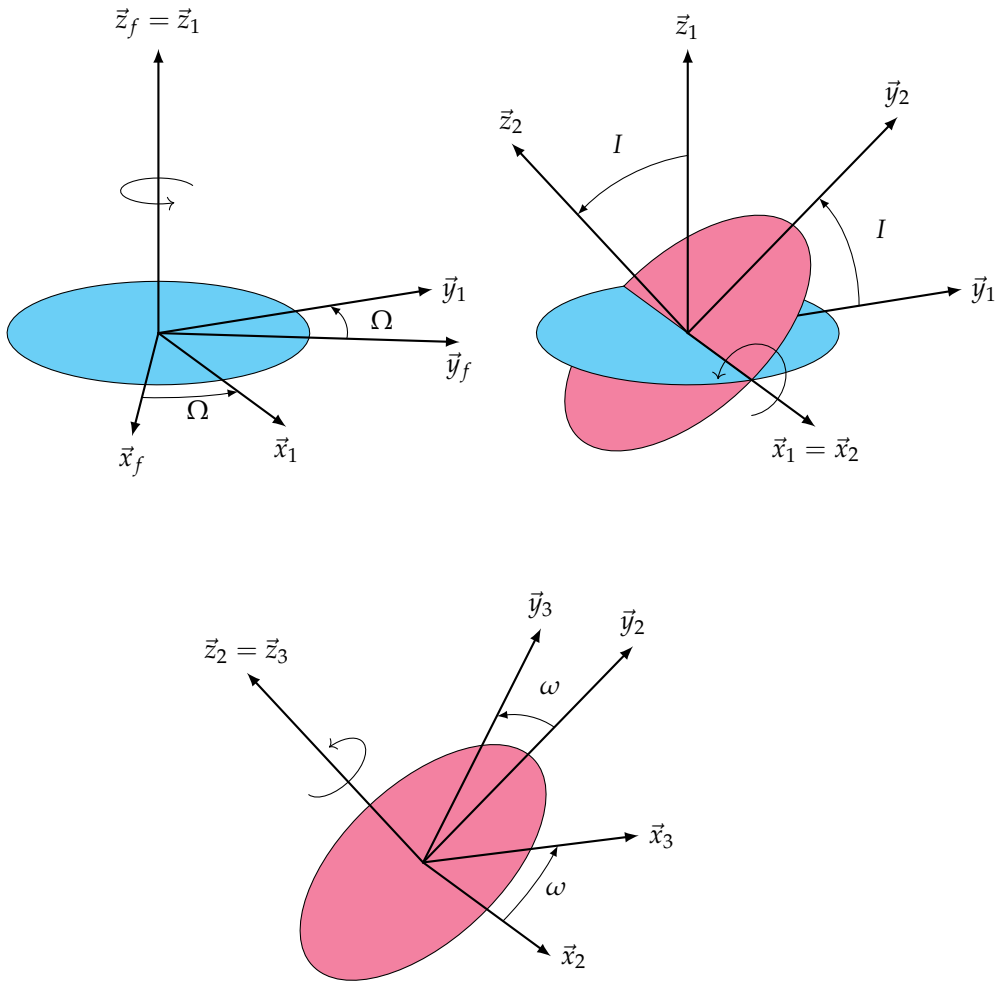

Figure 2.7: A procedure illustrating the transition between the blue orientation and the pink orientation by Euler angles. First rotating about Ω around the z-axis to be able to rotate the plane by an angle of I correctly. Finally, rotating ω around the z-axis to obtain the correct orientation within the plane.

result in a normal vector (direction of angular velocity) of the ellipse to be moved to

$$\vec{n} = \begin{pmatrix} \sin(\Omega)\sin(I) \\ -\cos(\Omega)\sin(I) \\ \cos(I) \end{pmatrix}. \tag{2.47}$$

I : The inclination, defined by the angle between plane of reference and plane of orbit.

Ω : Longitude of ascending node, the angle with which the plane has to be rotated horizontally after being inclined.

ω : Argument of periapsis, the angle between the periapsis and the reference vector of the plane.

With the first 5 orbital elements the orbit of the body is completely given. However, there is one last variable describing the position of the body on this trajectory, for this the variable ν is used, which is the angle from the perihelion to the body calculated from the Sun in the plane of the ellipse. Figure 2.8 shows how a, e, ν and ω can be expressed visually.

ν : True anomaly, angle between periapsis and object.

The true anomaly, while geometrically significant, is not particularly useful for analytical purposes due to its complex dependence on time. As noted in section 2.3, the rate at which the true anomaly changes is proportional to the area swept out by the orbiting body, which is a nonlinear function

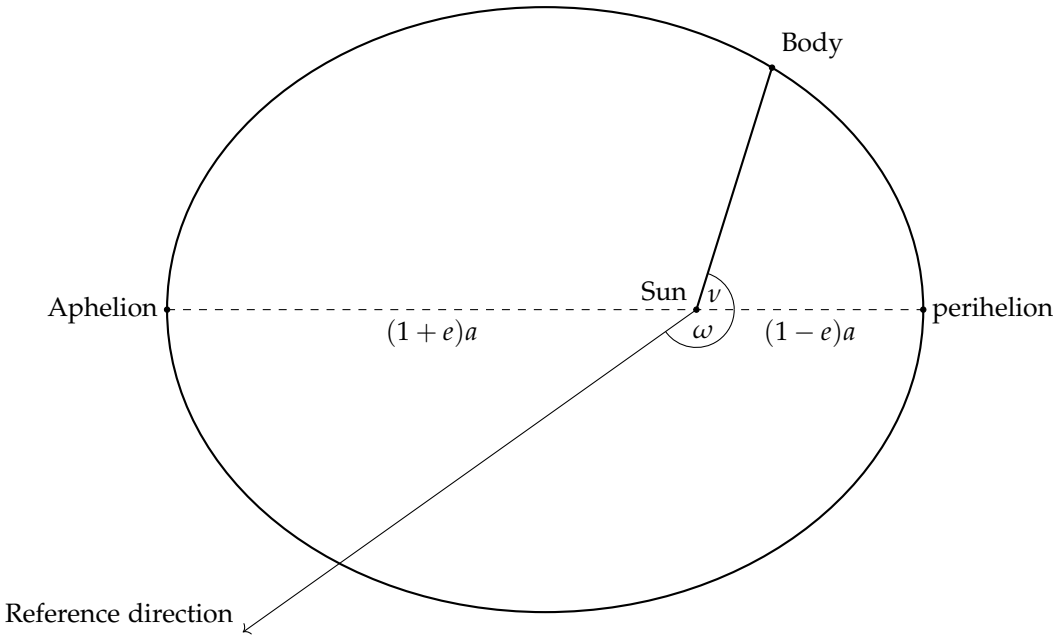

Figure 2.8: A figure showing a few notable quantities within the plane of an orbit. The reference direction refers to the direction through which the plane has been rotated. The perihelion and the Aphehlion are the closest and farthest point away from the Sun respectively and have values of $(1-e)a$ and $(1+e)a$. ω is the angle from the reference direction to the perihelion and ν is the angle from the perihelion to the body.

of time due to the elliptical shape of the orbit. To simplify the analysis, a "pseudo-angle" known as the mean anomaly, denoted by M, is typically used instead. Unlike the true anomaly, the mean anomaly varies linearly with time, increasing by 2π every orbital period. It reaches integer multiples of 2π each time the orbiting body passes through perihelion. The mean anomaly can be expressed as $M = n(t - t_0)$, where n is the average angular velocity, and t_0 is the time of perihelion passage. At the reference time $t = 0$ (epoch), the mean anomaly is denoted as M_0, which is time-independent and serves as an alternative to the true anomaly ν.

M_0 Mean anomaly at epoch, linearilised pseudo-angle between periapsis and object at a chosen reference time.

Thus this section the orbital elements $a, e, \omega, I, \Omega, \nu$ and M_0 have been described. In the literature more can be found, however, for a basic understanding of the orbital elements these are deemed sufficient.

2.5.2 Calculating orbital elements from Cartesian coordinates

As has been shown in the previous section, the orbital elements consist of six variables which tend to be intuitive due to their geometrical nature. This section shall focus on calculating these variables when a particular position $\vec{r}$ and velocity $\vec{v}$ have been given. The derivation of orbital elements from Cartesian coordinates involves using conserved quantities such as energy and angular momentum. These quantities are straightforward to compute at a specific point in the orbit using Cartesian coordinates. By expressing these conserved quantities in terms of the orbital elements and solving the corresponding equations, the relationship between Cartesian coordinates and orbital elements can be established, thereby determining the orbital parameters.

The first step is finding the position and velocity at this particular point in terms of orbital elements; the perihelion is chosen for this because of its symmetry leveraging more simplistic derivations. The expression of distance from the Sun at the perihelion in terms of orbital elements is $(1-e)a$ according to elliptical geometry, so only the expression for velocity in orbital elements has to be found.

The velocity at the perihelion is determined by examining the ratio of acceleration to velocity at this point. This ratio is related to the curvature of the ellipse, which can be derived from elliptical geometry. Since acceleration is centripetal at the perihelion, this relationship simplifies the calculation of velocity by linking it directly to the curvature of the orbit. Indeed, consider the fact that the velocity is tangent to the distance but the acceleration parallel to it, this means that the parallel distance to the perihelion can be described by $x(t) = r_0 + \frac{1}{2}\|\vec{a}\|_0 t^2 + \mathcal{O}(t^3)$ while the tangent distance is $y = v_0 t + \mathcal{O}(t^2)$. These expressions can be combined to obtain

$$x(y) = r_0 + \frac{1}{2}\frac{\|\vec{a}\|_0}{v_0^2} y^2 + \mathcal{O}(y^3), \tag{2.48}$$

where $r_0, v_0, \|\vec{a}\|_0$ are the position, velocity and acceleration respectively. Differentiating this expression gives that $\frac{d^2x}{dy^2} = \frac{\|\vec{a}\|_0}{v_0^2}$. However, this curvature can also be described by the geometry of the ellipse. Differentiating equation (2.6) twice at the right most point gives that $\frac{d^2x}{dy^2} = \frac{1}{(1-e^2)a}$. This means that the relationship between curvature and the velocity fraction is easily obtained by equation both $\frac{d^2x}{dy^2}$.

$$\frac{\|\vec{a}\|_0}{v_0^2} = \frac{1}{(1-e^2)a} \tag{2.49}$$

is this equation. Velocity is then found by substituting $\|\vec{a}\| = \frac{\mathcal{G}M_\odot}{((1-e)a)^2}$, which means that

$$v_0 = \sqrt{\frac{\mathcal{G}M_\odot}{a}\frac{1+e}{1-e}}. \tag{2.50}$$

Now these quantities of $r_0 = (1-e)a$ and $v_0 = \sqrt{\frac{\mathcal{G}M_\odot}{a}\frac{1+e}{1-e}}$ are used in finding conserved quantities and relating them to Cartesian coordinate formulas.

The first conserved quantity comes from energy divided by mass. Equation (2.7) can also be written as

$$\frac{d^2\vec{r}}{dt^2} = -\nabla U, \qquad \text{with} \qquad U = -\frac{GM_\odot}{r}. \tag{2.51}$$

This means that the conserved quantity for the energy is $\frac{1}{2}mv^2 - \frac{\mathcal{G}mM_\odot}{r}$, which can be reduced to

$$\epsilon = \frac{1}{2}v^2 - \frac{\mathcal{G}M_\odot}{r}. \tag{2.52}$$

This can be written in terms of orbital elements:

$$\epsilon = -\frac{\mathcal{G}M_\odot}{r} + \frac{1}{2}v^2 \tag{2.53a}$$

$$= -\frac{\mathcal{G}M_\odot}{(1-e)a} + \frac{1}{2}\frac{\mathcal{G}M_\odot}{a}\frac{1+e}{1-e} \tag{2.53b}$$

$$= \frac{\mathcal{G}M_\odot}{2a}. \tag{2.53c}$$

This expression only depends on the semi-major axis a which means that the semi-major axis can be derived from the Cartesian state, this is given explicitly by

$$a = \frac{\mathcal{G}M_\odot}{2\epsilon} = \frac{\mathcal{G}M_\odot}{2\left(\frac{1}{2}v^2 - \frac{\mathcal{G}M_\odot}{r}\right)}. \tag{2.54}$$

The second conserved quantity which shall be considered stems from angular momentum divided by mass, also known as the reduced angular momentum h. This quantity is calculated by $h = \vec{r} \times \vec{v}$.

Since position and velocity were perpendicular, the expression can be simply found to be $\vec{h} = r_0 v_0 \vec{n}$, where $\vec{n}$ is the normal of the plane.

$$\vec{h} = \vec{r} \times \vec{v} \tag{2.55a}$$
$$= r_0 v_0 \vec{n} \tag{2.55b}$$
$$= (1-e)a\sqrt{\frac{\mathcal{G}\mathrm{M}_\odot}{a}\frac{1+e}{1-e}}\vec{n} \tag{2.55c}$$
$$= \sqrt{\mathcal{G}\mathrm{M}_\odot(1-e^2)a}\,\vec{n} \tag{2.55d}$$

is then this reduced angular momentum expressed in terms of orbital elements. By comparing this equation of $\vec{n}$ with the one given by equation (2.47) its relation to orbital elements can be found. From this relation I and Ω can be found with inverse trigonometric functions:

$$I = \cos^{-1}\left(\frac{\vec{h}\cdot\hat{z}}{h}\right), \tag{2.56}$$

$$\Omega = \mathrm{atan2}(h_y, h_x). \tag{2.57}$$

The eccentricity e can be found using this equation as well, however, these is a simpler way of doing so using the next conserved quantity.

The final equation is a more unfamiliar conserved quantity as it's specific to the case of Kepler orbits (or more generally, inverse quadratic forces). This conserved quantity is the "Laplace-Runge-Lenz vector" and is a vector which points from the focus to the periapsis with length e. This gives a clear relationship to this conserved quantity and the eccentricity. This quantity is defined by

$$\frac{\vec{v}\times\vec{h}}{\mathcal{G}\mathrm{M}_\odot} - \frac{\vec{r}}{r}. \tag{2.58}$$

In this equation $\vec{h} = \vec{r}\times\vec{r}$ is the reduced angular momentum as mentioned before. Before this supposedly conserved quantity is used, it is first proven that it is indeed a conserved quantity by showing that the time-derivative is equal to 0. Consider just the time derivative of only $\frac{\vec{v}\times\vec{h}}{\mathcal{G}\mathrm{M}_\odot}$:

$$\frac{d}{dt}\frac{\vec{v}\times\vec{h}}{\mathcal{G}\mathrm{M}_\odot} = \frac{\vec{a}\times\vec{h}}{\mathcal{G}\mathrm{M}_\odot} \tag{2.59a}$$
$$= \frac{-\frac{\mathcal{G}\mathrm{M}_\odot}{r^3}\vec{r}\times\vec{h}}{\mathcal{G}\mathrm{M}_\odot} \tag{2.59b}$$
$$= -\frac{\vec{r}\times\vec{h}}{r^3} \tag{2.59c}$$
$$= -\frac{(\vec{r}\cdot\vec{v})\vec{r} - r^2\vec{v}}{r^3} \tag{2.59d}$$
$$= \frac{d}{dt}\frac{\vec{r}}{r} \tag{2.59e}$$

So with the $\frac{\vec{r}}{r}$ subtracted the time-derivative will be 0 and therefore will be a conserved quantity. It can then be shown that this vector points towards the perihelion and that it has magnitude of e by computing this vector for the special case of the perihelion:

$$\vec{e} = \frac{\vec{v_0}\times\vec{h}}{\mathcal{G}\mathrm{M}_\odot} - \frac{\vec{r_0}}{r_0}, \tag{2.60a}$$
$$= \frac{v_0^2\vec{r_0}}{\mathcal{G}\mathrm{M}_\odot} - \frac{\vec{r_0}}{r_0}, \tag{2.60b}$$
$$= \frac{(1+e)\vec{r_0}}{r_0} - \frac{\vec{r_0}}{r_0}, \tag{2.60c}$$
$$= e\frac{\vec{r_0}}{r_0}. \tag{2.60d}$$

Which is indeed a vector of length e pointing towards $\vec{r}_0$, or in other words, the perihelion. The simpler way of calculating the eccentricity e, as mentioned before, is then

$$e = |\vec{e}| \tag{2.61}$$

And furthermore a way to obtain ω. Let $\vec{\Omega} = \begin{pmatrix} \cos\Omega \\ \sin\Omega \\ 0 \end{pmatrix}$, then:

$$\omega = \text{atan2}(\vec{\Omega} \cdot (\vec{e} \times \vec{n}), \vec{\Omega} \cdot \vec{e}) \tag{2.62}$$

Where $\vec{n}$ is once again given as in equation (2.47).

In this section the conserved quantities of energy and angular momentum (both divided by mass) were expressed in terms of orbital elements by considering the special point of the perihelion. The energy was completely a function of the semi-major axis a and the angular momentum pointed in the normal vector which allowed for the determination of the longitude of ascending node Ω and inclindation I. Additionally, a new conserved quantity quantity known as the "Laplace-Runge-Lenz vector" was introduced which gave information about the eccentricity e and the location of the perihelion from which the argument of periapsis ω could be found.

2.6 Perturbations of the planets' motion

This section explores how the elliptical orbits of a planet are perturbed by the gravitational influence of other planets. The aim is to derive equations that describe the changes in orbital elements due to these perturbations, which is essential for understanding the dynamics of multiple-planet systems.

The one-body problem is finding the solution to the differential equation (2.7 and equation (2.51):

$$\ddot{\vec{r}} = -\frac{\mathcal{G}M_\odot}{r^3}\vec{r} = -\nabla U. \tag{2.63}$$

The one-body problem describes a single body orbiting a central mass. However, to account for the gravitational perturbations from other bodies, the N-body problem (2.3) has to be considered, where the equation can be rewritten as:

$$\frac{d^2\vec{r}}{dt^2} = -\nabla(U + \mathcal{R}), \qquad \text{with} \qquad \mathcal{R} = -\sum_j \frac{Gm_j}{r_j}, \tag{2.64}$$

where m_j is any mass other than the Sun and r_j the distance to that mass.

The change in orbital elements can then be found by the Lagrange planetary equations

$$\frac{da}{dt} = -\frac{2}{na}\frac{\partial\mathcal{R}}{\partial M_0}, \tag{2.65a}$$

$$\frac{de}{dt} = \frac{b}{na^3e}\frac{\partial\mathcal{R}}{\partial\omega} - \frac{b^2}{na^4e}\frac{\partial\mathcal{R}}{\partial M_0}, \tag{2.65b}$$

$$\frac{dM_0}{dt} = \frac{2}{na}\frac{\partial\mathcal{R}}{\partial a} + \frac{b^2}{na^4e}\frac{\partial\mathcal{R}}{\partial e}, \tag{2.65c}$$

$$\frac{d\omega}{dt} = \frac{\cos I}{nab\sin I}\frac{\partial\mathcal{R}}{\partial I} - \frac{b}{na^3e}\frac{\partial\mathcal{R}}{\partial e}, \tag{2.65d}$$

$$\frac{dI}{dt} = \frac{1}{nab\sin I}\frac{\partial\mathcal{R}}{\partial\Omega} - \frac{\cos I}{nab\sin I}\frac{\partial\mathcal{R}}{\partial\omega}, \tag{2.65e}$$

$$\frac{d\Omega}{dt} = -\frac{1}{nab\sin I}\frac{\partial\mathcal{R}}{\partial I}, \tag{2.65f}$$

where we refer to [Fitzpatrick, 2023] for a derivation. In these equations n is used which has been briefly mentioned for the average angular velocity. This quantity simplifies the equations but can

also be rewritten as $n^2a^3 = \mathcal{G}M_\odot$, according to the third Kepler law [Murray and Dermott, 2000, p. 3]. As $\mathcal{R}$ is typically small, the resulting changes are also minor. To illustrate this, consider two planets each with a mass of 10^{27}kg, orbiting in circular, co-planar paths with semi-major axes of 5AU and 10AU, analogous to Jupiter and Saturn. At their closest approach, the perturbation $\mathcal{R}$ for each planet would be:

$$\mathcal{R} = -\frac{G \cdot 10^{27}\,\mathrm{kg}}{5\,\mathrm{AU}} = -8.9 \times 10^4\,\mathrm{J/kg}. \tag{2.66}$$

For the innermost planet with a semi-major axis $a = 5\,\mathrm{AU}$, the mean motion n is approximately:

$$n \approx 1.7 \times 10^{-8}\,\mathrm{s}^{-1}. \tag{2.67}$$

Thus, the rate of change of the semi-major axis $\frac{da}{dt}$ can be estimated as:

$$\left|\frac{da}{dt}\right| \approx \frac{2}{na} \cdot \frac{|\mathcal{R}|}{\frac{1}{2}T} = \frac{2|\mathcal{R}|}{\pi a} = 5.7 \times 10^4\,\mathrm{m/s} = 3.8 \times 10^{-7}\,\mathrm{AU/s}. \tag{2.68}$$

This variation is small relative to the size of their orbits. Nonetheless, over extended periods, such small perturbations can accumulate, as discussed in section 2.7.

2.7 Orbital resonance

This section applies the Lagrange planetary equations to the gravitational interactions between two co-planar bodies, with a significantly lighter inner body compared to the outer body. The heavier body is positioned along the positive x-axis, and both bodies orbit in a counter-clockwise direction. These initial conditions are illustrated in figure 2.9. By analyzing the gravitational potential over multiple periods and averaging it, the phenomenon of "orbital resonance" emerges. This resonance effect plays a crucial role in the long-term evolution of planetary systems, including the Solar System.

For co-planar orbits, the Lagrange planetary equations simplify by eliminating Ω and I, and substituting ω with ϖ. The equations describing the change of orbital elements are then

$$\frac{da}{dt} = -\frac{2}{na}\frac{\partial \mathcal{R}}{\partial M_0}, \tag{2.69a}$$

$$\frac{de}{dt} = \frac{\sqrt{1-e^2}}{na^2e}\frac{\partial \mathcal{R}}{\partial \varpi} - \frac{1-e^2}{na^2e}\frac{\partial \mathcal{R}}{\partial M_0}, \tag{2.69b}$$

$$\frac{dM_0}{dt} = \frac{2}{na}\frac{\partial \mathcal{R}}{\partial a} + \frac{1-e^2}{na^2e}\frac{\partial \mathcal{R}}{\partial e}, \tag{2.69c}$$

$$\frac{d\varpi}{dt} = -\frac{\sqrt{1-e^2}}{na^2e}\frac{\partial \mathcal{R}}{\partial e}. \tag{2.69d}$$

Because of the difficulty of solving these equations an approximation shall be made: instead of considering $\mathcal{R}$, the average value $\langle \mathcal{R} \rangle$ shall be considered. This average value for one (outer) period can approximately be found by considering figure 2.10, where it can be seen that there's some base level with the contribution of a peak added. From this the approximation

$$\langle \mathcal{R} \rangle = \text{base level} + \alpha(\text{peak} - \text{base level}) \tag{2.70}$$

This peak is found by considering the point at which the two planets are closest, as this point has the highest value. At the closest approach, $\mathcal{R}$ for the inner planet is $\mathcal{R} = -\frac{\mathcal{G}m}{r}$, where m is the mass of the outer planet. Here, r is the distance between the two bodies, computed as the difference between their distances from the central body. The distance of the outer orbit to the center is simply its radius R, the inner orbit is a more complicated expression, however. The distance from the inner orbit to the center is $af(\phi, e)$, where a is the semi-major axis and f is some function in terms of the mean anomaly ϕ and the eccentricity e. A figure of this function f has been made for $e = 0.3$ in

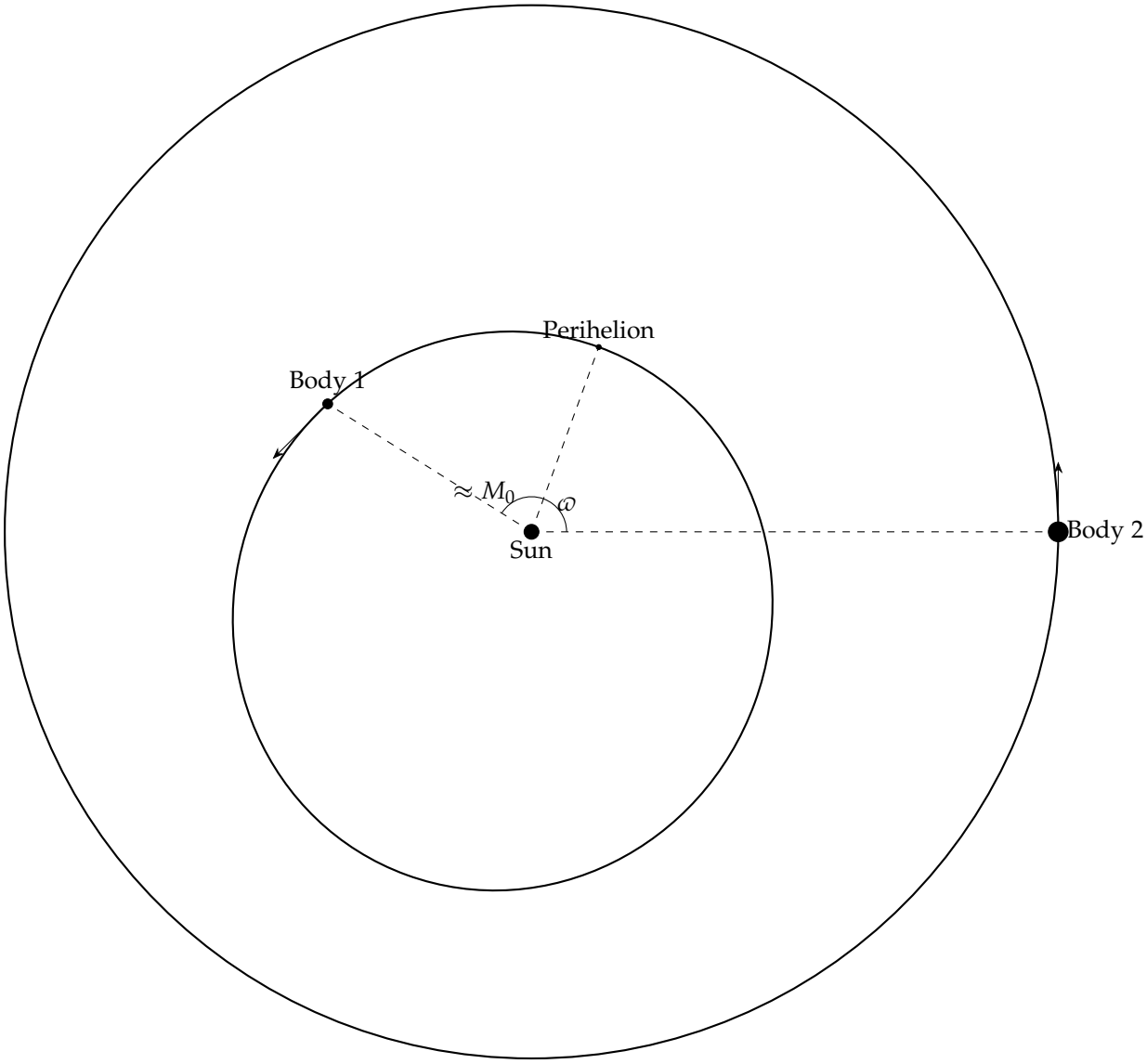

Figure 2.9: A figure showing the initial conditions of a small inner body in a Kepler orbit and a large outer body in a circular orbit.

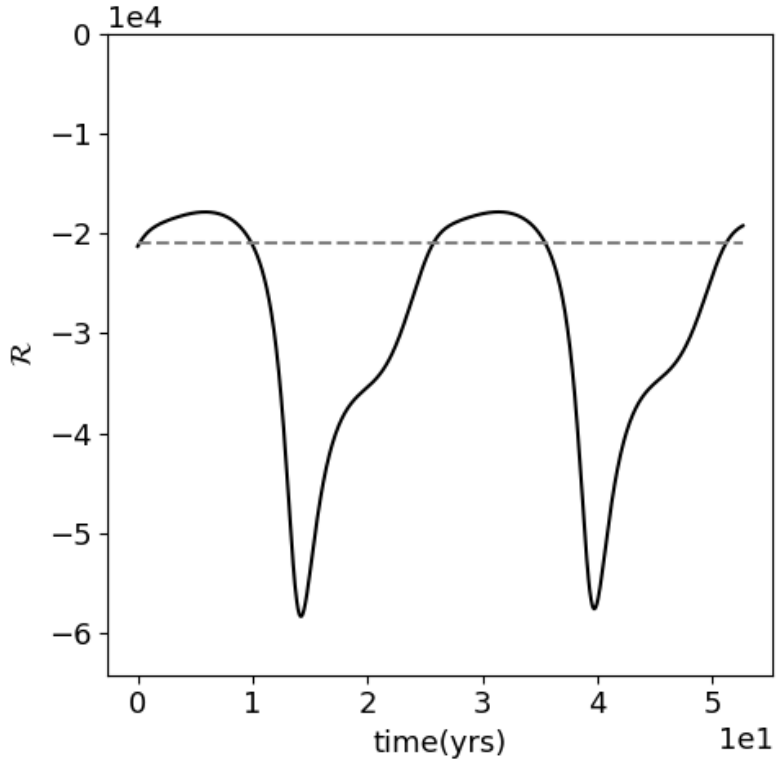

Figure 2.10: The disturbing potential $\mathcal{R}$. Notice that there's some base-level shown by the grey dotted line and peaks.

figure 2.11. The base level is found by $-\frac{\mathcal{G}m}{R+a}$, which is the scale when the planets are approximately opposite to each other. From this the full approximation of $\langle\mathcal{R}\rangle$ is

$$\langle\mathcal{R}\rangle \approx -(1-\alpha)\frac{\mathcal{G}m}{R+a} - \alpha\frac{\mathcal{G}m}{R-af(\phi,e)}, \tag{2.71}$$

where α is some constant associated with the consideration of only the closest point. Typically, the pseudo-angle ϕ at which the planets align varies over time, so $\langle\mathcal{R}\rangle$ must be averaged over ϕ and depends on a and e. However, if the orbital periods are commensurate (i.e., their ratio is a fraction of integers), ϕ remains constant. This effect is known as orbital resonance. To illustrate this, consider the 2:1 resonance, which means that the inner planet has a period 2 times that of the outer planet. Consider that the planets are in conjunction at a pseudo-angle (pseudo-angles will be used to make the mathematics easier) of ϕ. The next time these planets will meet is when $\phi + 2nt = \phi + nt + k \cdot 2\pi$, which is when $nt = k \cdot 2\pi$, or when plugged into $\phi + 2nt$ and $\phi + nt$, the same angle. The angle ϕ can be calculated from the orbital elements as follows. If the inner planet starts with a mean anomaly M_0 and a longitude of periapsis ϖ, and the outer planet starts at an angle θ_0, the evolution of the pseudo-angles can be described as $M_0 + \varpi + 2nt$ for the inner planet and $\theta_0 + nt$ for the outer planet. Equating these gives the pseudo-angle at which they meet as

$$\phi = 2\theta_0 - 2\varpi - M_0. \tag{2.72}$$

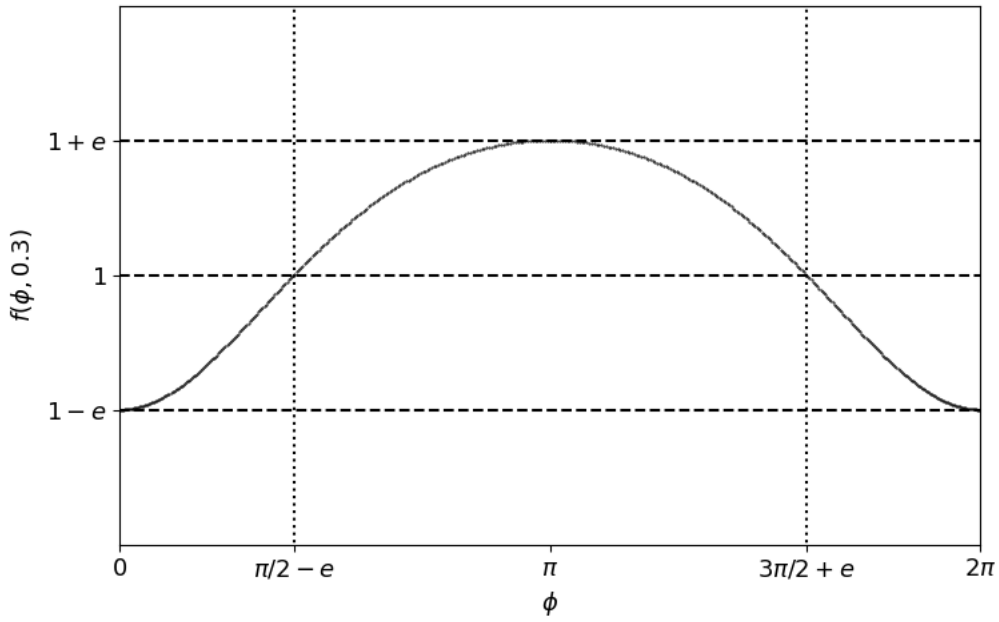

Figure 2.11: The oscillation function for $e = 0.3$. This function describes the distance divided by the semi-major axis from the focal point closest to the periapsis to a point that makes a pseudo-angle ϕ relative to the periapsis.

With the significance of ϕ the Lagrange orbital equations are

$$\frac{\partial\langle\mathcal{R}\rangle}{\partial a} = (1-\alpha)\frac{\mathcal{G}m}{(R+a)^2} - \alpha\frac{\mathcal{G}m}{(R-af(\phi,e))^2}f(\phi,e), \tag{2.73a}$$

$$\frac{\partial\langle\mathcal{R}\rangle}{\partial e} = -a\alpha\frac{\mathcal{G}m}{(R-af(\phi,e))^2}\frac{\partial f}{\partial e}(\phi,e), \tag{2.73b}$$

$$\frac{\partial\langle\mathcal{R}\rangle}{\partial \varpi} = -a\alpha\frac{\mathcal{G}m}{(R-af(\phi,e))^2}\frac{\partial f}{\partial \phi}(\phi,e)\frac{\partial \phi}{\partial \varpi} = 2a\alpha\frac{\mathcal{G}m}{(R-af(\phi,e))^2}\frac{\partial f}{\partial \phi}(\phi,e), \tag{2.73c}$$

$$\frac{\partial\langle\mathcal{R}\rangle}{\partial M_0} = -a\alpha\frac{\mathcal{G}m}{(R-af(\phi,e))^2}\frac{\partial f}{\partial \phi}(\phi,e)\frac{\partial \phi}{\partial M_0} = a\alpha\frac{\mathcal{G}m}{(R-af(\phi,e))^2}\frac{\partial f}{\partial \phi}(\phi,e). \tag{2.73d}$$

$$\tag{2.73e}$$

To understand these equations, it is crucial to analyze the function f. The function f reaches its extreme values at perihelion and aphelion, corresponding to $\phi = 0 + k \cdot 2\pi$ (value $1 - e$) and $\phi = \pi + k \cdot 2\pi$ (value $1 + e$), respectively. The zeros of f occur at $\pi/2 - e + k \cdot 2\pi$ and $3\pi/2 + e + k \cdot 2\pi$. These zeros correspond to the eccentric anomaly $E = k \cdot \pi$ and the mean anomaly $M = E - e\sin E$. Further details regarding the relationship between eccentric and mean anomaly are provided through [Wikipedia, 2024b]. The observations of the zeros and the extreme values can be seen in figure 2.11. The extreme values and zeros are important because f's sign is determined by the zeros and $\frac{\partial f}{\partial \phi}$'s sign is determined by the extreme values. With this knowledge the sign of $\frac{da}{dt}$, $\frac{de}{dt}$, $\frac{d\varpi}{dt}$ and $\frac{dM_0}{dt}$ can be found. Generally, this angle slowly oscillates in resonance, causing all the relevant orbital elements, but most significantly e and a, to oscillate. This oscillation of e and a is most important for the context of orbital evolution.

2.8 Nice model

One of the most popular descriptions of the evolution of planetary orbits of the giants in the Solar system is known as the Nice model. The Nice model states that the giant planets began their evolution near their current resonances and operates through two main mechanisms:

1. Orbital Resonances: The planets' orbits have semi-major axes in specific resonant relationships.
2. Interactions with Planetoids: The planets interact with a population of planetoids.

The concept of orbital resonance has been discussed in (2.7) but the most important aspects shall be repeated, whereas the disk of planetoids shall not be discussed in detail as they shall be ignored during the simulations. According to the original Nice model [Tsiganis et al., 2005], the giant planets were positioned as follows:

1. Jupiter: 5.45 AU
2. Saturn: 8.65 AU
3. Neptune: 11–13 AU
4. Uranus: 13.5–17 AU

Here Uranus and Neptune are additionally separated by at least 2 AU. Additionally, the planets have an eccentricity e and inclination $i \sim 10^{-3}$. These semi-major axes make it so that the planets are placed in low integer resonances close to 2:1 and 3:2. specifically, $T_J : T_S \approx 2 : 1, T_S : T_N \approx 3 : 2$ and $T_N : T_U$, where T_J, T_S, T_N and T_U are the periods of Jupiter, Saturn, Neptune and Uranus respectively. These relationships result in the fact that they meet each other in the same point, causing them to strongly influence each other resulting in oscillations in e and a, allowing the planets to move closer to each other.

Additionally, the planets interact with planetoids, which have a total mass ranging from 30 to 50 times the mass of Earth (M_E). These planetoids are distributed from Neptune's orbit out to 30–35 AU, with their density falling off linearly within this range. These interactions primarily dampen the planets' eccentricities e and inclinations i, mitigating extreme variations and preventing excessive resonant effects. This is an important feature because during resonance, these values can vary quite drastically, but now these effects are dampened. Furthermore, and maybe more significantly, it allows for a mechanism to escape from "locking" as shall be described in the results chapter (4).

It is important to note that all orbits start as near-circular orbits, which implies that the argument proposed in section 2.7 seems to not apply, as the the oscillation function f would remain near constant. However, note that the denominator of $\frac{de}{\mathrm{dt}}$ contains a e term in equation (2.69), which means that the decrease of the f in the nominator is compensated for by the e term in the denominator.

Figure 2.12 illustrates the typical evolution of the Solar System under the Nice model. This plot, known as an $a/q/Q$ plot, depicts the semi-major axis a, the minimum heliocentric distance q, and the maximum heliocentric distance Q. Here q and Q are expressed as $(1-e)a$ and $(1+e)a$, respectively. These plots are used to show the range of heliocentric distance the planets can occupy and also provide a way to visualise the a and e parameter in one figure.

The original Nice model simulations revealed that Neptune and Uranus frequently switched positions, as shown in figure 2.12. This switching occurred after Jupiter and Saturn entered a 1:2 mean motion resonance, which perturbed their orbits and significantly impacted the eccentricities of Neptune and Uranus. After this, Neptune and Uranus have a series of encounters due to their orbits decreasing their relative distance. This series of encounters causes both planets to undergo drastic changes in semi-major axis a and eccentricity e, as can be observed from figure 2.12 and results in effects such as the swapping of positions and expansion into larger semi-major axis orbits.

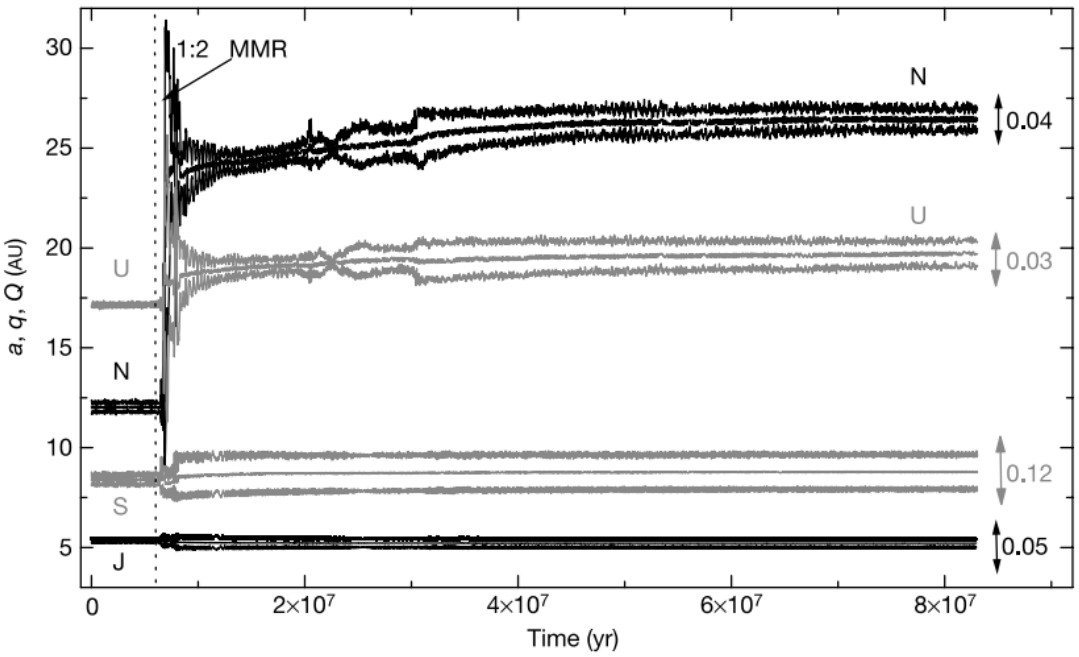

Figure 2.12: Evolution of the Solar System as depicted in the Nice model [Tsiganis et al., 2005]. This $a/q/Q$ plot displays the semi-major axis a (where $q = a(1-e)$), the perihelion distance q, and the Aphelion distance Q (where $Q = a(1+e)$). The plot illustrates how the semi-major axis and eccentricity of the planets evolve over time, providing insights into the dynamic changes and resonant interactions within the Solar System.

3 Numerical method

3.1 Mechanics

As mentioned in the N-body problem section 2.1, the algebraic solutions known to the n-body problem are of limited use so numerical solutions are instead utilised to solve the differential equations (2.3). This paper uses Leapfrog integration for numerical integration, suitable because acceleration depends only on position, not velocity. Before the numerical integration method is described, it is important to understand how each particle is described in the simulation; a particle i is initialised with a mass m_i (which stays constant throughout the run), a 3D-Cartesian position $\vec{r}_i = (x_i, y_i, z_i)$ and its corresponding velocity $\vec{v}_i$ in 3D-Cartesian coordinates, as well. These are then updated each time-step according to the Leapfrog integration, which is described by

$$\vec{r}_{i,n+1} = \vec{r}_{i,n} + \vec{v}_{i,n}\mathrm{d}t + \frac{1}{2}\vec{a}_{i,n}\mathrm{d}t^2 \tag{3.1a}$$

$$\vec{v}_{i,n+1} = \vec{v}_{i,n} + \frac{1}{2}(\vec{a}_{i,n} + \vec{a}_{i,n+1})\mathrm{d}t. \tag{3.1b}$$

In these equations $\vec{r_{i,n}}$ is the position vector of particle i at time-step n, $\vec{v_{i,n}}$ the velocity vector, $\vec{a_{i,n}}$ the acceleration vector and dt the size of the time-step. The time after n iterations would then be $t = n \cdot \mathrm{d}t$. At each iteration, $a_{i,n+1}$ is calculated using equation (2.3), which is computationally intensive due to its non-linear nature. For this reason, array multiplications in Numpy (Python) were used to save time over alternatives such as for-loops. To outline the computations executed, equation (2.3) shall be rewritten with their indices and quantities shall be defined to make particular steps simpler. First equation (2.3) can be rewritten by denoting a subscript for each vector component:

$$a_{i\chi} = \sum_{j \neq i} G m_j \frac{r_{j\chi} - r_{i\chi}}{|r_{j\chi} - r_{i\chi}|^3}, \tag{3.2}$$

where χ is this new index. To simplify this expression two related quantities shall be defined:

$$R_{ij\chi} \equiv r_{j\chi} - r_{i\chi} \tag{3.3}$$

and

$$T_{ij} \equiv \left(R_{ij0}^2 + R_{ij1}^2 + R_{ij2}^2\right)^{-3/2}, \tag{3.4}$$

where T_{ij} is ill-defined for $i = j$ as it would equal to the undefined $0^{-3/2}$. For this reason the definition is modified to

$$T_{ij} \equiv \left(R_{ij0}^2 + R_{ij1}^2 + R_{ij2}^2 + D\right)^{-3/2}, \tag{3.5}$$

where D_{ij} is a quantity defined by

$$D_{ij} = \begin{cases} \infty & i = j \\ 0 & \text{else.} \end{cases} \tag{3.6}$$

In the implementation, ∞ from the Python math library is used, which functionally represents a number that satisfies the following properties:

$$\infty + c = \infty, c \in \mathbb{R} \tag{3.7a}$$

$$\infty^{-3/2} = 0. \tag{3.7b}$$

Effectively, this has the same effect as the case of not computing $i = j$, however, due to limitations in software and knowledge the speed increase of arrays could not be combined with disallowing it to compute the entire operation. In conclusion, the acceleration is then computed by

$$a_{i\chi} = \sum_j G m_j R_{ij\chi} T_{ij}. \tag{3.8}$$

To outline how the algorithm functions, some pseudocode has been written:

$m \leftarrow m_{\text{initial}}$
$r \leftarrow r_{\text{initial}}$
$v \leftarrow v_{\text{initial}}$
gravity_interaction_constant$[i, j] \leftarrow G \cdot m$[:, newaxis]
$D \leftarrow \infty \cdot \text{diag}(\text{length}(m))$
procedure A(r)
    $R \leftarrow r[\text{newaxis}, :, :] - r[:, \text{newaxis}, :]$
    $T \leftarrow \left((r[i, j, 0]^2 + r[i, j, 1]^2 + r[i, j, 2]^2)\right)^{-3/2}$
    return $\sum_j$ gravity_interaction_constant$[i, j] R[i, j, \xi] T[i, j]^3$
end procedure
$a \leftarrow A(r)$
while Do_Iteration = True **do**
    $r \leftarrow r + v\text{dt} + \frac{1}{2} a \text{dt}^2$
    $a' \leftarrow A(r)$
    $v \leftarrow \frac{1}{2}(a + a')\text{dt}$
    $a \leftarrow a'$
end while

In following sections this program shall be used with varying initial conditions, initially to test accuracy and later to verify and find results. This algorithm shall, however, be slightly altered when the mechanics of interactions with the asteroid cloud are added.

3.2 Initialisation

To initialise leapfrog, the initial position and velocity need to be given. For every simulation it is outlined in detail how this is initialised.

Generally, the Sun (called the Sun because it has the mass of the Sun) will always have the position and velocity values such that $\sum m_i \vec{r}_i = \vec{0}$ and $\sum m_i \vec{v}_i = \vec{0}$, where i refers to all the other bodies, this is done to set the center of mass stationary at the origin. The Sun shall therefore be omitted from the specific initial conditions.

Asteroid in L_4
Parameters: δx, δy, $\delta \dot{x}$, and $\delta \dot{y}$ define deviations in position and velocity from the L_4 point in the rotating frame.
Constant values: distance between the outer body and the Sun $d = 5\text{AU}$ and the mass-ratio $\mu_2 = 0.01$.
First, the angular velocity was calculated by $n = \sqrt{\frac{\mathcal{G}\text{M}_\odot}{d^3(1-\mu_2)}}$. After this, the outer body was placed with position $\vec{r}_2 = ((1-\mu_2) \cdot d, 0, 0)$ and velocity $(0, (1-\mu_2)d \cdot n, 0)$. The test-particle was then positioned at $\vec{r}_3 = ((\frac{1}{2} - mu_2)d + \delta x, \frac{1}{2}\sqrt{3}d + \delta y, 0)$. The angle θ_3 and distance r_3 of this point were then calculated, after which the velocity was calculated by $\vec{v}_3 = (\cos\theta_3 nr + \delta \dot{x}, \sin\theta_3 nr + \delta \dot{y}, 0)$.

Test particle in 2:1 resonance
Parameters: a_0, e_0 and ϖ_0, describing the orbit of the test-particle.
Constant values: distance between the outer body and the Sun $d = 5\text{AU}$ and the mass-ratio $\mu_2 = 0.001$.
Two bodies were initialised. The outer body was placed similarly to last initial conditions at position $\vec{r}_2 = ((1-\mu_2) \cdot d, 0, 0)$ and velocity $(0, (1-\mu_2)d \cdot n, 0)$ with $n = \sqrt{\frac{\mathcal{G}\text{M}_\odot}{d^3(1-\mu_2)}}$. The particle

was then initialised at the positive x-axis. The parameter $\varpi_0 \in \{0, \pi\}$ gives two different initial conditions. If $\varpi_0 = 0$, the initial position is at perihelion, $\vec{r}_3 = ((1 - e_0)a_0, 0, 0)$, with velocity $\vec{v}_3 = (0, \sqrt{\frac{\mathcal{G}M_\odot}{a_0}\frac{1+e_0}{1-e_0}})$. For $\varpi_0 = \pi$, the position is $\vec{r}_3 = ((1 + e_0)a_0, 0, 0)$ and velocity is $\vec{v}_3 = (0, \sqrt{\frac{\mathcal{G}M_\odot}{a_0}\frac{1-e_0}{1+e_0}})$. Similarly, if $\varpi_0 = \pi$ the position would be $\vec{r}_3 = ((1 + e_0)a_0, 0, 0)$ and the velocity $\vec{v}_3 = (0, \sqrt{\frac{\mathcal{G}M_\odot}{a_0}\frac{1-e_0}{1+e_0}})$.

Two planets in 2:1 resonance
Parameters: a_0, e_0 and ϖ_0, describing the orbit of the test-particle.
Constant values: distance between the outer body and the Sun $d = 8.65$AU and the mass of Jupiter and Saturn for the inner and outer body respectively.
These are the same initial conditions as the previous simulation except for the fact that the test-particle had Jupiter's mass and the outer particle Saturn's. Furthermore, the distance to the outer object was set to be $d = 8.65$AU and a_0 was scaled appropriately.

Nice model
Parameters: In this simulation four planets were initialised with masses of Jupiter, Saturn, Uranus and Neptune, from inner to outer planet (note that this is different from the Nice paper as they initialised Uranus as the outer planet). These planets were initialised with a random e, ω, Ω and I, of which e and I were chosen from a uniform distribution between -10^{-3} and 10^{-3}, while ω and Ω were chosen from a uniform distribution between $-\pi$ and π. The semi-major axis of Uranus and Neptune were picked randomly from $11 - 13$AU and $13.5 - 17$AU with the initial condition that they are at least 2AU apart.
Constant values: Jupiter's and Saturn's semi-major axis with values of 5.45AU and 8.65AU respectively.
The initial values were calculated from these orbital elements by initialising the planet at position $\vec{r}_i = ((1 - e_i)a_i, 0, 0)$ and velocity $\vec{v}_i = (0, \sqrt{\frac{\mathcal{G}M_\odot}{a_i}\frac{1+e_i}{1-e_i}})$, which was afterwards rotated by $\hat{R}_z(\Omega)\hat{R}_x(I)\hat{R}_z(\omega)$.

3.3 Adaptive time-steps

The time-step dt was initially too large for accurate close-encounter calculations, but reducing dt significantly increased computation time. Therefore, instead of a constant dt, a variable dt was opted for. The basic principle for choosing the dt at a particular moment is that $\|\vec{a}\|\,\mathrm{dt} \ll \|\vec{v}\|$, so instead of a dt parameter, a parameter k was chosen such that dt could be found by a particular procedure: to find dt the minimum of $\{k \cdot \|\vec{v}\|_i \,/\, \|\vec{a}\|_i\}$ was considered, where v_i is the speed of body i and a_i the acceleration. This presents an issue, however. To use leapfrog correctly, the dt has to be consistent throughout the entire time-step. But, during the time-step the accelerational influences are calculated which are used to calculate the dt. So knowledge of the time-step has to be used before the time-step. To address this, an initial dt is selected based on the previous iteration and then adjusted if it proves insufficient during the attempted time-step. If the time-step necessary for the time-step is less than $0.9\times$ the used dt, the time-step is tried again but with this new value for dt. This process is iterated multiple times until an appropriate dt is found.

4 Results

In this chapter the results of various simulations are presented building up to simulating the Nice model (without the influence of a disk of planetoids). Various orbital resonances are considered, starting with 1:1 resonance of L_4 with a test particle and then proceeding to a 2:1 resonance with a test particle, after which the test particle is replaced by a particle with mass. These simulations give insight into the general principles of resonance and helps with finding suitable time-scales for the simulation of the Nice model. After this, the Nice model is considered without asteroids. From this several phenomena van be observed such as resonance, close-encounters, ejections and orbit-catching.

4.1 The 1:1 resonance, L_4

First, motions about L_4 are considered. This is done because L_4 is an example of a 1:1 resonance, the strongest resonance. Furthermore, L_4's (and that of L_5) analytical description is the most extensive, see section 2.4, which allows for a simpler analysis.

In the following tests two bodies were set in circular motions around each other with a distance of $d = 5\text{AU}$ and a mass ratio of $\mu_2 = 0.01$. This circular motion was initialised by placing the two bodies on the x-axis with corresponding speeds as described in equation (2.15).

First a test was ran to observe the deviation from the center point, since a test-particle should be stationary at L_4. For this the x-values of the test particle were transformed by $\Delta x/d = (x - (1 - \mu_2)d)/d$ and the y-values by $\Delta y/d = (y - (\frac{1}{2}\sqrt{3})d/d)$. Using these quantities the "absolute relative deviation" was then calculated by $\sqrt{\Delta y/d^2 + \Delta x/d^2}$. The results are shown for time-steps 10^4s in figure 4.1 and 10^5s in figure 4.2.

From these figures an oscillatory motion can be observed in figure 4.3 and figure 4.4. In these oscillations the maximum deviation is most important as that is an indicator of the precision of distance of the simulation. For this reason, the maximum deviation was plotted over time in figure 4.5. A least squares fit was made to a straight line of this figure was made, from which the relation $\log \frac{\delta r}{d} \approx 2.00 \log \mathrm{dt} - 36.38$ was found with a variance of 2.62×10^{-7} and 3.66×10^{-5} for the variables respectively. The scaling of the error is therefore quadratic, which agrees with the fact that Leapfrog is a second order integrator.

After these tests the analytical solution of a slight deviation $\Delta x/d = \Delta y/d = 10^{-5}$ was tested against the theoretical result of equation (2.44). The parameters were found to be sufficiently similar to the theoretical value, however, the phase of the solution and the simulation differed significantly. This phase difference differed with $-0.002\text{yr}/900\text{yr}$ with significant changes to dt (10^3s and 10^5s). This offset is illustrated in figure 4.6 and figure 4.7. Therefore, the phase difference is explained as an artifact of the theoretical approximation of Taylor series and the experimental value from 10^5s is considered sufficient to model the motion of planets close to L_4. The change of $-0.002\text{yr}/900\text{yr}$ is not deemed significant and therefore the

The phase off-set also means that the analytical solution is limited in testing the accuracy of the simulation as making the analytical solution more accurate would decrease the distance, but this would make the error from the simulation more significant. The key insights are that the error changes asymptotically quadratically and the scale of error is approximately 10^{-5} of the distance for time-steps of 10^5s.

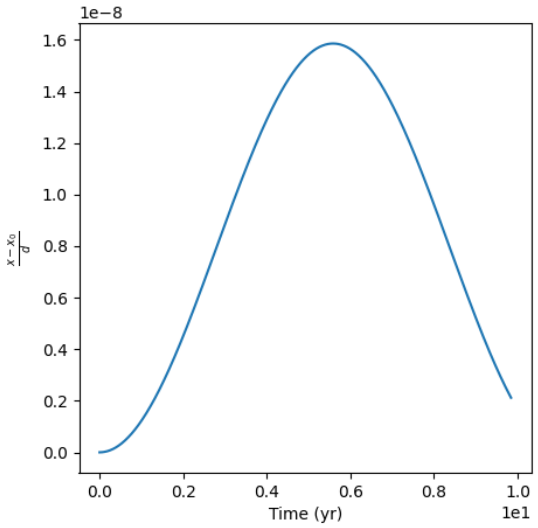

Figure 4.1: A plot of the relative distance from L_4, that is, the distance divided by the distance between the two large masses d. This simulation was ran with time-steps of 10^4 seconds.

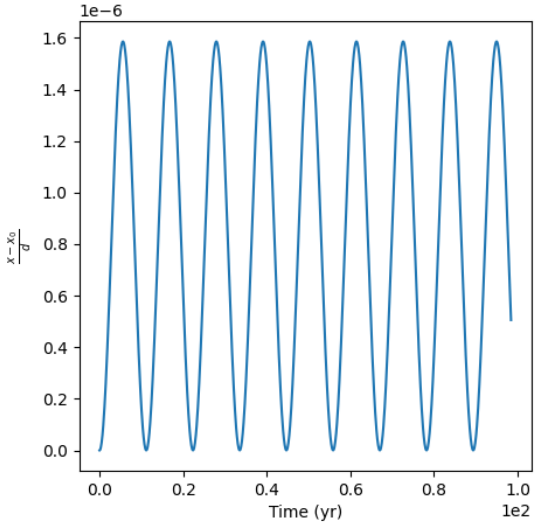

Figure 4.2: A similar plot to that of 4.1 but with time-steps of 10^5 seconds.

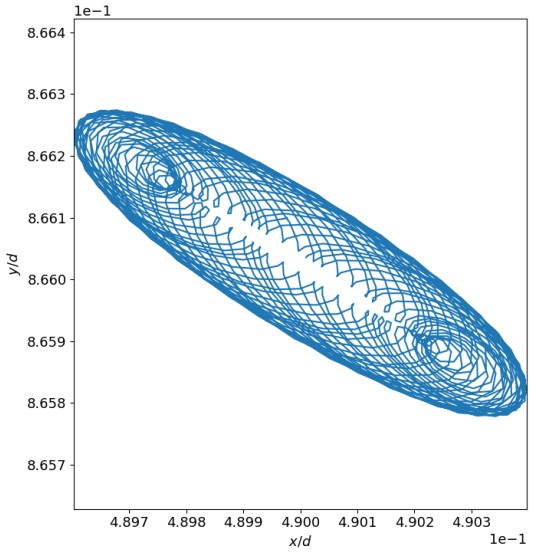

Figure 4.3: The path of an object starting close to L_4. It can be seen that it oscillates about this point. Additionally, this shape seems similar to that of a cycloid.

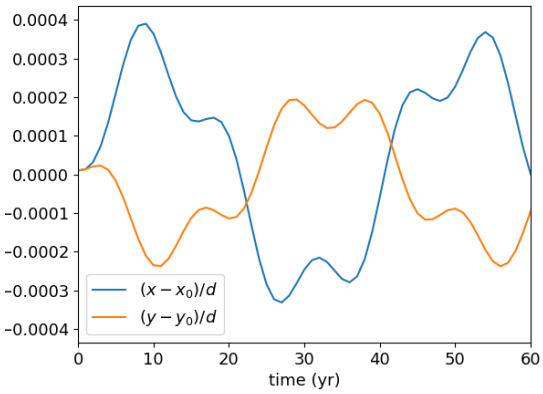

Figure 4.4: The x and y values divided by the separation between the Sun and the planet.

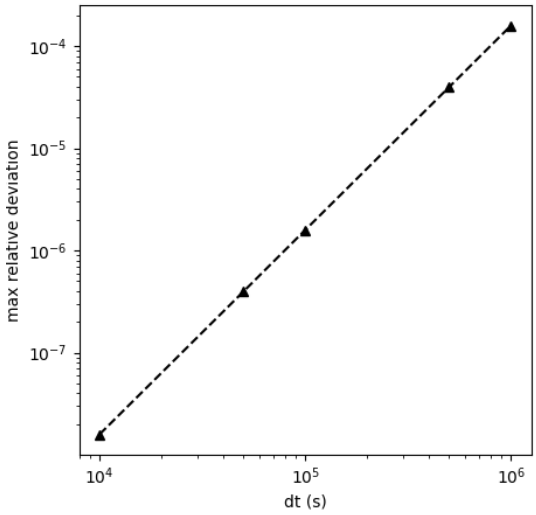

Figure 4.5: The maximum relative deviation against the time-steps of the simulation. A linear relation can be observed between $\log \mathrm{dt} = \log \frac{\Delta x}{d}$. It follows from the slope of 2 decades per decade that the error is quadratic in dt.

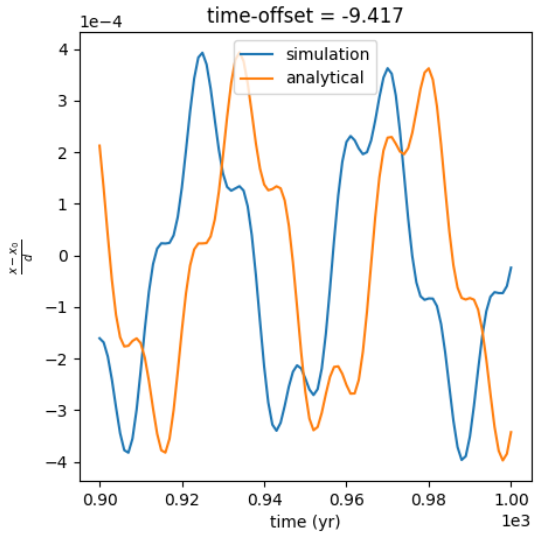

Figure 4.6: The numerical solution and the analytical solution near L_4 with starting conditions $x - x_0/d = y - y_0/d = 10^-5$ after 900yr. After this time the numerical solutions seems to lag behind the analytical solution with about 9.419yr

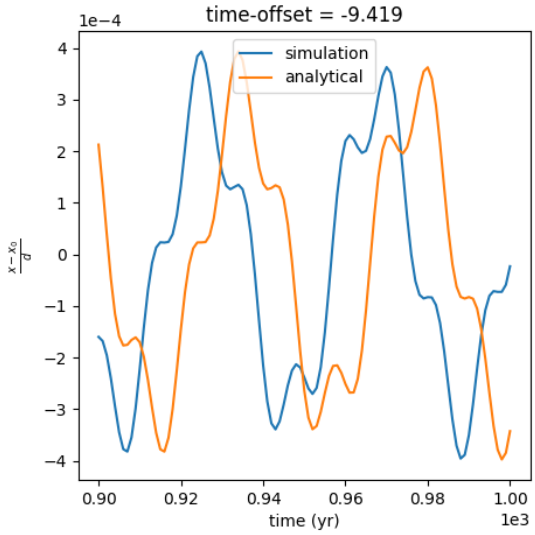

Figure 4.7: Similar test to 4.6 where the numerical and analytical solution of motion near L_4 with starting conditions $x - x_0/d = y - y_0/d = 10^{-5}$ are compared after 900yr.

Plot	a_0	e_0	ϖ_0
a	0.625277	0.128386	0
b	0.633424	0.0725011	0
c	0.637837	0.0122862	0
d	0.636705	0.060146	π
e	0.638222	0.0184545	π
f	0.610592	0.1975	0

Table 4.1: Initial conditions for the various tests which will be ran in this section, taken from [Murray and Dermott, 2000].

4.2 2:1 Resonance with test-particle

Now a more complex resonance is considered: the 2:1 resonance. The consideration of this resonance is important because such a resonance is forced between Jupiter and Saturn in the Nice model. First, a test-particle is considered in this section, as this allows to isolate certain effects of resonance and a sufficient time-scale can be observed by comparing the results with those out of the literature.

Taken from [Murray and Dermott, 2000] the following orbital elements were chosen as initial conditions for a variety of tests. These orbital elements were calculated as if the Sun was located at the origin (which coincides with center of mass). These values were chosen to research the 2:1 resonance. This particle was initialised with these orbital elements at the x-axis with a positive z-component of the angular velocity. The Sun and an outer object such that $\mu_2 = 0.001$ and $d = 5$AU were initialised at the x-axis with a positive z-component of the angular velocity, as well. The outer body was initialised at the positive x-axis, whereas the Sun at the negative x-axis. These two bodies were initialised such that they would orbit around each other with a $d = 5$AU and with the CM at the origin, so as described in 2.4.2.

From these tests plots were created of the orbital elements a, e and ϖ. Additionally, an angle describing an orbital resonance parameter (named the resonance angle in section 2.7) was plotted as well with the value $\varphi_1 = 2\nu_2 - \nu_1 - 2\varpi_1$, where the index 1 refers to the test particle and the index 2 to the massive body. The quantity φ_1 is important because it illustrates the angle from the periapsis at which the two objects have a close encounter. This can be confirmed by considering an arbitrary point at which the test-particle resides at angle $\nu_1 + \varpi_1$ and the outer body at angle ν_2 (there is no ϖ_2 term because the light body has a circular orbit, so the periapsis

is ill-defined, instead it is assumed to be 0 where it was initialised). The two bodies then meet at angle $\nu_1 + \varpi_1 + 2nt = \nu_2 + nt \implies nt = \nu_2 - \nu_1 - \varpi_1$, so the angle at which they meet has value $\nu_2 + (\nu_2 - \nu_1 - \varpi_1) = 2\nu_1 - \nu_2 - \varpi_2$. The angle from the periapsis is then minus ϖ_2, giving

$$\text{angle of close encounter from periapsis} = \varphi_1 = 2\nu_2 - \nu_1 - 2\varpi_1. \tag{4.1}$$

These plots have been made for time-steps of dt $= 10^5$s and dt $= 10^6$s shown in figures (4.8 and 4.9) respectively. Comparing the plots with results obtained in [Murray and Dermott, 2000], it can be seen that the dt $= 10^5$s closely resembles the plots obtained in that book, whereas dt $= 10^6$s strongly deviates for (e) and (f). The initial conditions of the test-particle deviated significantly between (e) and (f), yet the path of (f) in the 10^6s simulation resembles that of what (e)'s path is according to the 10^5s and the citation. This shows how sensitive resonances can be and the importance of choosing appropriate time-steps.

Additionally, the orbital elements seem to change in periodic ways. For all the plots the semi-major axis a and the eccentricity e seem to deviate around a particular value. (a), (b) and (c) can be categorised by the behaviour of φ_1 which deviates around 0 but never completes a full rotation, this is known as libration and it's a indicator for resonance. Furthermore, in the (a), (b) and (c) plots the semi-major axis a deviates around its resonance ratio of $2^{2/3}$. (d) has the bodies pass each other opposite of the periapsis as can be seen from φ_1. The resonance ratio can be found by considering a_2/a_1 in the third Kepler law, equation (2.8), given that $T_2/T_1 = 1/2$.

Furthermore, for the plots (a)-(d) in figure 4.8 it can be observed that the motion is in a specific kind of resonance because the resonant angle ϕ librates but does not circulate. Whereas in (e) and (f) in figure 4.8 they do circulate. From this it is concluded that these are different types of resonance, for (a)-(d) there is a particular "force" keeping the resonant-angle to a particular value, but for (e) and (f) this force is not strong enough.

In conclusion, it was observed that resonances are highly sensitive to errors by comparing computations with time-steps 10^5s and 10^6s. From this it was also found that 10^5s is a sufficient time-step for resonance at a distance of approximately 3AU. Furthermore, it was observed that planet's semi-major axis a and eccentricity e oscillate when in resonance and that the type of resonance can be observed from a quantity $\varphi_1 = 2\nu_2 - \nu_1 - \varpi_1$.

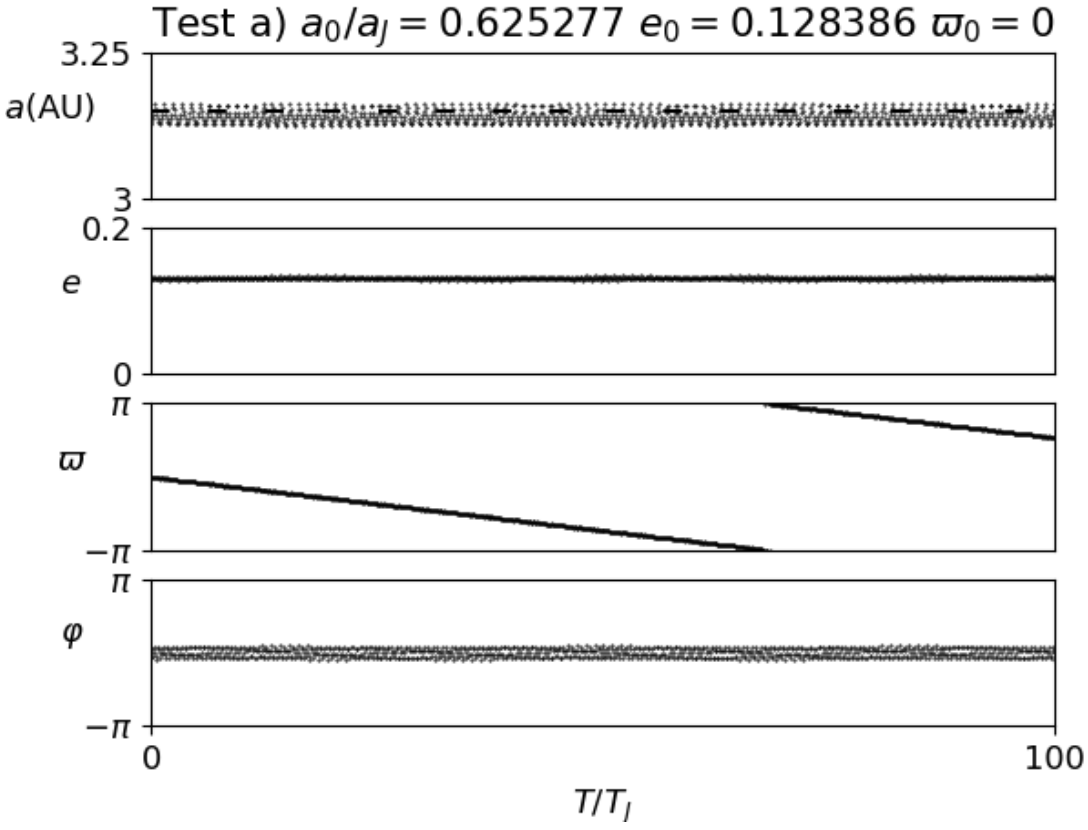
Test a) $a_0/a_J = 0.625277$ $e_0 = 0.128386$ $\varpi_0 = 0$
3.25
a(AU)
3
0.2
e
0
π
ϖ
$-\pi$
π
φ
$-\pi$
0
100
T/T_J

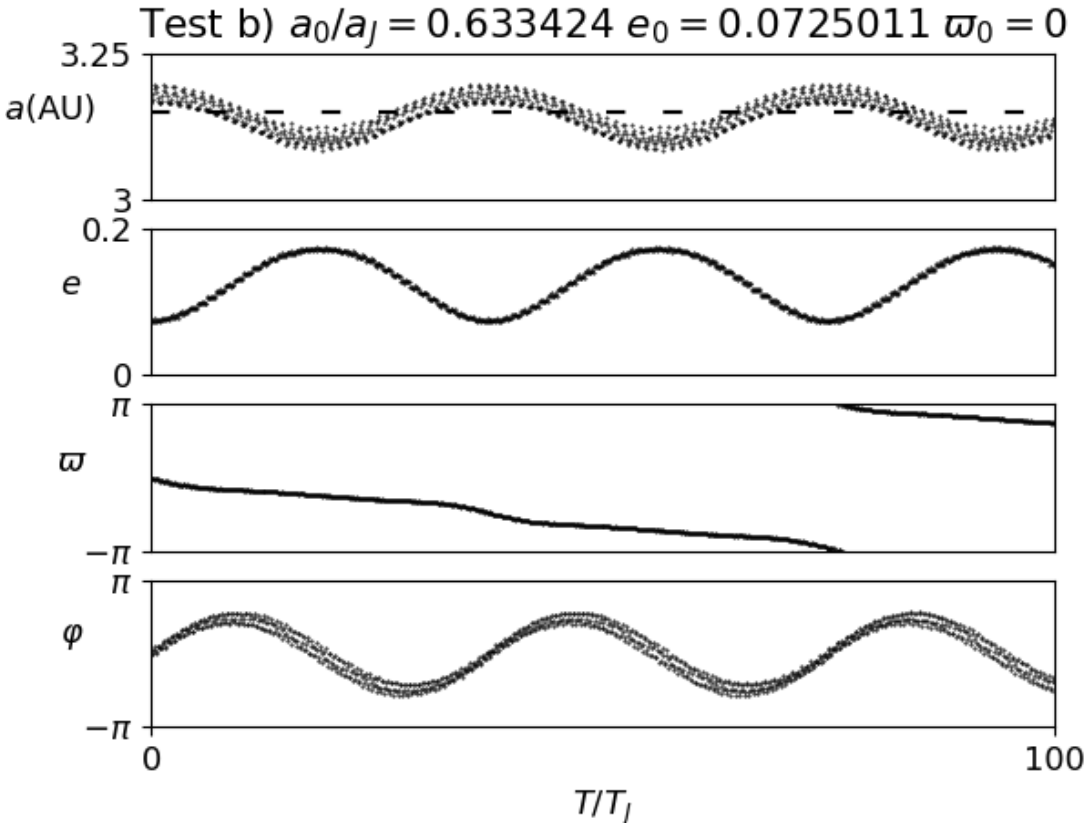
Test b) $a_0/a_J = 0.633424$ $e_0 = 0.0725011$ $\varpi_0 = 0$
3.25
a(AU)
3
0.2
e
0
π
ϖ
$-\pi$
π
φ
$-\pi$
0
100
T/T_J

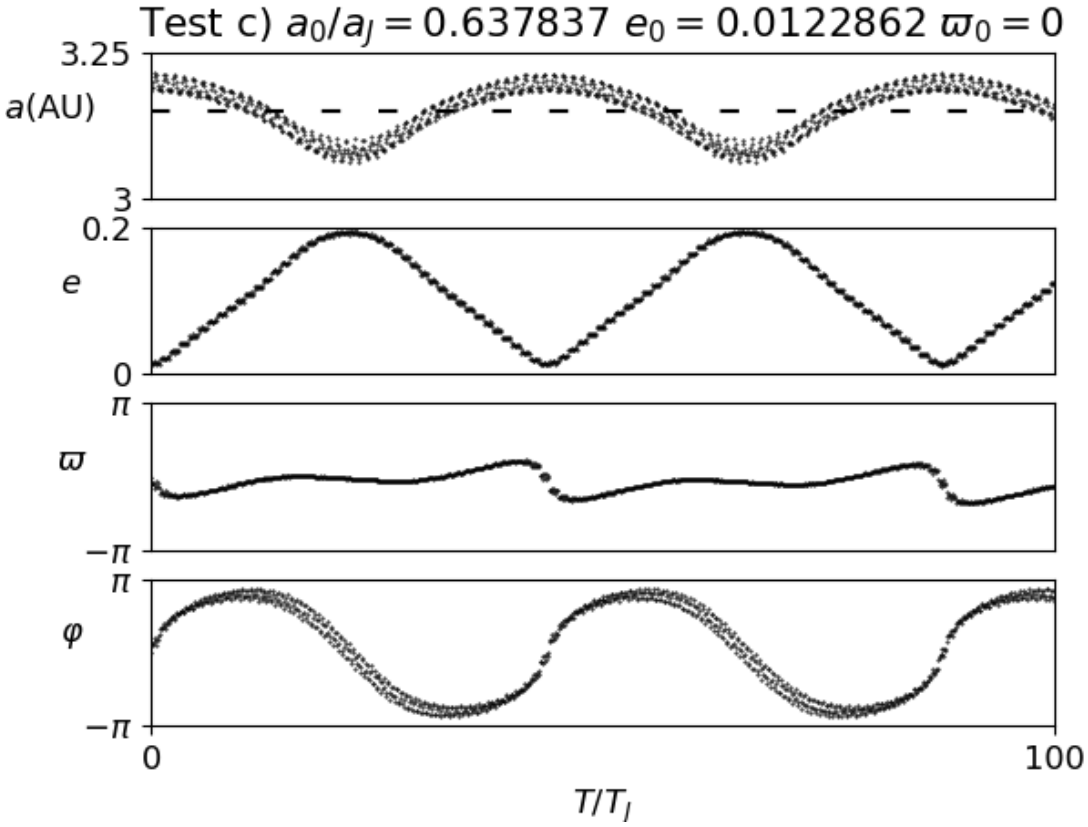
Test c) $a_0/a_J = 0.637837$ $e_0 = 0.0122862$ $\varpi_0 = 0$
3.25
a(AU)
3
0.2
e
0
π
ϖ
−π
π
φ
−π
0
100
T/T_J

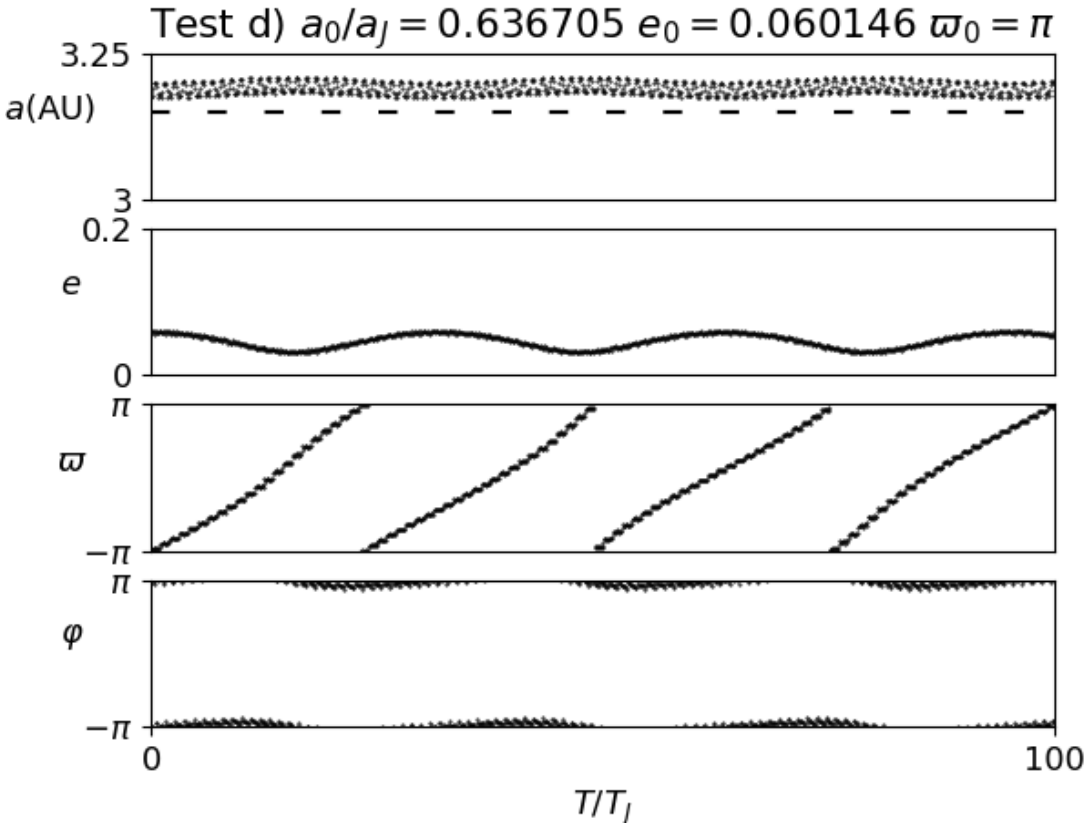
Test d) $a_0/a_J = 0.636705$ $e_0 = 0.060146$ $\varpi_0 = \pi$
3.25
a(AU)
3
0.2
e
0
π
ϖ
−π
π
φ
−π
0
100
T/T_J

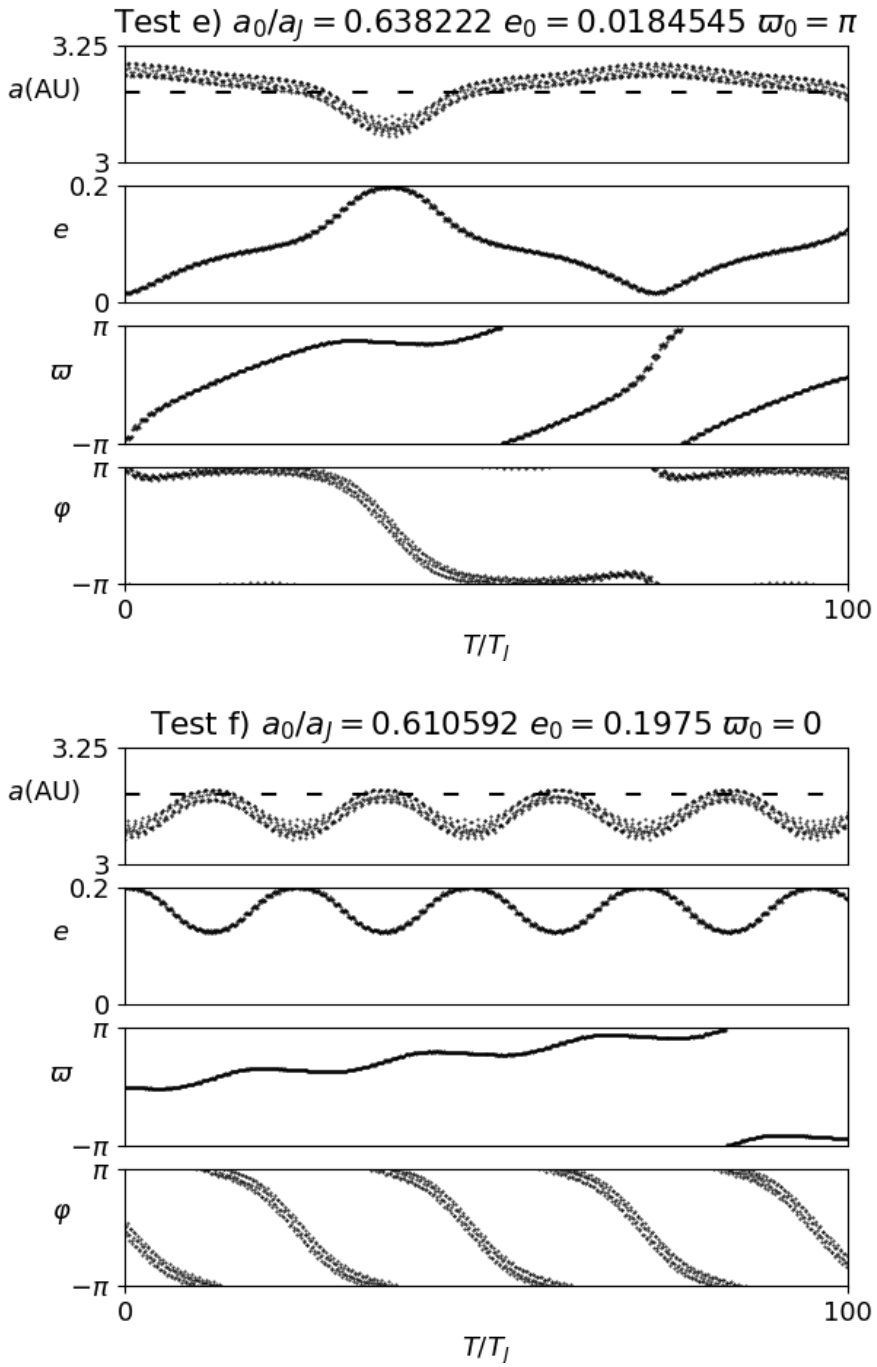

Figure 4.8: These figures show the variance of orbital elements of different 2:1 resonances over a time-scale of 100 circulations of an outer body with $\mu_2 = 0.001$. In each plot a is the semi-major axis (on a scale from 3AU to 3.25AU), e represents the eccentricity (on a scale from 0 to 0.2), ϖ longitude of periapsis (on a scale from $-\pi$ to π rad) and φ a quantity defined by $2\nu_2 - \nu_1 - 2\varpi$ (on a scale from $-\pi$ to π rad). The initial values are given in table 4.1. All of these figures were created with time-steps of 10^5s.

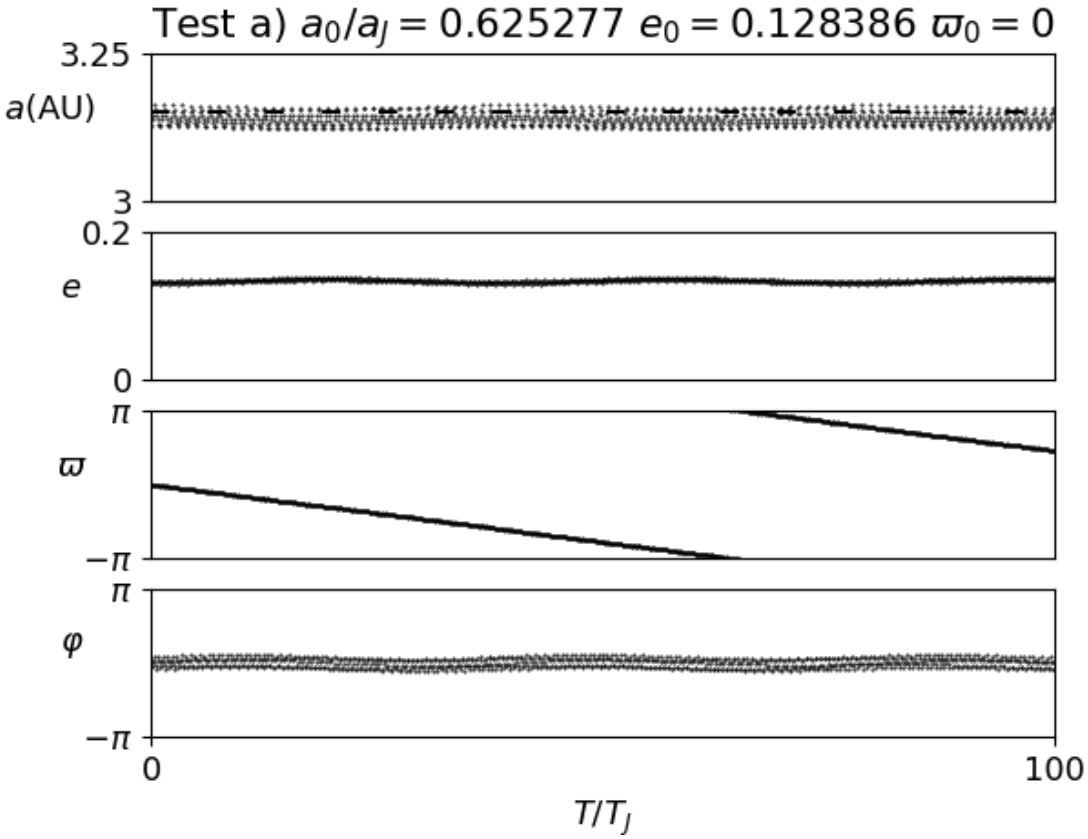
Test a) $a_0/a_J = 0.625277$ $e_0 = 0.128386$ $\varpi_0 = 0$
3.25
a(AU)
3
0.2
e
0
π
ϖ
$-\pi$
π
φ
$-\pi$
0
100
T/T_J

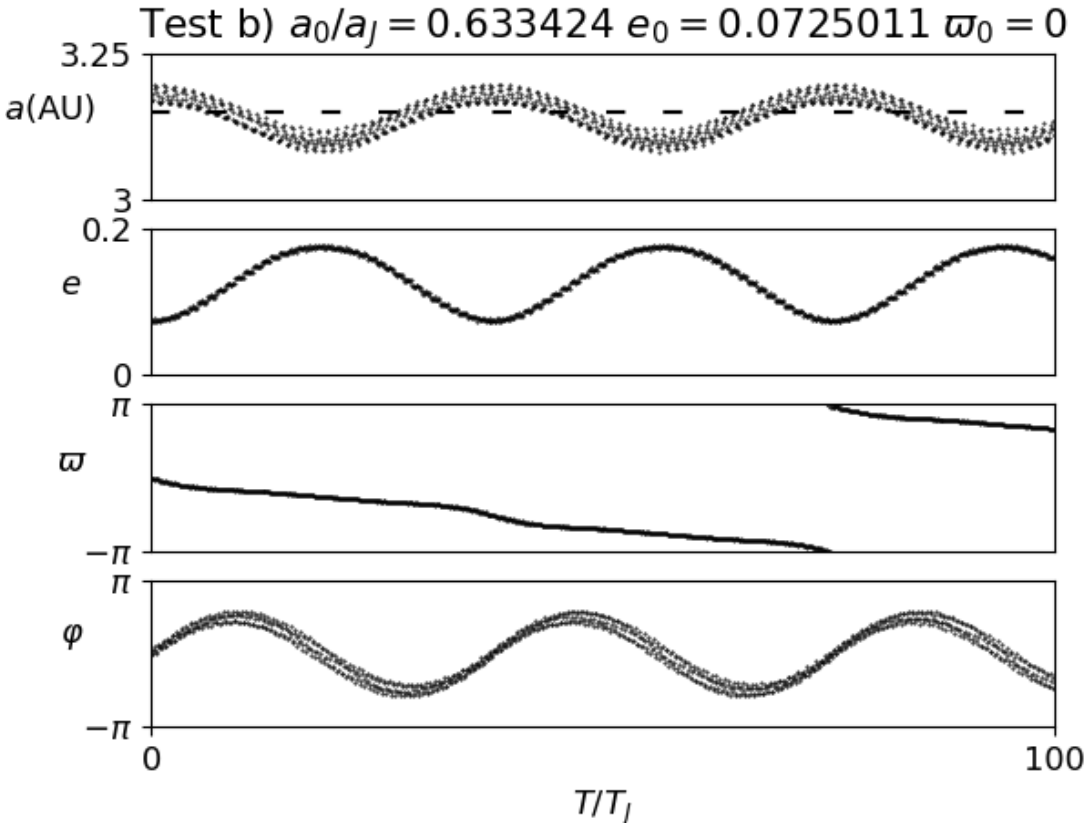
Test b) $a_0/a_J = 0.633424$ $e_0 = 0.0725011$ $\varpi_0 = 0$
3.25
a(AU)
3
0.2
e
0
π
ϖ
$-\pi$
π
φ
$-\pi$
0
100
T/T_J

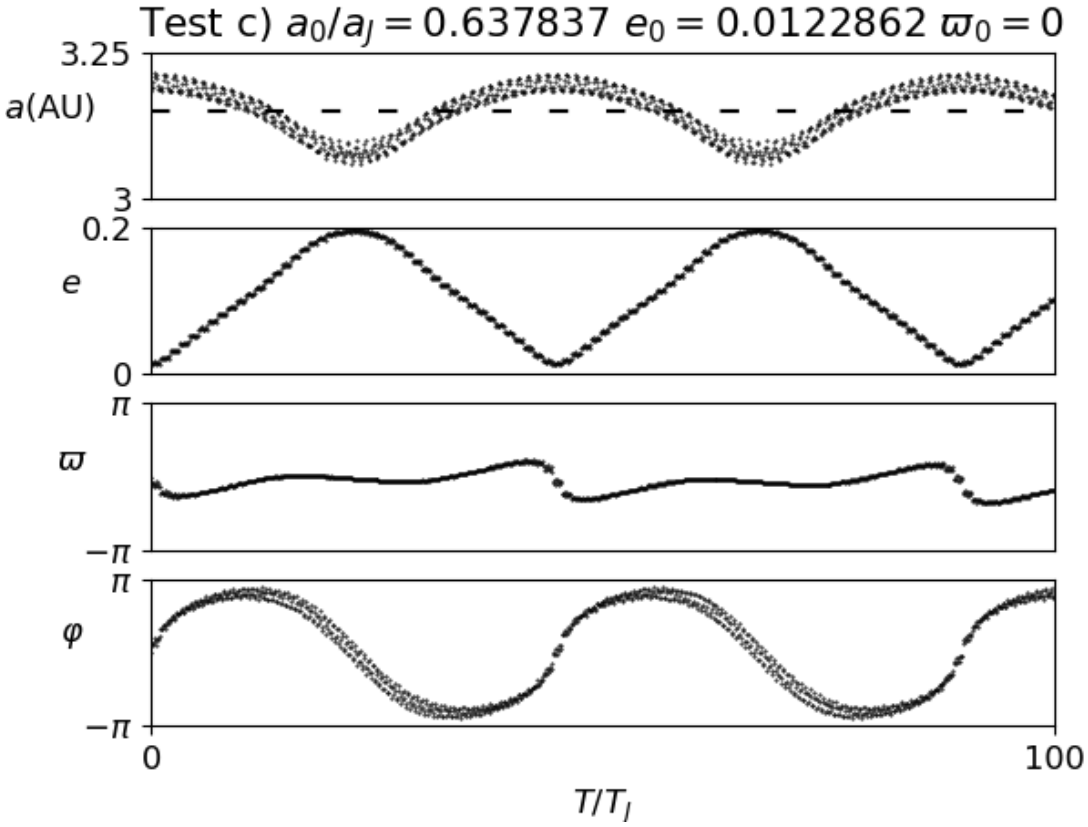
Test c) $a_0/a_J = 0.637837$ $e_0 = 0.0122862$ $\varpi_0 = 0$
3.25
a(AU)
3
0.2
e
0
π
ϖ
$-\pi$
π
φ
$-\pi$
0
100
T/T_J

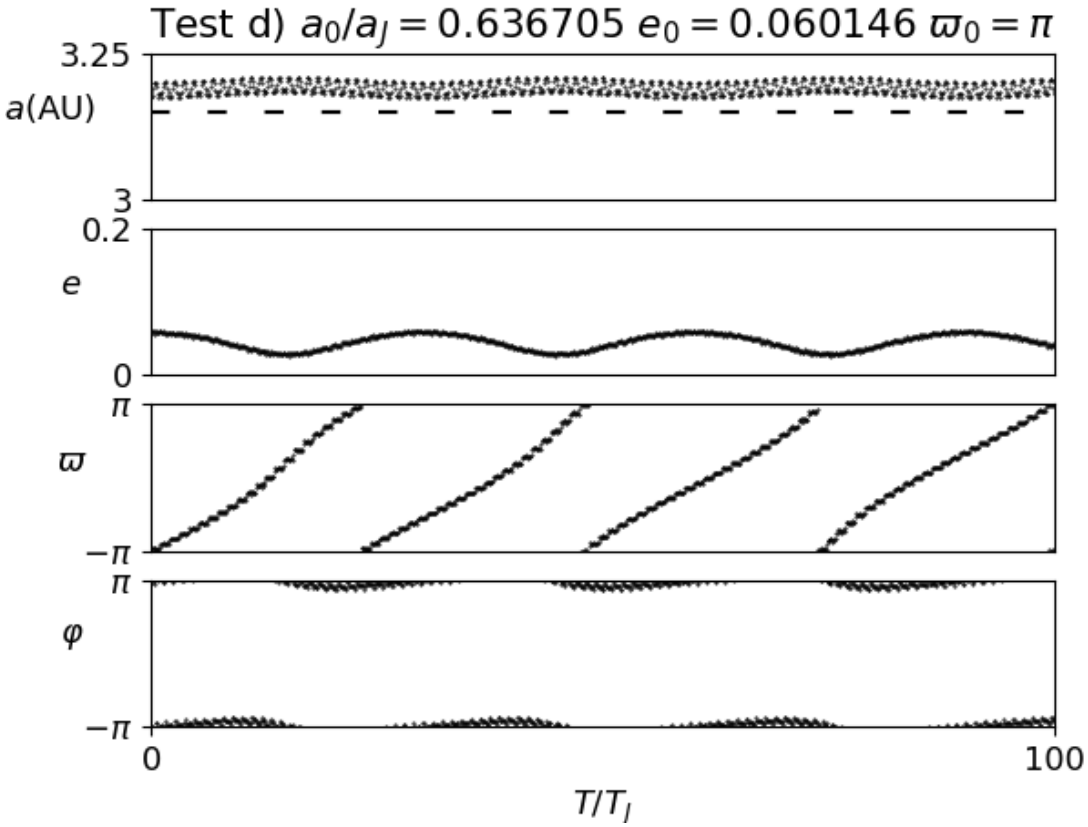
Test d) $a_0/a_J = 0.636705$ $e_0 = 0.060146$ $\varpi_0 = \pi$
3.25
a(AU)
3
0.2
e
0
π
ϖ
$-\pi$
π
φ
$-\pi$
0
100
T/T_J

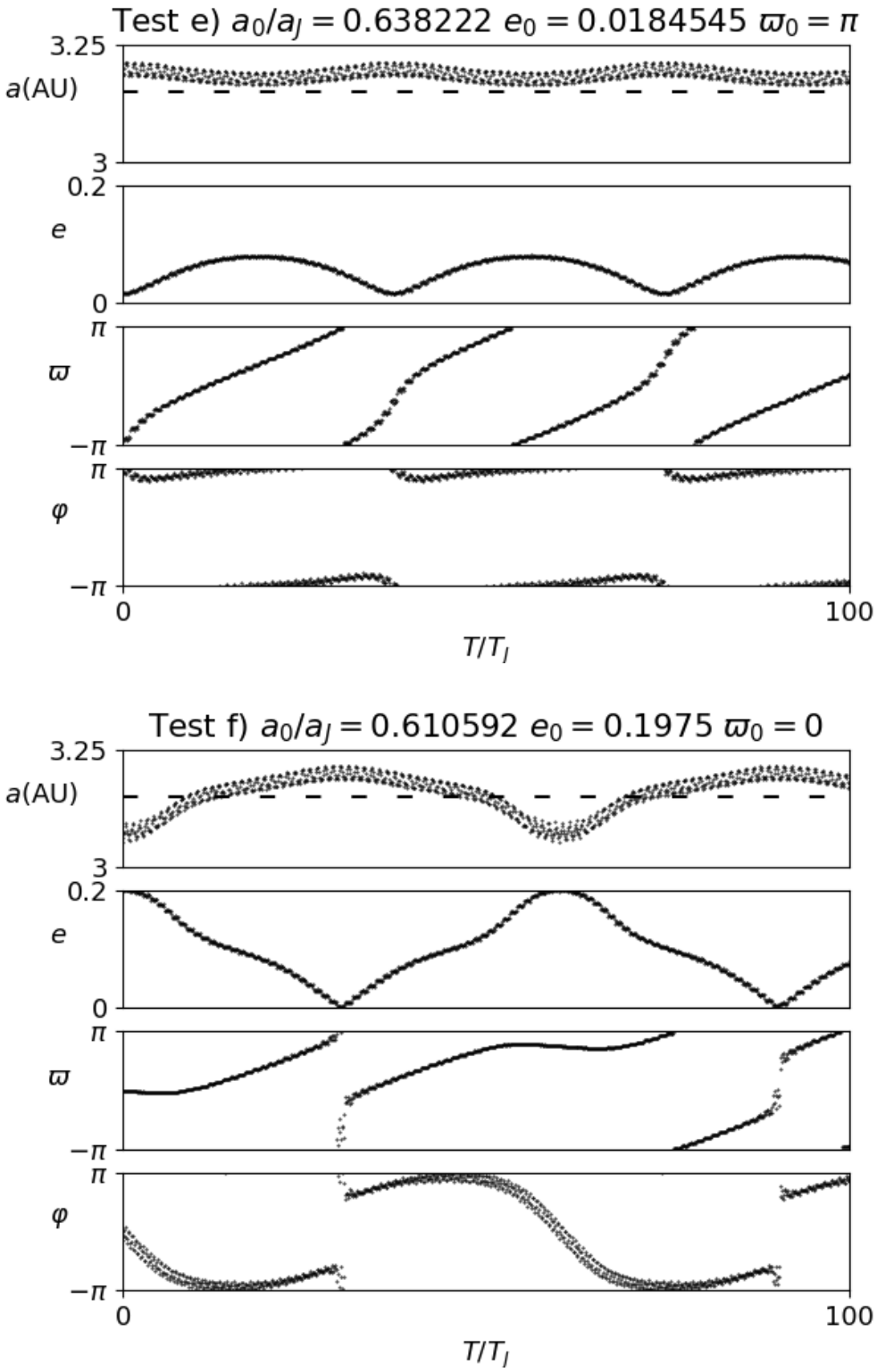

Figure 4.9: Plots of different orbital elements for different types of 2:1 resonances, described more precisely in figure 4.8, which is identical to these plots except that time-steps of 10^5s were used to create the plots instead of 10^6s, which were used for these plots.

4.3 2:1 resonance tests of planets

The tests from previous section were executed again, except no longer a test-particle is used as the inner object, but instead a body Jupiter's and the outer body has been given Saturn's mass. Additionally, the outer planet was placed at a distance of 8.65AU to mimic that of Saturn in the Nice model.

The key difference between these two simulations is that both orbiting bodies influence each other's orbits instead of only the outer body influencing the inner. This results in more variables, which is why there are now two plots for every a, e and ϖ.

Comparing these plots with those of the previous section it can be observed that (a), (b) and (c) have similar plots for the orbital elements except that deviations in a and e are dampened for (b) and (c) and is less constant for (a). Furthermore, the change in ϖ is dampened for all of these plots. The plots of (d), (e) and (f) have significantly different patterns and most notably is the (e) plot which seems strongly resonant. For most plots e increases, suggesting that the plots are not periodic for larger time-steps. To illustrate this, the most aperiodic plots (c) and (e) have been simulated for 1000 cycles of the outer body.

It is also interesting to consider Jupiter and Saturn in their initial conditions as they would be in the Nice model. That is, Jupiter at 5.45AU and Saturn at 8.65, both in near circular co-planar orbits (e and i on the scale of 10^{-3}).

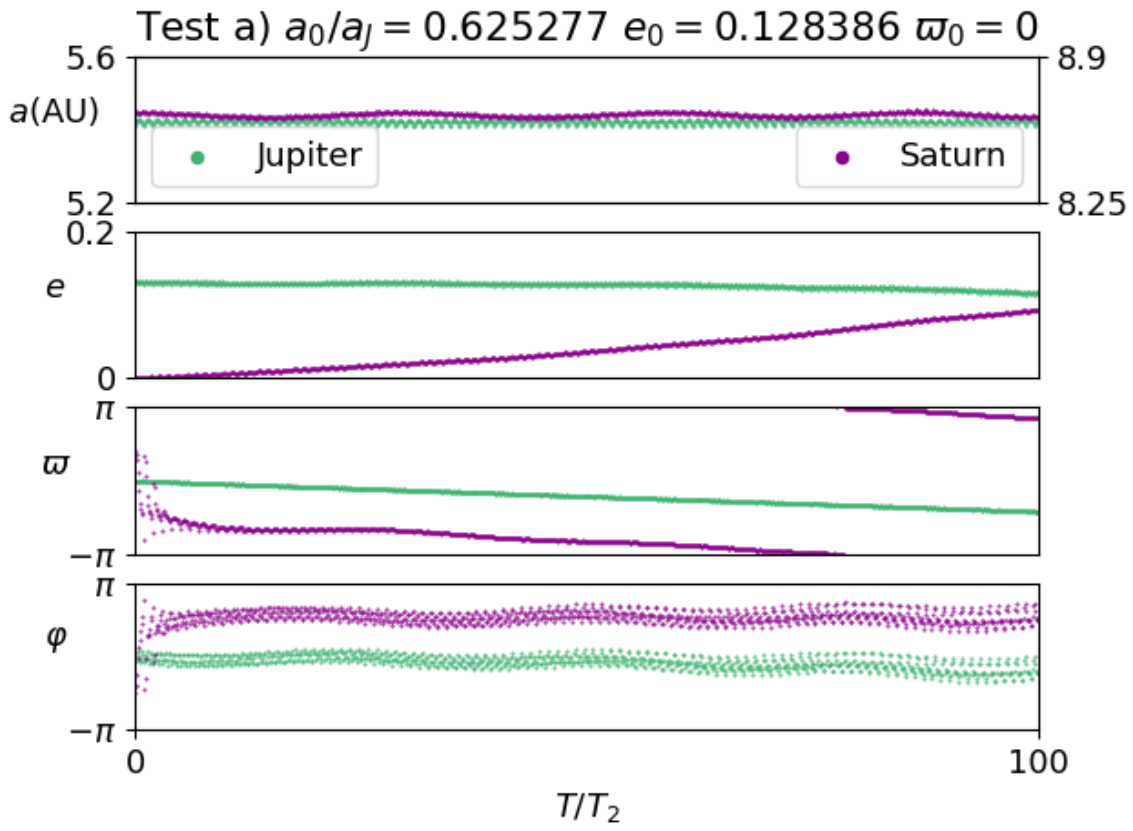
Test a) $a_0/a_J = 0.625277$ $e_0 = 0.128386$ $\varpi_0 = 0$
5.6
8.9
a(AU)
Jupiter
Saturn
5.2
8.25
0.2
e
0
π
ϖ
$-\pi$
π
φ
$-\pi$
0
100
T/T_2

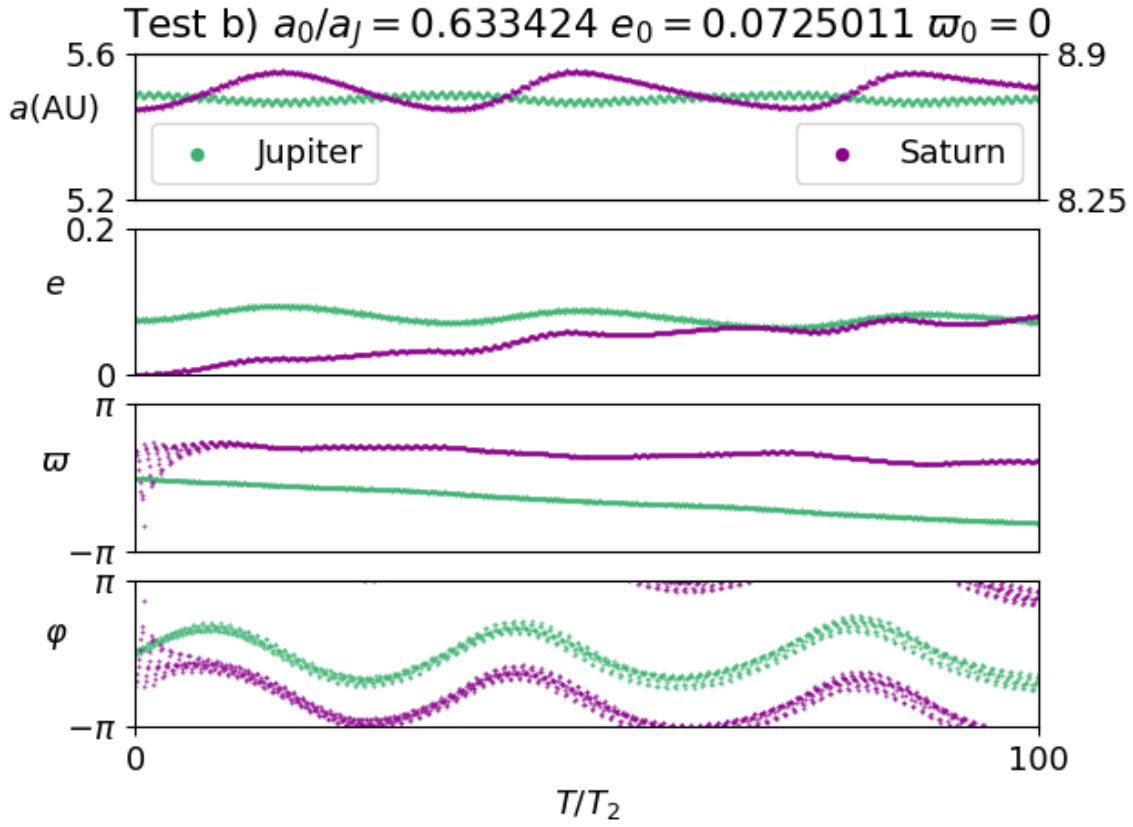
Test b) $a_0/a_J = 0.633424$ $e_0 = 0.0725011$ $\varpi_0 = 0$
5.6
8.9
a(AU)
Jupiter
Saturn
5.2
8.25
0.2
e
0
π
ϖ
$-\pi$
π
φ
$-\pi$
0
100
T/T_2

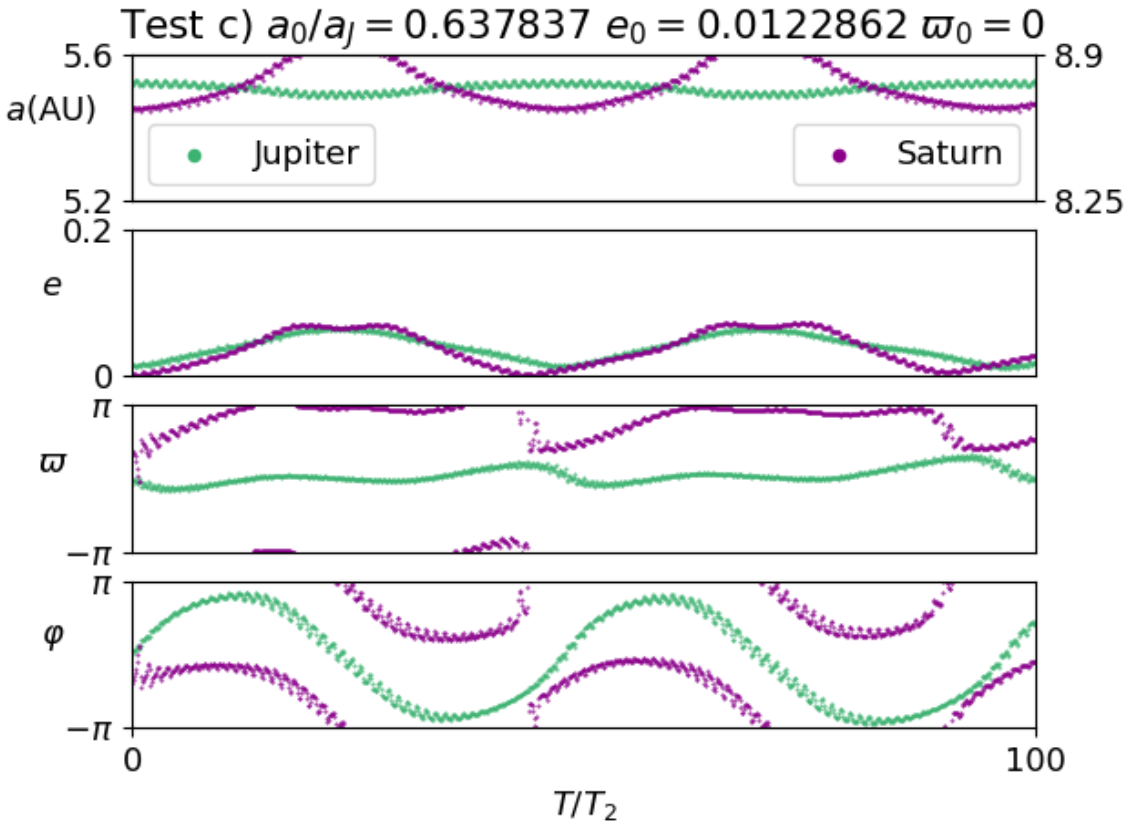
Test c) $a_0/a_J = 0.637837$ $e_0 = 0.0122862$ $\varpi_0 = 0$
5.6
8.9
a(AU)
Jupiter
Saturn
5.2
8.25
0.2
e
0
π
ϖ
$-\pi$
π
φ
$-\pi$
0
100
T/T_2

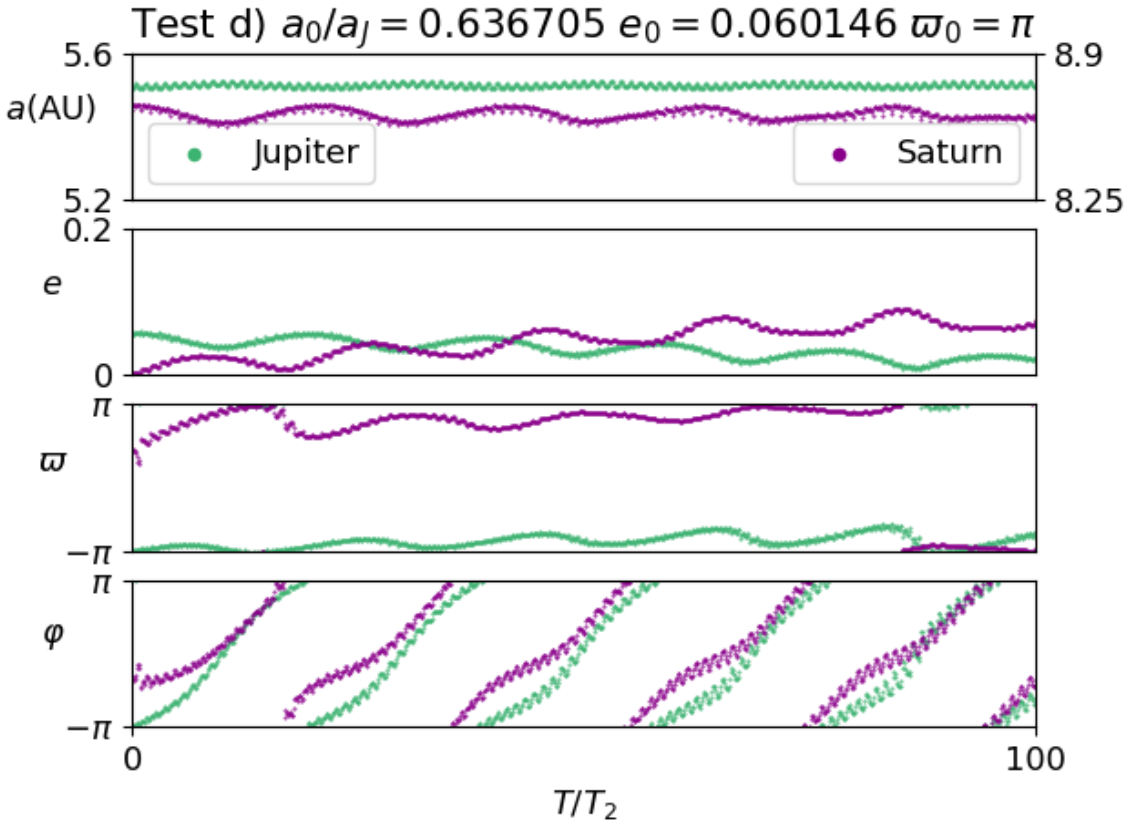
Test d) $a_0/a_J = 0.636705$ $e_0 = 0.060146$ $\varpi_0 = \pi$
5.6
8.9
a(AU)
Jupiter
Saturn
5.2
8.25
0.2
e
0
π
ϖ
$-\pi$
π
φ
$-\pi$
0
100
T/T_2

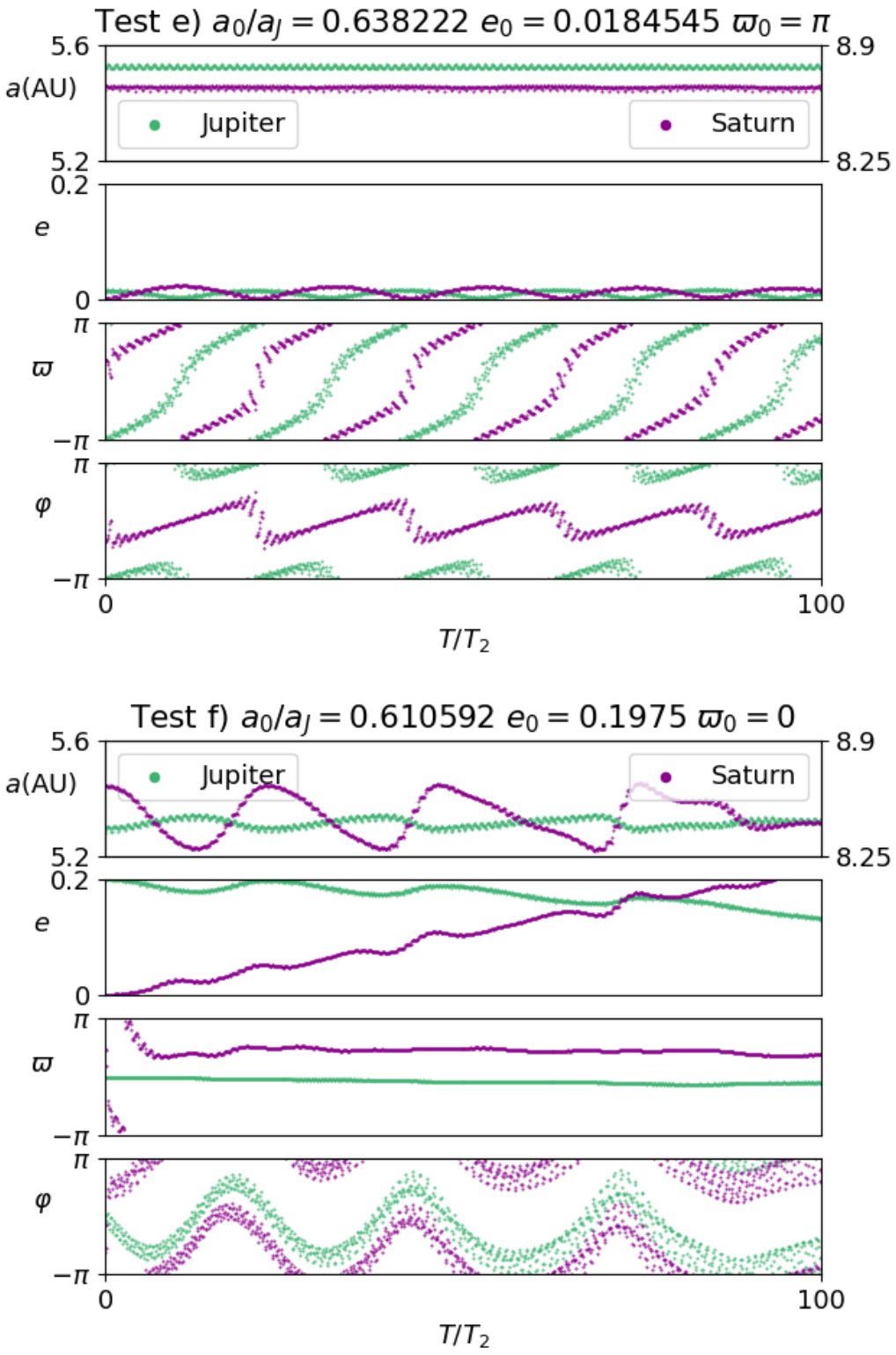

Figure 4.10: Orbital elements of two planets starting over a time-scale of 1000 circulations of the outer body. The inner and outer body were given the masses of Jupiter and Saturn respectively. In each plot a is the semi-major axis (on a scale from on a scale from 5.2 to 5.6AU for the inner body and 8.25 to 8.9AU for the outer), e represents the eccentricity (on a scale from 0 to 0.2 for both), ϖ longitude of periapsis (on a scale from $-\pi$ to π rad) and φ a quantity defined by $2\nu_2 - \nu_1 - 2\varpi$ (on a scale from $-\pi$ to π rad). The initial values are given in table (4.1).

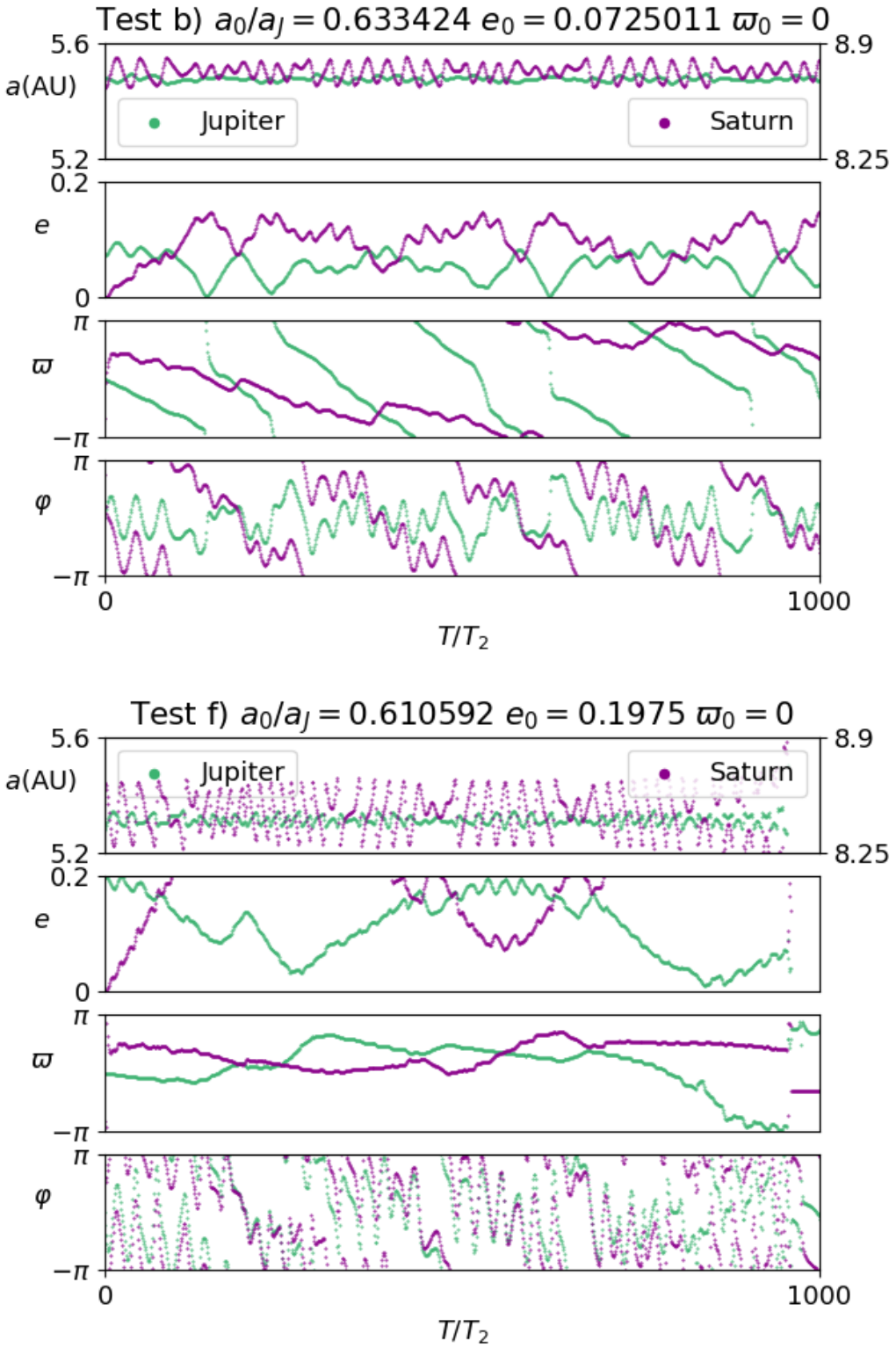

Figure 4.11: The orbital elements of initial conditions (b) and (f) respectively for 1000 outer periods. The specifics of these initial conditions are also given in the titles of the respective plots. These plots were shown for 100 outer periods in 4.3 and were both plotted because the eccentricity e did not appear periodic in these plots. It is in this figure that that this is indeed the case.

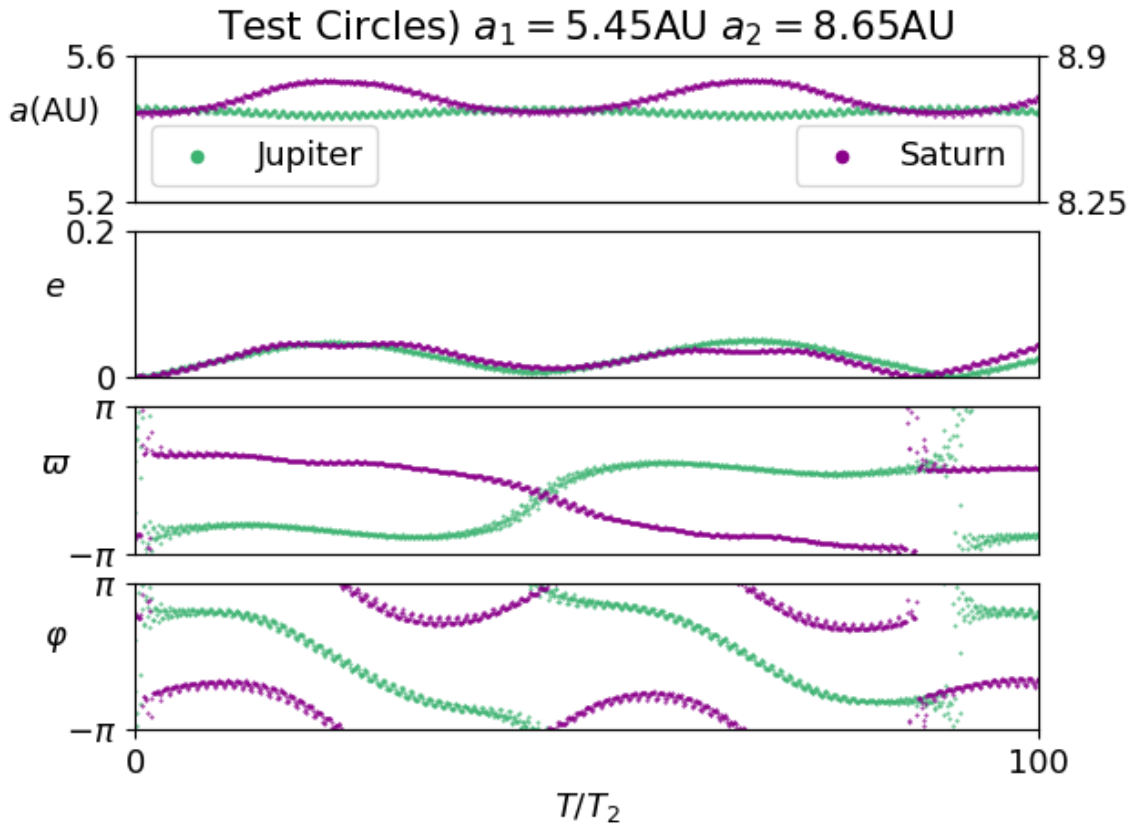

Figure 4.12: Orbital elements of Jupiter and Saturn initialised as in the Nice model. a is the semi-major axis (on a scale from on a scale from 5.2 to 5.6AU for the inner body and 8.25 to 8.9AU for the outer), e represents the eccentricity (on a scale from 0 to 0.2 for both), ϖ longitude of periapsis (on a scale from $-\pi$ to π rad) and φ a quantity defined by $2\nu_2 - \nu_1 - 2\varpi$ (on a scale from $-\pi$ to π rad).

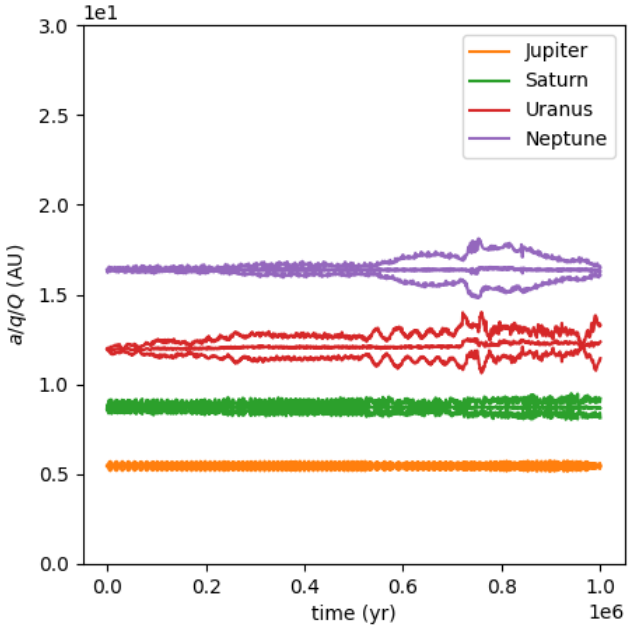

Figure 4.13: Run of our Nice model depicting oscilations due to resonance.

4.4 Four planets in resonance chain

To study the effects of orbital resonance, a "resonance-chain" has been created. That is, a multitude of planets which have initial semi-major axes so that the frequencies of the neighbouring orbits are close to resonance just like in the Nice model. This model differs significantly from the Nice model, however, as it does not include a disk of planetoids. To attain this resonance the planets have been initialised close to $T_J : T_S \approx 2 : 1, T_S : T_U \approx 3 : 2$ and $T_U : T_N$, where T_J, T_S, T_U and T_N are the periods of Jupiter, Saturn, Uranus and Neptune respectively. Additionally, the eccentricities and inclinations were chosen from a uniform distribution between -10^{-3} and 10^{-3}. The semi-major axis values given to the planets to attain these values close to resonance are

1. Jupiter : 5.45 AU
2. Saturn : 8.65 AU
3. Uranus : 11-13 AU
4. Neptune : 13.5-17 AU,

where Uranus and Neptune are additionally separated by at least 2 AU.

From these plots particular phenomena could be observed. Firstly, as noted in section 4.3, the semi-major and the eccentricity oscillate when in resonance as can be observed in figure 4.13. The eccentricity tends to oscillate most significantly which causes the distance between the different orbits to decrease. It can also be observed that these effects are most notable for the lightest outer planets Uranus and Neptune. When two planets' orbits cross they can start having close-encounters, shown in figure 4.14. In these cases the semi-major axis and eccentricity change drastically. In that figure it can also be observed that the orbits of Uranus and Neptune stay close to one another, this is explained because the point at which the planets change orbit should be included in the new path. The influence of the two planets can sometimes be so great that one of the planets is ejected as shown in figure 4.15. The effect of two planets having a prolonged close-distance is labeled "locking" in this paper. When Uranus and Neptune are displaced by a larger distance, Uranus can first lock with Saturn as shown in figure 4.16. When this happens, like in the previous case, the orbits of Saturn and Uranus significantly change each other's semi-major axis and eccentricity causing one of the orbits to cross Neptune's orbit as well. Due to this "multi-locking" the Solar

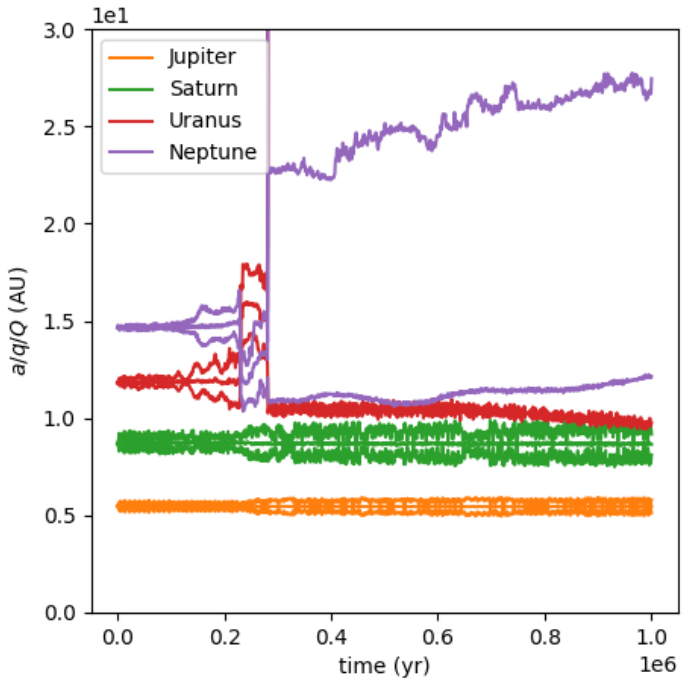

Figure 4.14: Run of our Nice model depicting Uranus and Neptune closing in on each other, after which at around $t \approx 0.3 \times 10^6$yr they have a close encounter and Neptune is ejected into an eccentric orbit.

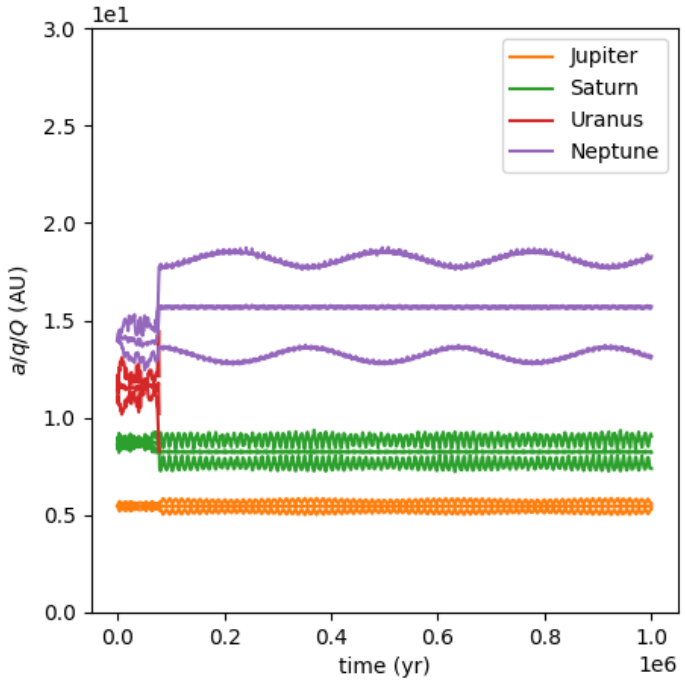

Figure 4.15: Run of our Nice model depicting an ejection of Uranus at around $t \approx 0.1 \times 10^6$yr, after which Neptune is knocked into a more eccentric orbit with higher semi-major axis.

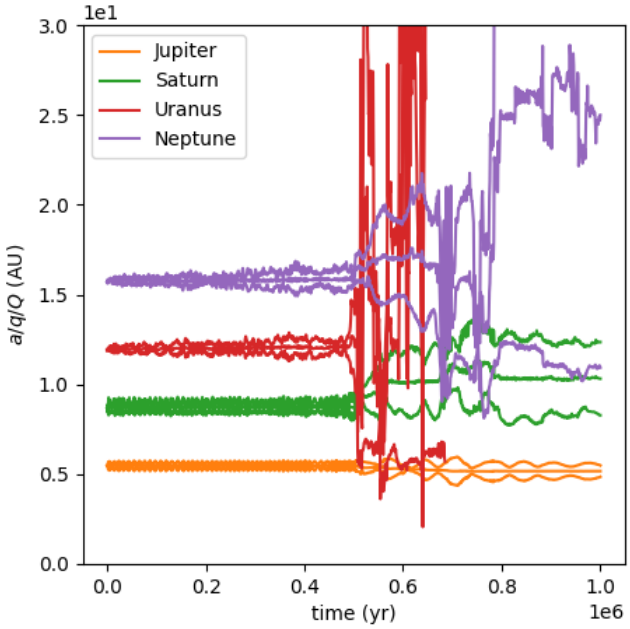

Figure 4.16: Run of our Nice model depicting Uranus influencing Saturn's and Neptune's orbit strongly due to the distance between the orbits from around $t = 0.5 \times 10^6$yr. After chaotic changes, Uranus is ejected from the Solar System at around 0.7×10^6yr, after which Saturn and Neptune keep changing each other's orbit.

system undergoes a chaotic evolution. In the case of figure 4.16 Uranus is ejected from the Solar system, Jupiter ends up with a significant eccentricity and Saturn and Neptune remain locked with each other, resulting in significant changes in the future.

Error analysis We tested the accuracy of our simulations by studying the constants of motion: energy, linear momentum and angular momentum. These values are theoretically constant and therefore provide an indication of the error. These values are calculated by

$$E = \sum_i \frac{1}{2} m_i \vec{v}_i \cdot \vec{v}_i - \sum_{ij} \frac{\mathcal{G} m_i m_j}{r_{ij}} \tag{4.2a}$$

$$\vec{p} = \sum_i m_i \vec{v}_i \tag{4.2b}$$

$$\vec{L} = \sum_i m_i \vec{r}_i \times \vec{v}_i, \tag{4.2c}$$

where $E, \vec{p}$ and $\vec{L}$ are the energy, linear momentum and angular momentum respectively, m_i, $\vec{r}_i$ and $\vec{v}_i$ the mass, position and velocity of body i and r_{ij} the distance between body i and body j. The total energy, absolute value of linear momentum, and the z-value of angular momentum of the systems were plotted, as shown in Figures (4.17, 4.18, 4.19 and 4.20). These plots reveal key insights into the behavior of these conserved quantities under different dynamical scenarios.

In figure 4.17, the total energy exhibits oscillations around a mean value, with deviates on the order of 2×10^{-3}. Similarly, the linear momentum oscillates with deviations around 1×10^{-1}, and the angular momentum fluctuates approximately 1.0×10^{-3}, thought with a shifting mean. There variations are attributed to noise inherent in these simulations. Examining figure 4.18 it becomes evident that close encounters result in significant changes in the mean values of both total energy and angular momentum. Additionally, the noises levels for both linear and angular momentum increase following these encounters. In the case of an ejection event following a close encounter, as shown in figure 4.19, the mean value of the momentum shifts, resulting in the center of mass (CM) of the system moving over time. Consequently, the angular momentum error grows linearly. Aside from this effect, the total energy exhibits a discontinuous jump to a new mean value, and

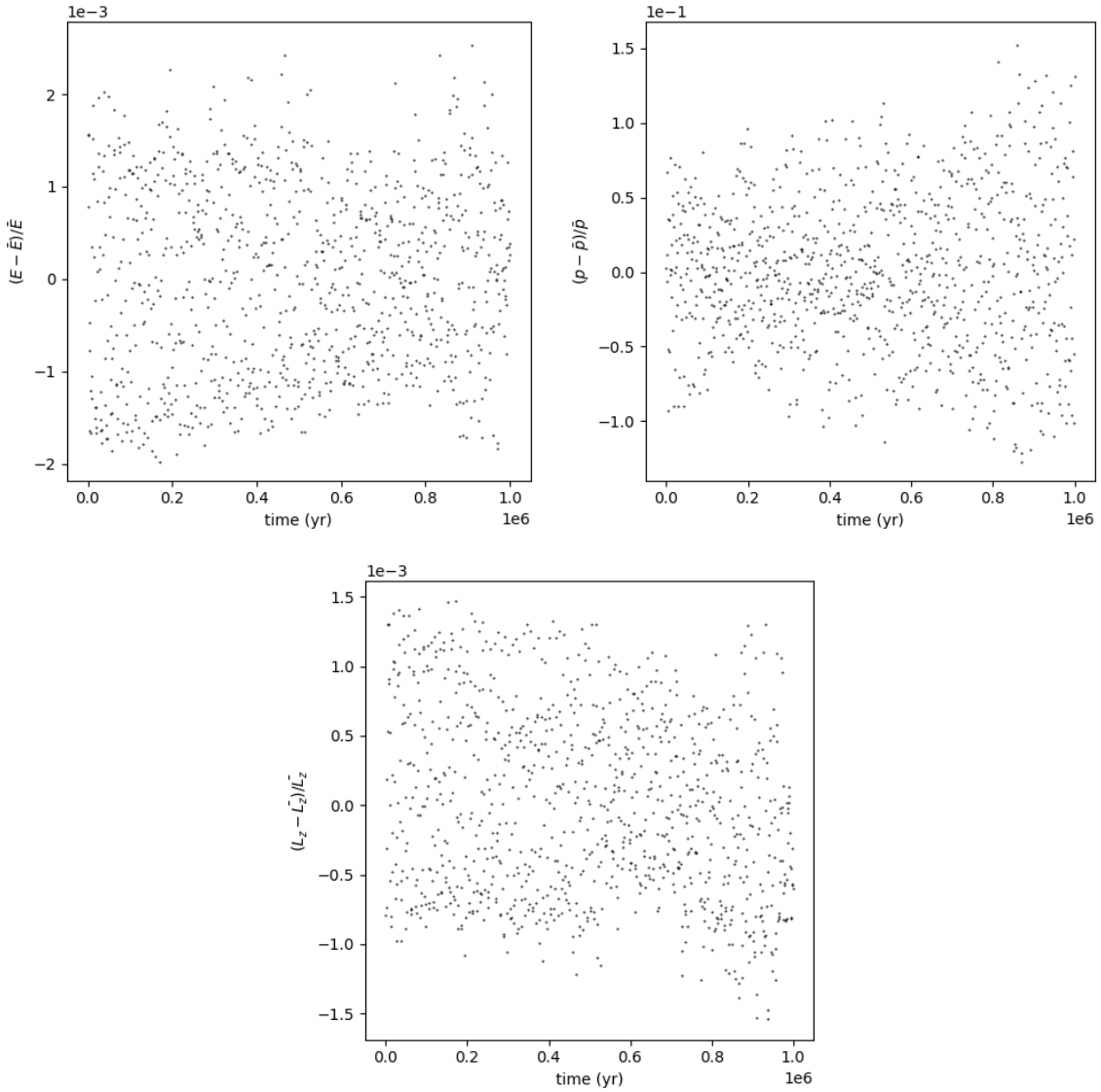

Figure 4.17: Relative deviation of total energy, linear momentum and angular momentum of figure 4.13. It can be observed that all the conserved quantities have a noise-like error which is on the scale of 10^{-3} for the energy and the angular momentum, while it is on the scale of 10^{-1} for the momentum.

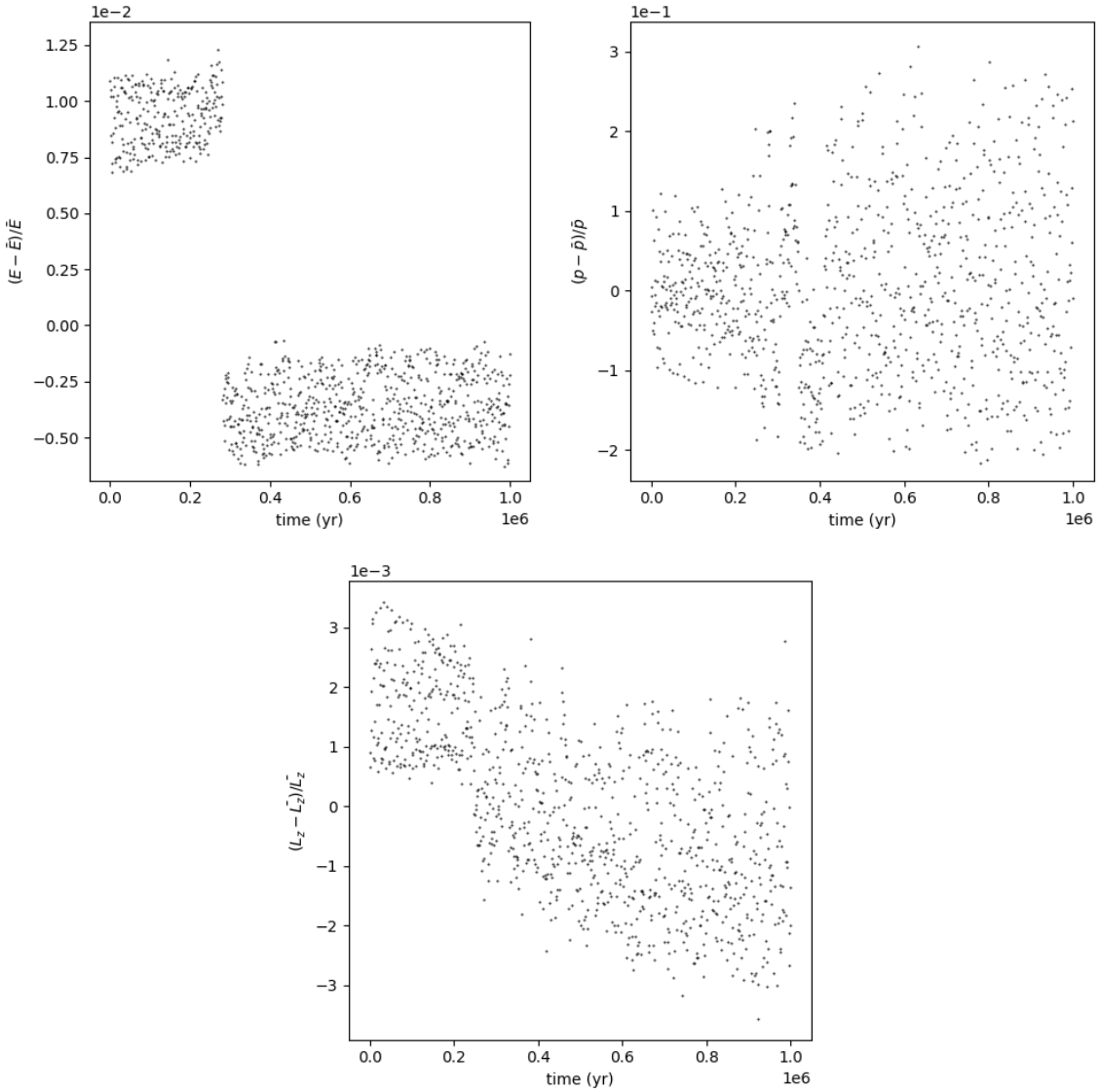

Figure 4.18: Relative deviation of total energy, linear momentum and angular momentum of figure 4.14. A discontinuity can be observed in the energy and angular momentum plot around $t = 0.3 \times 10^6$yr. Additionally, the angular momentum and the linear momentum increase their noise-like error after this event.

the noise in the momentum also increases after the event, similar to what is observed during close encounters. Finally, the cumulative effect for multiple close encounters and a single ejection is presented in figure 4.20. This plot illustrates the combined impact on the conserved quantities, reinforcing the observations made in the previous scenarios. In summary, the analysis of these plots indicates that while noise is present in all simulations, close encounters and ejections lead to noticeable discontinuities in energy and angular momentum. These events also cause a marked increase in noise levels, particularly in linear and angular momentum, due to the shifting center of mass and other dynamical effects.

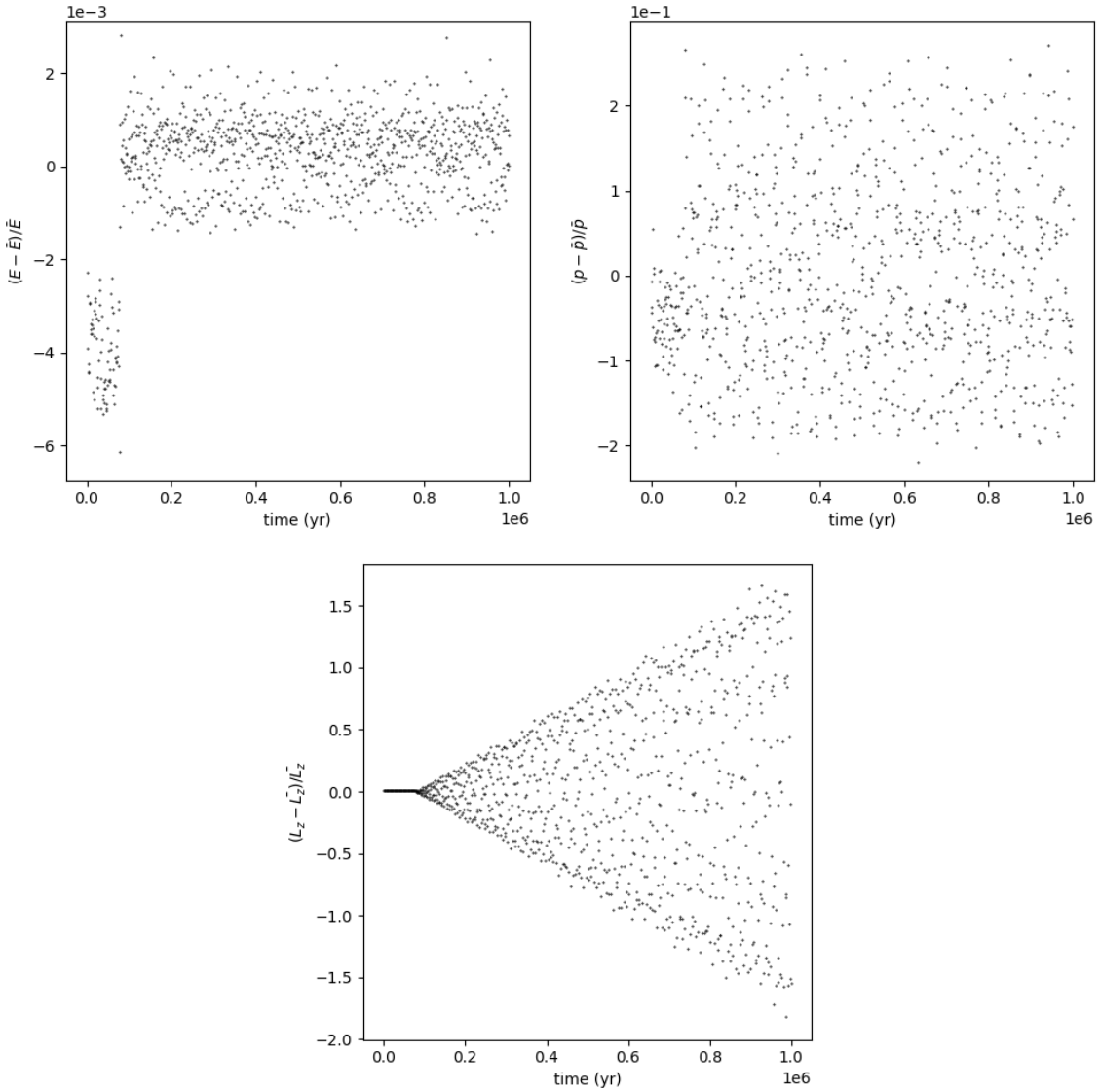

Figure 4.19: Relative deviation of total energy, linear momentum and angular momentum of figure 4.15. A discontinuity can be observed in the energy and linear momentum plot around $t = 0.1 \times 10^6$yr. Additionally, the noise of the linear momentum increases after this point. Because of the moving center of mass (the average of p is not constant) the angular momentum's error increases linear from $t = 0.1 \times 10^6$yr.

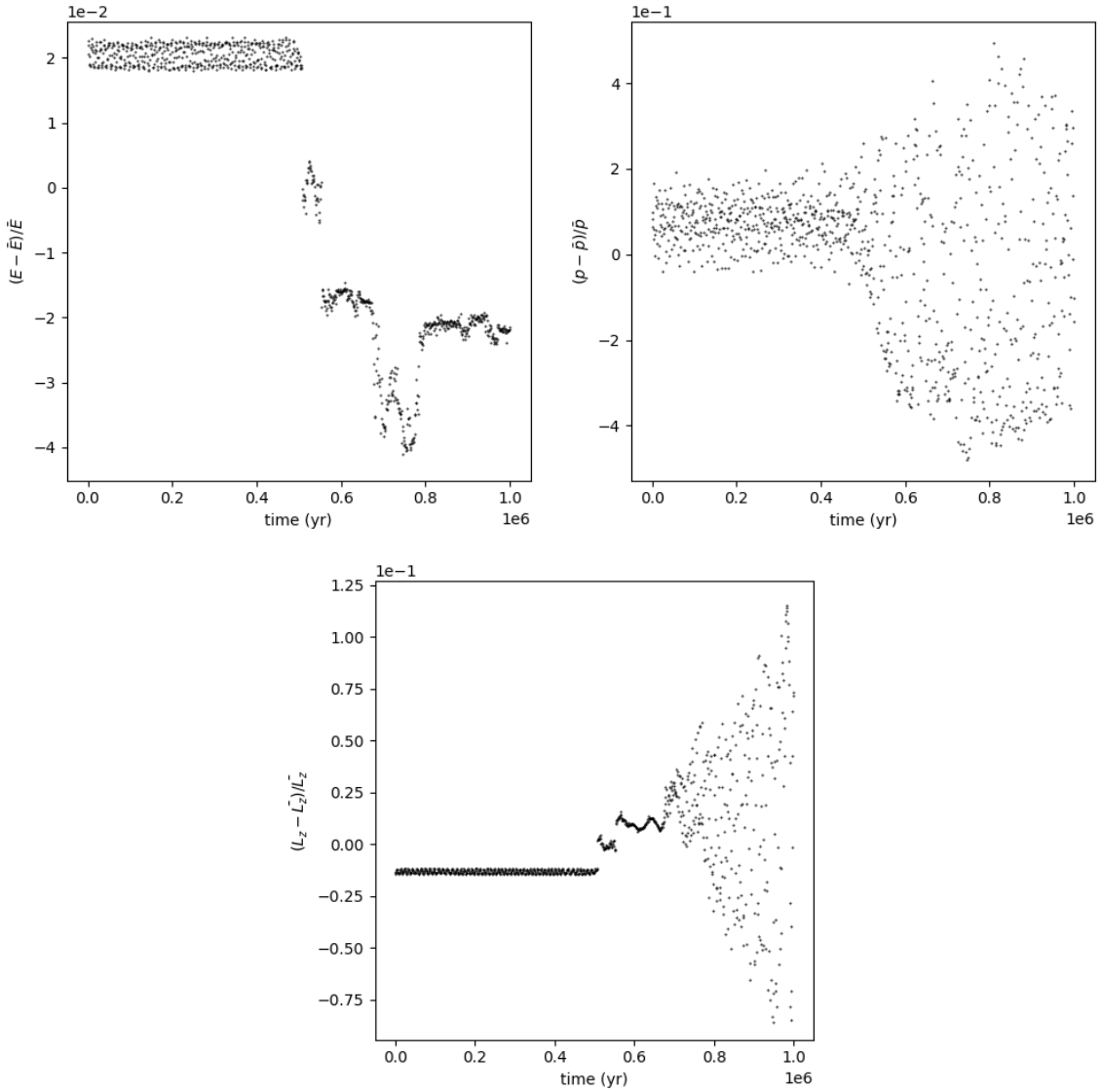

Figure 4.20: Relative deviation of total energy, linear momentum and angular momentum of figure 4.16. Significant results can be found around $t = 0.5 \times 10^6$yr, during which all the conserved quantities change and an event around 0.7×10^6yr after which the angular momentum linearly increases, suggesting an ejection, as can be verified from figure 4.16.

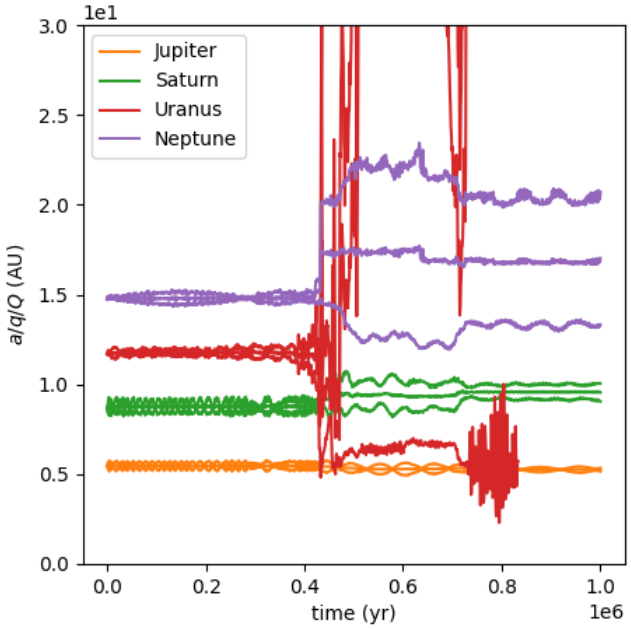

Figure 4.21: Run of our Nice model with adaptive time-steps. Most notable is the ejection of Uranus at approximately $t = 0.8 \times 10^6$yr

4.4.1 Resonance chain with adaptive time-steps

To reduce the uncertainty in energy, linear momentum and angular momentum, adaptive time-steps have been implemented as outlined in in section 3.3. While the improvement in accuracy was not drastic, it was nonetheless significant. Figure 4.21 illustrates the evolution of the Solar System with adaptive time-steps, showing features similar to those observed in figure 4.16, considered previously, without adaptive time-steps.

error analysis The errors in total energy, linear momentum, and angular momentum are presented in figure 4.22. These results are compared with those from the similar scenario depicted in figure 4.20. The energy profile in the adaptive time-step scenario displays multiple jumps, but over a smaller range (from -1.5 to 1.5×10^{-2}), compared to the larger range observed in the non-adaptive case (from -4.5 to $2.5\times^{-2}$), This general trend of reduced error is consistent across all conserved quantities, including total energy, linear momentum, and angular momentum.

A particularly promising observation is that, during the ejection event, the energy profile does not exhibit a continuous jump. The absence of discontinuity strengthens the confidence that ejections are a physically plausible outcome in the Solar System, as captured by the simulations with adaptive time-steps.

In summary, the implementation of adaptive time-steps has led to a notable reduction in the uncertainties associated with energy and momentum. The more stable behavior of conserved quantities, particularly during critical events such as ejections, enhances the confidence that these events represent realistic dynamical features of the Solar System.

The plots have shown various dynamical conditions of oscillating eccentricities e, locking, close-encounters and ejections. These results suggest that resonance is a strong explanation for rapid evolution of the Solar System as is suggested in the Nice model. Furthermore, ejections of planets such as observed in revisions of the Nice model are seen in this paper as well, increasing the likelihood of such a conclusion. Additionally, this paper has strong educational relevance in understanding the effects of resonance, due to the different types considered and the approach of isolating resonance from all other effects which are usually considered in the Nice model.

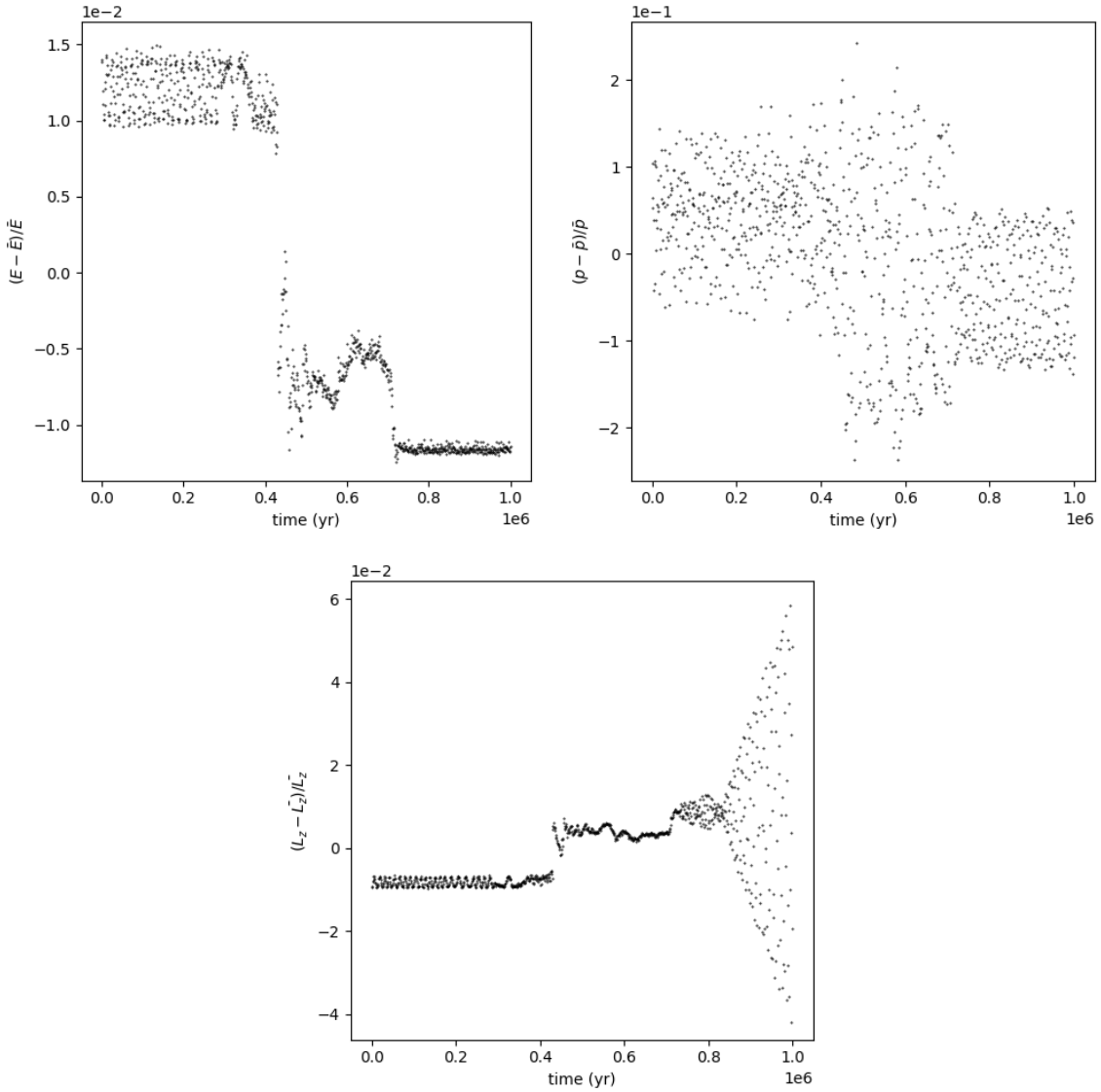

Figure 4.22: Relative deviation of total energy and momentum of figure 4.21. From the angular momentum plot it can be seen that there are 2 significant events at around 0.45×10^6yr and 0.8×10^6yr. By comparing the timescale with that of figure 4.21 it can be seen that the first event is when Uranus starts having close encounters with Saturn and Neptune, changing its semi-major axis significantly and the last event is the ejection of Uranus.

5 Conclusion

In this paper, we investigated gravitational resonances using a variety of initial conditions for bodies in co-planar orbits around a central massive object, at least 1000 times heavier than the orbiting bodies. Simulations were conducted using a second-order leapfrog integrator, which calculated accelerations via optimized brute-force methods based on array multiplication.

We began by examining motions near the L_4 Lagrange point. This provided an estimate of the simulation's numerical deviation and insights into the analytical solution near L_4. The analytical solution, which involves a Taylor approximation of the potential, deviates from the numerical results, leading to a gradual phase shift. A comparison between the analytical and numerical solutions revealed that the solution shifted by 9.42 years over a 1000-year period, indicating the limitations of the analytical approximation in capturing long-term behavior.

Next, we explored the 2:1 resonance, both with and without a test particle. Different initial conditions were used to trigger various types of resonances, revealing the sensitive nature of these systems. Even small changes in time-steps could lead to significantly different outcomes and resonance patterns. In these simulations, the semi-major axis a and eccentricity e were observed to oscillate, with the resonance angle φ serving as a valuable tool for analyzing the types of resonances. The test-particle scenario exhibited strong periodicity, while simulations involving two massive bodies tended to display chaotic behavior. This chaotic behavior was particularly evident as the eccentricity of the outer body increased, leading to more pronounced dynamical effects.

Finally, we simulated the Solar System using a configuration similar to the Nice model, excluding planetoids, and with Uranus and Neptune swapped from their current positions. These simulations revealed consistent phenomena across different runs. Initially, the planets' orbits oscillated in both semi-major axis a and eccentricity e, causing their orbits to gradually converge. Once the planets reached a critical proximity, close encounters occurred, but these encounters did not increase the distance between the planets. Instead, the planets became "locked" in their orbits unless one was eventually ejected from the Solar System, resulting in chaotic outcomes where one planet was typically expelled.

The plots have shown various dynamical conditions of oscillating eccentricities e, locking, close-encounters and ejections. These results suggest that resonance is a strong explanation for rapid evolution of the Solar System as is suggested in the Nice model. Furthermore, ejections of planets such as observed in revisions of the Nice model are seen in this paper as well. Overall the significance of these results is that resonance is found as a strong factor of these drastic dynamics.

6 Further Research

Due to time constraints, this study only scratches the surface of the complexities involved in the evolution of the Solar System under Nice model conditions. We propose three areas for further research:

1. Planetoid Disc: As discussed in Section 2.8, planetoids play a crucial role in damping eccentricity and inclination, allowing planets to escape from orbital locking. Future studies could model planetoids as a homogeneous disc extending from Neptune's initial position to approximately 30 AU. Alternatively, planetoids could be modeled individually and calculated via brute force, as in the original Nice model study [Tsiganis et al., 2005].

2. More Accurate Integrator: The simulations exhibited significant errors in conserved quantities such as energy and momentum. Using a more accurate integrator could help mitigate these errors, leading to more precise results.

3. More Efficient Algorithm or Enhanced Computing Power: The accuracy of the simulations could also be improved by decreasing the time-step Δt, but this was not feasible in our study due to the inefficiency of Python and limited access to high-end computing resources. Utilizing more efficient algorithms or more powerful computational tools could alleviate this issue.

Bibliography

[Alvarez et al., 1980] Alvarez, L. W., Alvarez, W., Asaro, F., and Michel, H. V. (1980). Extraterrestrial Cause for the Cretaceous-Tertiary Extinction. *Science*, 208:1095–1108. ADS Bibcode: 1980Sci...208.1095A.

[Fitzpatrick, 2023] Fitzpatrick, R. (2023). Derivation of Lagrange planetary equations.

[Gomes et al., 2005] Gomes, R., Levison, H. F., Tsiganis, K., and Morbidelli, A. (2005). Origin of the cataclysmic Late Heavy Bombardment period of the terrestrial planets. *Nature*, 435(7041):466–469.

[Li et al., 2023] Li, J., Xia, Z. J., Yoshida, F., Georgakarakos, N., and Li, X. (2023). Asymmetry in the number of L4 and L5 Jupiter Trojans driven by jumping Jupiter. *Astronomy & Astrophysics*, 669:A68.

[Morbidelli et al., 2005] Morbidelli, A., Levison, H. F., Tsiganis, K., and Gomes, R. (2005). Chaotic capture of Jupiter's Trojan asteroids in the early Solar System. *Nature*, 435(7041):462–465.

[Murray and Dermott, 2000] Murray, C. D. and Dermott, S. F. (2000). *Solar System Dynamics*. Cambridge University Press, Cambridge.

[NIST, 2022] NIST (2022). CODATA Value: Newtonian constant of gravitation.

[Sundman, 1913] Sundman, K. F. (1913). Mémoire sur le problème des trois corps. *Acta Mathematica*, 36(none):105–179. Publisher: Institut Mittag-Leffler.

[Tsiganis et al., 2005] Tsiganis, K., Gomes, R., Morbidelli, A., and Levison, H. F. (2005). Origin of the orbital architecture of the giant planets of the Solar System. *Nature*, 435(7041):459–461.

[Wang, 1991] Wang, Q.-D. (1991). The global solution of the n-body problem. *Celestial Mechanics and Dynamical Astronomy*, 50:73–88. Publisher: Springer ADS Bibcode: 1991CeMDA..50...73W.

[Wikipedia, 2024a] Wikipedia (2024a). Ellipse.

[Wikipedia, 2024b] Wikipedia (2024b). Mean anomaly. Page Version ID: 1241160993.